AERODYNAMIC CHARACTERISTICS OF THE
SCOUT 133R VEHICLE DETERMINED FROM
WIND TUNNEL TESTS

26 October 1972

By F. B. Abramson, T. G. Muir, H. L. Simmons

TABLE OF CONTENTS

LIST OF TABLES

LIST OF FIGURES

LIST OF FIGURES (Cont'd.)

DEFINITION OF SYMBOLS

Symbol	Definition

B — Refers to the nose boom

C_N — Normal force coefficient

C_{N_α} — Slope of normal force coefficient curve at $\alpha = 0°$, $\dfrac{dC_N}{d\alpha}$, per degree

C_{N_δ} — Rate of change of normal force coefficient with fin tip control deflection at $\alpha = 0°$, $dC_N/_{d\delta}$, per degree

C_m — Pitching moment coefficient

C_{m_α} — Slope of pitching moment coefficient curve at $\alpha = 0°$, $dCm/_{d\alpha}$, per degree

C_{m_δ} — Rate of change of pitching moment coefficient with fin tip control deflection at $\alpha = 0°$, $dCm/_{d\delta}$, per degree

C_p — Pressure coefficient

$c_{N_\alpha} S$ — Normal load distribution parameter, $\dfrac{dC_{N_\alpha}}{dX} S$, $ft/_{deg.}$

c_N — Local normal force coefficient, $\dfrac{dC_N}{dX}$, per ft.

c_{N_α} — Local normal force coefficient slope, $\dfrac{dC_{N_\alpha}}{dX}$, $1/ft - deg$

$\dfrac{dC_N}{dX}$ — Rate of change of normal force coefficient, $1/ft.$

$\dfrac{dC_{N_\alpha}}{dX}$ — Rate of change of normal force coefficient slope, $1/ft\text{-}deg$

$d_{ref.}$ — Reference diameter, 2.58 ft.

F — Refers to vehicle fins

FS — Refers to full-scale vehicle dimensions or stations

MS — Refers to model dimensions or stations

M — Mach number

P — Refers to protuberances (includes protuberances and wiring tunnels)

S — Vehicle reference area, $5.25 \, ft^2$

X_{cp} — Center of pressure location, inches

DEFINITION OF SYMBOLS (Cont'd.)

Symbol	Definition
X_l	Station location of vehicle base, inches
X_{ref}	Reference moment center, station 427.8
α	Angle of attack, degrees
δ	Fin tip control deflection angle, positive provides nose down pitching moment, degrees
ϕ	Radial angle measured around the body circumference, degrees
ψ	Yaw angle, positive nose right, degrees

Subscripts

o	Conditions at zero angle of attack
FIN	Refers to one fin

Superscripts

o	Indicates nose boom aligned with vehicle centerline
3	Indicates nose boom inclined at 3° nose up to the vehicle centerline

AERODYNAMIC CHARACTERISTICS OF THE
SCOUT 133R VEHICLE DETERMINED FROM
WIND TUNNEL TESTS

SUMMARY

Bending moments and other associated parameters were measured on a Scout vehicle during a launch through high velocity horizontal winds. Comparison of the measured data with predictions revealed some unexplained discrepancies. Possible sources of error in the experimental data and predictions were considered; one of which is the predicted aerodynamic characteristics. A wind tunnel investigation was initiated, including supersonic force and pressure tests, to better define the aerodynamics.

The purpose of this study was to reduce and analyze the wind tunnel tests data and establish aerodynamic coefficients in the pitch plane. Prior to this study, very little experimental data existed which defined the flow characteristics in the vicinity of protuberances and wiring tunnels. In addition to basic aerodynamic coefficients from the force test, detailed pressure and load distributions along the body were established from the pressure test. Pressure coefficients were integrated to determine normal load distributions, total normal force, and total pitching moment of the body. Comparison of the normal forces from pressure and force tests resulted in agreement within 15%. Comparison of pitching moment data from the two tests resulted in larger differences. Moment coefficients determined from the force data are considered more accurate than integrated pressure data because moments obtained from pressure distributions are too sensitive to local loadings (i.e., a small variation in loading on the heatshield may result in a large change in moment because of the long moment arm involved).

1.0 INTRODUCTION

One of the most severe sources of loading on a launch vehicle is the horizontal wind. The wind produces high dynamic and static loadings on launch vehicles and results in substantial bending moments for long slender vehicles. The number of flight tests in which adequate load measurements have been made are few. An exception is the measured data

obtained by NASA/Langley during the flight of Scout 133R through a high wind velocity (200 fps). Strain gages were installed on the vehicle for measurement of bending moments in the structure, and were monitored throughout the flight. A comparison of the measured bending moments with values which were calculated for flight through the same wind profile indicated that dynamic loads due to excitation of oscillatory rigid and flexible body modes were in satisfactory agreement, but the calculated quasi-steady loads differed significantly from measured values. There is also a corresponding difference in calculated and measured angle of attack time histories. The evidence indicates an appreciable pitching moment not accounted for in the nominal design aerodynamic forces.

In view of these differences and because no experimental aerodynamic data existed for the particular vehicle configuration used for the flight loads measurements, wind tunnel force and pressure tests were conducted in the supersonic speed range with a model of the Scout 133R vehicle. Aerodynamic forces and moments were measured during the force test as a function of angle of attack and Mach number, and numerous pressure measurements were made on the model surface during the pressure tests. The study effort reported herein was initiated to reduce the wind tunnel data, and better define the aerodynamic derivatives and normal load distributions.

The ultimate goal is to eventually prove the validity of a technique for predicting loads on launch vehicles and spacecraft. The next step required to accomplish this will be to use the revised aerodynamic data generated in this study and re-calculate vehicle loads for comparison to flight measurements.

2.0 DISCUSSION

This study involved the reduction and analysis of data from force and pressure wind tunnel tests of Scout 133R models. Aerodynamic coefficients and derivatives were derived directly from the force test data, and the pressure test data were plotted and integrated over the length of the body, to obtain the same parameters. Discussion of the tests, and data reduction and analysis techniques are presented in the following paragraphs.

2.1 WIND TUNNEL TEST DESCRIPTIONS

2.1.1 Test Facility

Both tests were conducted at the LTV Vought Aeronautics Company High Speed Wind Tunnel in the supersonic test section. This

2

facility is an atmospheric exhaust, blow-down tunnel with a 4 foot by 4 foot test section size. The tunnel is a transonic-supersonic (inter-changeable test section and diffuser) installation with a Mach number range of .5 to 5.0. The nozzle upstream from the test section is an adjustable contour type, consisting of two flexible stainless steel plates and two fixed walls.

2.1.2 Models and Instrumentation

Aerodynamically, the force and pressure models were identical, but the force model was instrumented with a strain gage balance and the pressure model was instrumented with pressure transducers, Scanivalves, etc. Both models were 1/15 scale models of the Scout 133R vehicle (Figure 1).

2.1.2.1 Force Test

The model was mounted on a sting using a six component internal strain gage balance. This balance was used to measure total forces and moments acting on the model, and fin number one was instrumented to measure normal force, pitch plane moment, and root bending moments acting on the fin in the presence of the body. Fin tip controls of fins 1 and 3 were movable and were deflected at various angles during the test.

In order to present some means of determining data accuracies, static accuracies of the VB-13 six component balance are presented. The tabulated accuracies were obtained by computing a root mean square devia-tion between applied and measured loads over the maximum load range and ratioed to the maximum balance design limits. Results in the pitch plane are as follows:

Normal force	0.09%
Pitching moment	0.50%

This means that the best possible accuracy of normal force and pitching moments are 0.09% and 0.50% respectively of the balance maximum load limits (1500 lb. normal force and 2400 in lb. pitching moment). Or, in coefficient form $C_N = \pm .023$, $C_m = \pm .10$. These values apply for static loads; therefore, the test (or dynamic) loads are probably not as accurate. The fin balance data accuracy was estimated to be $\pm 3\%$ for normal force, or $C_N = \pm .0412$, and Mach number accuracy was $\pm 0.50\%$.

The 133R vehicle included a nose boom which is not standard for the Scout configuration; therefore, the model included a removable boom in aligned and inclined (3°) positions. Also included were the standard

3

wiring tunnels, protuberances, etc. The various configurations tested included combinations of body, fins, protuberances, and nose boom, as shown in Table I. Detailed dimensions of the Scout vehicle may be found in reference 1.

2.1.2.2 Pressure Test

The pressure model was sting mounted without the use of a strain gage balance. Removable nose booms in the aligned and 3° inclined positions were included, with the standard wiring tunnels, protuberances, etc., and the fins were attached during all data runs.

The model was instrumented to provide body circumferential and longitudinal pressure distributions. Circumferentially arranged pressure orifices were located at 38 longitudinal stations, with most stations located along the forward section of the model. Station number one had 4 pressure orifices, stations 9, 20-25, and 30 had 16 orifices each, and the remaining stations had 8 orifices each, totaling 364 taps. Model pressure orifice locations are presented in Table II and Figure 1. Pressure data sampling was accomplished using an eight-head Scanivalve pressure switch mounted aft of the model in the test section. Pressure tubing connected to the model pressure orifices were routed through the model and hollow sting to the Scanivalve. Each Scanivalve head could sample 48 pressures and was instrumented with a pressure transducer. Three pressure calibrations were made on all transducers during the test using a precision manometer. All calibrations checked within $\pm$ 0.5%.

2.1.3 Test Procedures

2.1.3.1 Force Test

The model configuration was tested at Mach numbers of 1.61, 2.01, 2.41, 2.61, and 2.80 and the corresponding test conditions as shown in Table III. A typical data run included taking model weight tares, wind-off zeros, wind on zeros, and data measurements. After flow in the tunnel was established and wind-on zeros were taken, the model was pitched to the maximum negative angle of attack. The model was then pitched to the maximum positive angle of attack at a rate of 2 degrees per second and data were sampled continuously at 10 points per second. The model was returned to zero angle of attack and a wind-on zero measurement was taken again. The test was conducted over an angle of attack range of -5° to $+4^{\circ}$. The measured data were digitized and recorded on magnetic tape. At the end of each run the data were transferred from tape to punched cards for reduction to proper units on a computer. Static force and moment data were reduced to obtain non-dimensional force and moment coefficients.

4

The model was tested both upright and inverted to determine angularity of the tunnel flow, and incremental angle of attack corrections were then applied to the data. This procedure was followed for all configurations and Mach numbers. At the conclusion of the test, the M = 1.61 data were ruled invalid because of a reflected bow shock that was acting on the aft end of the model.

2.1.3.2 Pressure Test

The test was conducted for four model configurations, as defined in Table I, at Mach numbers of 1.61, 2.01, 2.41, 2.61, 2.80. (The M = 1.61 data are questionable because of the reflected bow shock impingment on the body.) The configurations were chosen to yield the effects of wiring tunnels, protuberances, and nose boom on the pressure distributions. The run schedule and test conditions are defined in Table IV. Each run began by obtaining data at zero angle of attack, then pitching to other angles of attack (tested α increments between -4° and $+4^{\circ}$) and taking measurements. Several pressures were monitored to make sure the free-stream conditions had stabilized before taking data, then data were sampled at 20 times per second until readings were obtained from all static taps. The data were digitized and recorded on magnetic tape, then at the conclusion of a run the data were transferred to computer cards for processing to tabulated output in coefficient (C_p) form. On-line oscillograph traces were also monitored to insure that the Scanivalves and pressure transducers were functioning properly. The data were corrected for tunnel flow angularity in the same manner as the force test (i.e., angle of attack correction).

2.2   DATA REDUCTION AND ANALYSIS

2.2.1 .   Force Test Data

The primary purpose of this study was to establish vehicle longitudinal aerodynamic data by correlation of force test measurements and the corresponding values obtained by integration of pressure distributions. Therefore, the following force test data are omitted from this report: side force, yawing moment, rolling moment, axial force, fin pitch plane moments, and fin root bending moment.

The aerodynamic coefficients obtained during the force test were presented in tabulated and machine-plotted formats as a function of angle of attack for the various Mach numbers and configurations. To obtain the vehicle derivatives C_{N_α} and C_{m_α} the slopes were read from the plotted curves between the angles of attack $\pm 2^{\circ}$. The accuracy was checked by handplotting some cases from the tabulated data, sloping the

curves, and comparing the derivatives to those obtained from the original plots. Values of C_{N_o} and C_{m_o} were also obtained from the machine-plotted curves and checked using tabulated data. The fin aerodynamic characteristics, $C_{N_\alpha FIN}$ and $C_{N_o FIN}$ were also taken from machine-plotted curves. To obtain fin effectiveness parameters, C_{N_δ} and C_{m_δ}, the main model internal balance data were used. These parameters were calculated at all angles of attack, but effectiveness was found to vary little with α, so the only values presented are those at $\alpha = 0^o$. The results are discussed in Section 2.3.

2.2.2   Pressure Test Data

A computer program was developed to analyze pressure data from the wind tunnel test. Generally, this involved examination of the data, circumferential integration of pressure coefficients at each body station to obtain local loading, and integration of local loading over the length of the body to determine aerodynamic derivatives. Test data consisting of pressure coefficients, pressure tap identification, free stream Mach number, and angles of attack were transferred to punch cards preparatory to the plotting and integration tasks described below.

For a given configuration, Mach number (M), and angle of attack (α), local pressure coefficients (Cp) at each station were machine-plotted as a function of tap angular location (ϕ). The plotted data were reviewed and erroneous data points corrected. Questionable points were first checked for keypunch accuracy and, if correctly punched, obvious erroneous points were extracted and replaced with interpolated pressure coefficients.

To facilitate integration of the corrected pressure data, it was necessary to estimate supplemental Cp values for angular limits not defined by pressure taps, i.e., for $\phi = 0^o$ and 180° (or 360° where the taps encircled the body). The additional values were established by merely repeating the C_p of the ϕ nearest the appropriate limit. This approach was selected over a linear extrapolation technique which calculated a supplemental C_p from the two data points nearest the angular limit. Comparison of results obtained by the two methods showed minor differences except where the calculations involved sudden pressure changes in the vicinity of protuberances. For these situations, examination of the plotted data indicated the repeated-point result would generally give the better approximation to the actual (unknown) value.

6

The first integration produced local normal force coefficients according to the equation

$$c_N S = \frac{dC_N}{dX} S = r_{local} \int_0^{360} C_p \cos\phi \, d\phi \qquad (1)$$

where S = reference area, $\dfrac{dC_N}{dX}$ = rate of change of normal force coefficient

along the body axis, c_N = local normal force coefficient, and r_{local} = local body radius. It was assumed that the local radius did not vary with ϕ, i.e., the small cross-sectional area of the wiring tunnels and protuberances is neglected in this integration because the major effect of these items is felt through the pressure distribution on the main body. Incremental normal forces due to the protuberances and tunnels were calculated separately using a Second Order Shock Expansion technique (Reference 2). Basically this involved definition of the local Mach numbers in the vicinity of the wiring tunnels, etc., then analysis of the wiring tunnel as one half a body of revolution. These increments were found to be very small compared to the total local normal forces. A trapezoidal integration scheme was selected to perform the local integrations when it was found the irregularly-spaced intervals between tap angular positions made a more sophisticated algorithm impractical. Local force coefficients were computed at each α of a given configuration and M.

Eq. (1) is based on pressure taps lying in the range $0° < \phi < 360°$, but tap arrangements permit a 360° integration only at model axial stations 3, 20-25, and 30 (see Figure 1). All other stations have taps in the range $0° < \phi < 180°$, which suggests doubling the integral (evaluated from $\phi = 0°$ to 180°) to determine the remaining $c_N S$ values. A factor of two was applied to all cross-sections with (1) $0° < \phi < 180°$ and (2) symmetry with respect to a vertical plane through the model centerline. Not included in this calculation were Stations 18, 19, 26, and 27 when the wiring tunnels were in place (Figure 1). The presence of the tunnels violates the symmetry criterion at Stations 19 and 26 while sufficiently affecting Stations 18 and 27 to remove them from symmetry considerations also. The integration by Equation (1) at the excluded stations was evaluated only between $\phi = 0°$ and 180°. Normal force loading for the full circumference is provided by special treatment as described below.

Variation of $c_N S$ with angle of attack was defined by a least-squares polynomial curve-fit (LSPCF) subroutine which determined the local normal force coefficient ($c_{N_o} S$) and slope ($c_{N_\alpha} S$) at $\alpha = 0°$. A first-order, linear curve-fit was used for data over the range of $-2° < \alpha < +2°$. A linear variation over this range is consistent with the general behavior

of the integrated pressure data as well as the technique used to determine slopes with the force data. A fifth-order polynomial curve-fit through all the data points $(-4° \leqslant \alpha \leqslant +4°)$ was also investigated, but the resulting intercepts and slopes did not appear representative of the input data.

The LSPCF process was applied directly to all local normal force coefficients with the exception of those at the asymmetric stations 18, 19, 26, and 27. For each of these stations $c_{N_o}S$ and $c_{N_\alpha}S$ were calculated as follows:

(i) Normal force coefficients for the tapped half-body $(0° \leqslant \phi \leqslant 180°)$ were curve-fitted to a first order polynomial.

(ii) Normal force data points were reflected with respect to the $c_N S$ and α axes.

(iii) The reflected data points were curve-fitted.

(iv) The polynomial coefficients from (i) and (iii) were added to get a $c_{N_o}S$ and $c_{N_\alpha}S$ for the full body circumference.

The mirror symmetry used in this analysis is evident in the model sketch shown in Figure (1).

Total vehicle coefficients were obtained by integrating $c_{N_o}S$ and $c_{N_\alpha}S$ along the body axis according to

$$C_{N_o}S = \int_0^{X_1} (c_{N_o}S) \, dX \qquad (2)$$

and

$$C_{N_\alpha}S = \int_0^{X_1} (c_{N_\alpha}S) \, dX \qquad (3)$$

where $X = 0$ is the spherical nose tip and $X = X_1$ is the total body length. The values of $c_{N_o}S$ and $c_{N_\alpha}S$ at the upper and lower limits were set equal to zero, and linear variation of loading with X was assumed between pressure measurement stations. Comparisons with previous Scout load distributions (reference 1) indicate the assumption is a reasonable one. The total vehicle center of pressure location, X_{cp} was calculated as follows:

8

$$X_{cp} = \frac{\int_o^{X_1} (c_{N_\alpha} S)(X) \ dX}{C_{N_\alpha} S} \qquad (4)$$

and the corresponding pitching moment derivative by the equation:

$$C_{m_\alpha} = \frac{C_{N_\alpha} S (X_{ref} - X_{cp})}{S \ d_{ref.}} \qquad (5)$$

where: X_{ref} = longitudinal station of the moment reference center

2.3   RESULTS

2.3.1   Force Test Aerodynamic Parameters

The aerodynamic derivatives C_{N_α} and C_{m_α} are presented in Figures 2 and 3 respectively for all configuration, as a function of Mach number. The M = 1.61 data are not included because of the reflected bow shock problem discussed in Section 2.1.3. In analysis of the model build-up it can be seen that addition of the fins approximately doubles the magnitude of C_{N_α} and results in a stabilizing moment about the reference center of Station 427.8. The effects of adding the aligned nose boom resulted in increased C_{N_α} and a destabilizing moment. Adding protuberances and wiring tunnels results in a positive increment to C_{N_α} and negligible effects on C_{m_α}. The effects of an inclined nose boom (3°) were very small and inconsistent. At some Mach numbers the incremental C_{N_α} was positive, resulting in destabilizing moments, and at other Mach numbers the contributions were reversed. This phenomenon is discussed in the Section 2.3.2, but basically it appears to be a result of flow separation on the boom and the corresponding effects on the vehicle nose.

The coefficients C_{N_o} and C_{m_o} are presented in Figure 4. The magnitudes of C_{N_o} are relatively small for all configurations, but the corresponding C_{m_o} values are rather large for some configurations. The measurement inaccuracies discussed in Section 2.1.2 must be considered in drawing conclusions from these data.

Incremental C_{m_o} values for the various configurations may be explained by the rationalizations described below. The configuration with fins on, but protuberances and boom removed resulted in large negative C_{m_o}'s, possibly due to fin misalignment of positive incidence or flow angularity in the tunnel. When the nose boom was added at zero inclination, the incremental change in C_{m_o} generally resulted in small positive changes. This may be due to a small boom misalignment or tunnel flow angularity. Adding the protuberances and wiring tunnels resulted in large positive increments. It is assumed that this is due to increased pressures on the upper surface of the body (at the aft end) and fins, caused by the launch fitting fairing near the vehicle base. This is consistent with previous analyses of C_{m_o} and values shown in Reference 1. When the boom is deflected to a 3° positive inclination, the incremental C_{m_o} is positive, as expected. Next, the fins were removed and this resulted in small positive increments. This tends to substantiate the belief that the fins may have had a positive incidence misalignment, and it also indicates that the positive C_{m_o} caused by the launch fitting fairing is attributed more to high pressures acting on the body than on the fins.

Fin C_{N_α} and C_{N_0} are presented in Figure 5. $C_{N_{\alpha \text{ FINS}}}$ was determined from the main model balance ($C_{N_\alpha \text{ FINS}} = C_{N_\alpha \text{ FINS ON}} - C_{N_\alpha \text{FINS}}$ OFF) and fin internal balance. Both sets of data are presented, and differences between the two are attributed to fin carryover load on the body, which is not included in the fin balance measurements.

Control effectiveness parameters C_{N_δ} and C_{m_δ} are presented in Figure 6. The incremental normal force coefficients for 2 fin tips deflected were obtained from the vehicle balance. The increment was also measured by the fin internal balance, and the value doubled for comparison to the vehicle balance measurements.

Fin internal balance measurements of normal force coefficient are also presented in Figure 7 for tip deflections of 0° and angles of attack of -5°, 0°, $+1^o$, and $+5^o$ for the model configuration including protuberances, fins, and the aligned nose boom.

2.3.2   Normal Load Distributions

Normal load distributions on the body are presented in Figures 8 through 23 for the various configurations and Mach numbers. (Note

10

scale changes on parts b and c of each figure.) These were established from th~~ pressure data using the integration technique described in Section 2.2.2.

Clean body distributions (boom and protuberances off) are shown in Figures 8 through 11, with the exception of M = 1.61, which was deleted because of wind tunnel data reduction errors. The effects of adding protuberances and wiring tunnels may be seen by comparing these to the load distributions of Figures 12 through 15. The effects of protuberances are very localized in the vicinity of the protuberances, and wiring tunnels simply result in small changes in magnitude of $c_{N_\alpha} S$

along the body.

Load distributions for the configuration including protuberances, wiring tunnels and the nose boom (aligned at 0°) are presented in Figures 16 through 19. Effects of the nose boom are confined to the heatshield. $c_{N_\alpha} S$ is increased substantially at the nose tip, but loadings along the

heatshield are reduced. It is believed that flow separation on the nose boom is the major contributing factor to this unusual loading. Two load distributions are shown for this configuration, representing basic data obtained during the tests and additional data from repeat runs. (M = 2.80 repeatability data was invalid because of a data reduction error.) Trends of the two sets of data are in agreement and the only significant differences are in magnitudes of the M = 2.01 data.

Normal load distributions with the nose-boom inclined at 3° from the body centerline are shown in Figures 20 through 23. The only significant effect is seen near the nose tip, where the loading is decreased. This effect is present because the 3° incline and the corresponding flow separation results in a higher effective angle of attack of the nose tip. The curve c_N vs. α at the station near the nose tip is linear between $\pm 2^\circ$ and begins to level off above 2°; therefore, the value of c_{N_α} is decreased because the effective α is greater than 2°.

2.3.3   Pressure Test Aerodynamic Parameters

Aerodynamic coefficients were obtained from pressure test data by utilizing the integration technique described in Section 2.2.2. The parameters include C_{N_α}, C_{m_α}, and C_{N_0} of the body, excluding fins.

C_{N_α} and C_{m_α} are presented in Figures 24 and 25 as a function of Mach number for the four configurations tested. The M = 2.61 data for the clean configuration, and the M = 2.80 repeat run for the complete

configuration were eliminated because of data reduction errors. Effects of adding the nose boom protuberances, and wiring tunnels are very inconclusive as there are no definite patterns established. Erratic variation with Mach number is believed to be caused by flow separation on the nose boom. Separation varies with Mach number. Therefore, the resulting radial pressure distributions differ accordingly.

Normal force at zero angle of attack, C_N, is presented in Figure 26. The incremental force due to protuberances is positive and the increment due to the nose boom is negative. The trends of nose boom increment are questionable based on the small magnitudes of the coefficients and flow separation on the boom.

2.3.4   Correlation of Aerodynamic Data

Correlation of the aerodynamic parameters obtained from force test data and integrated pressure test data are presented in Figures 27 through 29 for the body alone. The measured C_{N_α}, C_{m_α}, and C_{N_o} from the force test are presented for the configuration including protuberances and wiring tunnels and nose boom aligned at 0°, with fins removed. These data are compared to the integrated pressure data for the configurations including protuberances and wiring tunnels, nose boom aligned at 0°, and fins. (Note: Pressure integrations were over the body only. Therefore, the contribution of fins to the parameters are not included.) Two sets of results are presented from the pressure test, which includes data from the basic wind tunnel runs and hysteresis runs.

Comparison of C_{N_α} is shown in Figure 27, and indicates agreement within about 15%, with the exception of one point at M = 2.01. Differences in C_{m_α} (Figure 28) are much larger, probably because C_{m_α} obtained by integration of pressure distributions is very sensitive to local load distribution on the heatshield and the aft end of the body. It would be possible to obtain agreement with the force data by adjusting the load distributions a small percentage. Therefore, the force test data should be used in defining the aerodynamic derivatives. Comparison of the two sets of data for C_{N_o} are presented in Figure 29.

Another consideration for differences between the force data and integrated pressure data involves the flow angularity that existed in the tunnel during both tests. Corrections for the flow angularity essentially involved shifting the angle of attack scale an amount determined by rerunning the force model in the upright and inverted positions. However,

the local angle of attack along the model from nose to base may have been exposed to varying degrees of flow angularity. Therefore, the local pressures and corresponding aerodynamic parameters may reflect a small degree of error. This would particularly be the case for C_{N_o}.

3.0 CONCLUSIONS AND RECOMMENDATIONS

Running load distributions, normal force, and pitching moment coefficients were determined through an angle of attack range at various supersonic Mach numbers from both force and pressure measurements on a scale model of Scout 133R. Effects of the nose boom, wiring tunnels, and other protuberances were determined. The nose boom appears to destabilize the configuration slightly, but differences in forces and moments due to the wiring tunnels and other protuberances were less than the repeatability of the measurements.

Running load distributions defined from the pressure measurements were substantiated by comparison with the total normal force coefficient determined from force measurements. However, small adjustments to the running load distributions are required to obtain good agreement with pitching moment coefficients from the force test. It is recommended that the adjustments be made and the running load distribution be refined to conformance with measurements from the force test.

Predicted aerodynamic characteristics (Reference 3) were used in a previous load analysis of the flight vehicle (Reference 4), and did not include data for all flow conditions obtained in the present study. The experimental data presented herein should be compared to the predicted data and another loads analysis conducted utilizing the experimental data. This would serve to increase the confidence level in the validity of the technique for predicting flexible body loads and bending moments.

REFERENCES

1. Muir, T. G., "Scout Aerodynamic Design Data Report", LTV Report No. 23.390, Revision A, January, 1971.

2. Damstrom, E. K., "'Local Flow Conditions and Aerodynamic Parameters by a Second-Order Shock Expansion Method Applicable to Bodies of Revolution Near Zero Lift and at Supersonic Speeds, " LTV Report No. 00.83, September, 1962.

3. Poucher, D. E., "Aerodynamic Design Data Report", LTV Report No. AST/E1R-12431, February, 1961.

4. Kreiter, G. W., "Comparison of Calculated and Measured Flight Loads for Scout Vehicle S-133R", LTV Report No. 00.853, September, 1966.

14

TABLE I — MODEL CONFIGURATIONS

FORCE TEST

Nose Boom	Protuberances	Fins
OFF	OFF	ON
ON^o	ON	OFF
ON^o	ON	ON
ON^3	ON	ON
ON^o	OFF	ON

PRESSURE TEST

Nose Boom	Protuberances	Fins
OFF	OFF	ON
ON^o	ON	ON
ON^3	ON	ON
OFF	ON	ON

15

TABLE II.- PRESSURE ORIFICE LOCATIONS

ϕ_{tap} (looking fwd.)
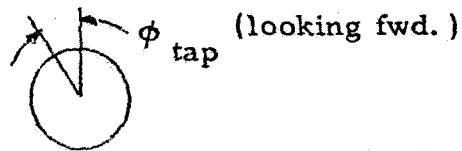
ϕ_{tap}, Deg	Station Number				
	1	2-8 / 10-19	9	20-25 / 30	26-29 / 31-38
7.2		✓	✓	✓	✓
22.	✓	↓	↓	↓	↓
38.7		↓	↓		
45.				✓	✓
61.	✓	✓	✓		
65.				✓	✓
115.				↓	↓
119.	✓	✓	✓		
135.				✓	✓
141.3		✓	✓		
158.	✓	↓		✓	✓
172.8		↓			↓
187.2			↓		
202.				↓	
218.7			↓		
225.				✓	
241.			✓		
245.				✓	
295.				↓	
299.			✓		
315.				✓	
321.3			✓		
338.			↓	✓	
352.8			↓	↓	

16

TABLE III - FORCE TEST RUN SCHEDULE

Run No.	Configuration B	P	F	Mach No.	q PSF	α Range Deg's	δ_1	δ_2	δ_3	δ_4	Comments
1	on°	on	on	1.61	--	-5/5	0°	0°	0°	0°	Void
2	on°	on	on	2.01	2588	"	"	"	"	"	
3	on³	on	on	"	2586	"	"	"	"	"	
4	on°	on	on	"	1270	"	"	"	"	"	
5	on°	on	on	"	2597	"	5°	0°	5°	0°	
6	on°	on	on	"	2584	"	15°	0°	15°	0°	
7	on°	on	on	1.61	2462	"	15°	0°	15°	0°	
8	on°	on	on	"	2451	"	5°	0°	50	0°	
9	on°	on	on	"	2465	"	0°	0°	0°	0°	{Repeat of Run 1
10	on°	on	on	"	2480	0/-4/4/0	"	"	"	"	Hysteresis
11	on³	on	on	"	2472	-5/5	"	"	"	"	
12	off	on	on	"	2471	"	"	"	"	"	
13	on°	on	on	2.41	2606	"	"	"	"	"	
14	on°	on	on	"	2602	"	5°	0°	5°	0°	
15	on°	on	on	"	2590	"	15°	0°	15°	0°	
16	on°	on	on	"	1319	"	0°	0°	0°	0°	
17	on³	on	on	"	2597	"	"	"	"	"	
18	on³	on	on	2.61	2673	"	"	"	"	"	
19	on°	on	on	"	2667	"	"	"	"	"	
20	on°	on	on	"	1433	"	"	"	"	"	
21	on°	on	on	"	2658	"	5°	0°	5°	0°	
22	on°	on	on	"	--	"	15°	0°	15°	0°	Void
23	on°	on	on	"	2657	"	15°	0°	15°	0°	{Repeat of Run 22
24	on°	on	on	2.80	2664	-5/5	15°	0°	15°	0°	

TABLE III -FORCE TEST RUN SCHEDULE (Concluded)

Run No.	Configuration B	P	F	Mach No.	q PSF	α Range Deg's	δ_1	δ_2	δ_3	δ_4	Comments
25	on°	on	on	2.80	2655	-5/5	5°	0°	5°	0°	
26	on°	on	on	"	2664	"	0°	0°	0°	0°	
27	on°	on	on	"	--	-5/5/-5	"	"	"	"	Void
28	on°	on	on	"	--	"	"	"	"	"	Void
29	on³	on	on	"	2642	-5/5	"	"	"	"	
30	on°	on	on	"	3678	-5/5-5	"	"	"	"	Repeat of Runs 27, 28
31	off	on	on	"	2640	-5/5	"	"	"	"	
32	off	on	on	"	2641	$\alpha = 4$ $\psi = 5/-5$	"	"	"	"	Yaw run
33	off	off	on	"	2648	-5/5	"	"	"	"	
34	on°	off	on	"	2647	"	"	"	"	"	
35	on°	off	on	2.61	2649	"	"	"	"	"	
36	off	off	on	"	2650	"	"	"	"	"	
37	off	off	on	2.41	2588	"	"	"	"	"	
38	on°	off	on	"	2596	"	"	"	"	"	
39	on°	off	on	2.01	2565	"	"	"	"	"	
40	off	off	on	"	2560	"	"	"	"	"	
41	off	off	on	1.61	2437	"	"	"	"	"	
42	on°	off	on	"	2436	"	"	"	"	"	
43	on°	on	off	"	2431	"	off	off	off	off	
44	on°	on	off	2.01	2579	"	"	"	"	"	
45	on°	on	off	2.41	2595	-5/5	off	off	off	off	
46	on°	on	off	2.61	2655	"	"	"	"	"	
47	on°	on	off	2.80	2659	"	"	"	"	"	

TABLE IV - PRESSURE TEST RUN SCHEDULE

Run No.	Configuration			Mach No.	q PSF	α Deg's	Comments
	B	P	F				
1	off	on	on	1.61	--	0, +1, +2, +3, +4	Void: Scanivalve Problems
2	off	on	on	"	--	"	"
3	off	on	on	"	--	"	"
4	off	on	on	"	--	"	"
5	off	on	on	"	--	"	"
6				"	2700	+2, +3	Good Run
7				"	--	+1, +4	{Void: Model Cart Problems
8				"	--	"	"
9				"	2660	"	Good Run
10				"	2700	0, -1	
11				"	2700	-2, -3	
12				"	2678	-3, -4	
13				2.01	--	0, +1	Void: Tunnel Unstart
14				"	2628	0, +1, +2	Good Run
15				"	2629	+3, +4	
16				"	--	-1, -2	{Void: Data System Problem
17				"	2627	"	Good Run
18				"	2620	-3, -4	
19				2.41	2445	0, +1, +2	
20				"	--	+3, +4	Void: Scanivalve Problems
21				"	2438	+4, -1	
22				"	2433	+3, -2, -3	

19

TABLE IV – PRESSURE TEST RUN SCHEDULE (Cont'd.)

Run No.	Configuration B	P	F	Mach No.	q PSF	α Deg's	Comments
23	off	on	on	2.41	2443	-4	
24	off	on	on	2.61	2438	+2, +4	
25	↓	↓	↓	"	2307	+3, +1, 0	
26				"	2306	0, -1, -2	
27				"	2308	-4, -3, -2	
28				2.80	2181	-4, -3, -2	
29				"	2186	-1, +1, +2, 0	
30	↓	↓	↓	"	2195	+4, +3, 0	
31	on°	on	on	"	2183	-4, -3, -2, -1, 0	
32				"	2187	+4, +3, +2, +1	
33				2.61	2296	+4, +3, +2, +1, 0	
34				"	2296	-4, -3, -2, -1, 0	
35				2.41	2420	+4, +3, +2, +1	
36				"	2423	-4, -3, -2	
37				"	2420	-1, 0, +1	
38				2.01	2606	-4, -3, -2	
39				"	2607	-1, 0, +1	
40				"	2597	+2, +3, +4	
41				1.61	2661	-2, -3	
42				"	2667	-1, 0	
43	↓	↓	↓	"	2670	-4, +1	

TABLE IV - PRESSURE TEST RUN SCHEDULE (Cont'd.)

Run No.	Configuration B	P	F	Mach No.	q PSF	α Deg's	Comments
44	on°	on	on	1.61	2698	+2, +3	
45				1.61	2668	+4	
46				"	--	0, +1	{Void: Scanvalve Problem
47				"	2731	0, +1	Hysteresis Run
48				"	2674	+2, +3	"
49				"	2673	+4, +3	"
50				"	--	+2, +1	{Void: Scanvalve Problem
51				"	2678	"	Hysteresis Run
52				"	2683	0, -1	"
53				"	2661	-2, -3	"
54				"	2677	-4, -3	"
55				"	2678	-2, -1, 0	"
56				2.01	1340	+4, +3, +2 +1, 0	
57				"	1340	-4, -3, -2 -1, 0	
58				2.41	--	-4, -3, -2	{Void: Control Problems
59				"	--	--	"
60				"	1366	+4, +3, +2 +1, 0	
61				"	1365	-4, -3, -2 -1, 0	
62	↓	↓	↓	2.61	--	--	{Void: Tunnel Control Problems

TABLE IV - PRESSURE TEST RUN SCHEDULE (Cont'd.)

Run No.	Configuration B	Configuration P	Configuration F	Mach No.	q PSF	α Deg's	Comments
63	on°	on	on	2.61	1336	+4, +3, +2 +1, 0	
64				"	1338	-4, -3, -2	
65				"	1373	-1, 0, +1	
66				2.80	2193	0, +1, +2 +3	Hysteresis Run
67	on°	on	on	2.80	2183	+3, +4, +3, +2	Hysteresis Run
68				"	2216	+1, 0, -1, -2, -3	"
69				"	2198	-3, -2, -1	"
70				"	2217	-4, 0	"
71	on³	on	on	"	--	0, +1, +2 +3	Void: Scanivalve Control Problems
72	on³	on	on	"	2209	"	
73				"	2190	+4, -1, -2 -3	
74				"	2185	-4	
75				2.61	--	0, +1, +2, +3, +4	Void: PO Off
76				"	--	"	Void: Scanivalve Problems
77				"	2328	"	
78				"	2330	-4, -3, -2 -1	
79				2.41	2434	-4, -3	
80				"	2440	-2, -1, 0	

TABLE IV - PRESSURE TEST RUN SCHEDULE (Cont'd.)

Run No.	Configuration			Mach No.	q PSF	α Deg's	Comments
	B	P	F				
81	on[3]	on	on	2.41	2431	+4, +3, +2	
82				"	2432	0, +1	
83				2.01	2620	-4, -3, -2	
84				"	2613	+4	
85				"	2605	+3	
86				"	2588	+2, +1, 0	
87				"	2615	-1, 0	
88				1.61	2665	+4, +3	
89				"	2668	-3	
90				"	--	+2, +1	{ Void: Scanivalve Problems
91				"	2656	"	
92				"	--	0, -1	{ Void: Scanivalve Problems
93				"	2571	"	
94	↓	↓	↓	"	2645	-2, -4	
95	off	off	on	"	2660	+1, +2	
96				"	2658	+3	
97				"	2664	+4	
98				"	2689	0, -1	
99				2.01	2616	+1, +2	
100				"	2632	+3, +4	
101				"	2544	0, -1	
102				2.41	2442	+2, +3, +4	
103				"	2437	-1, 0, +1	
104				2.61	2324	+2, +3	
105	↓	↓	↓	"	2326	+4, +1	

TABLE IV – PRESSURE TEST RUN SCHEDULE (Concluded)

Run No.	Configuration B	P	F	Mach No.	q PSF	α Deg's	Comments
106	off	off	on	2.61	2332	0, -1	
107	↓	↓	↓	2.80	2198	+4, +3, +2 +1, 0	
108	↓	↓	↓	"	2208	-1, 0, -1	
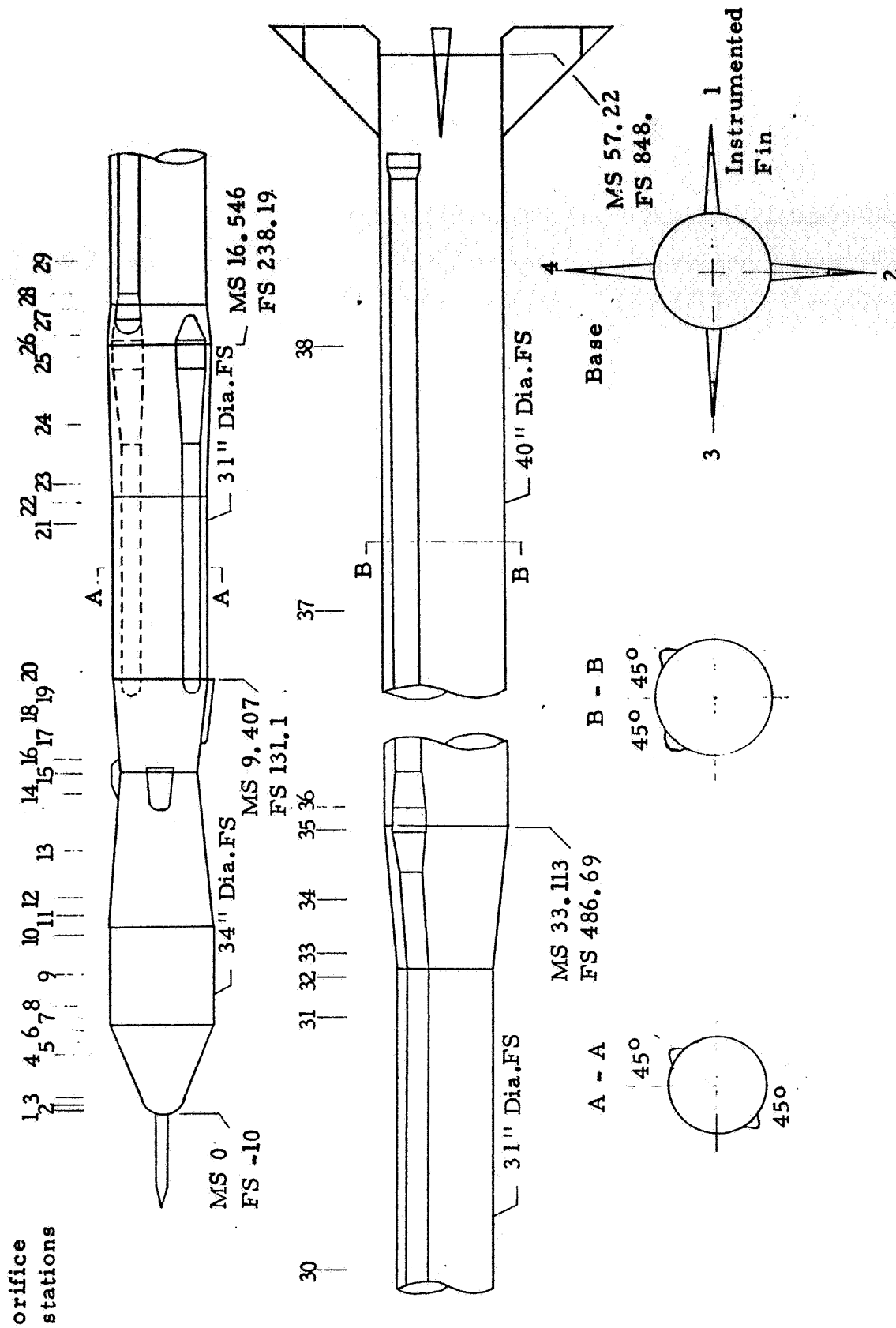
FIGURE 1. - SCOUT 133R WIND TUNNEL MODEL CONFIGURATION

	Boom	Protub.	Fins
O	off	off	on
□	on, 0	on	off
▽	on, 0	on	on
△	on, 3°	on	on
⊖	on, 0	off	on
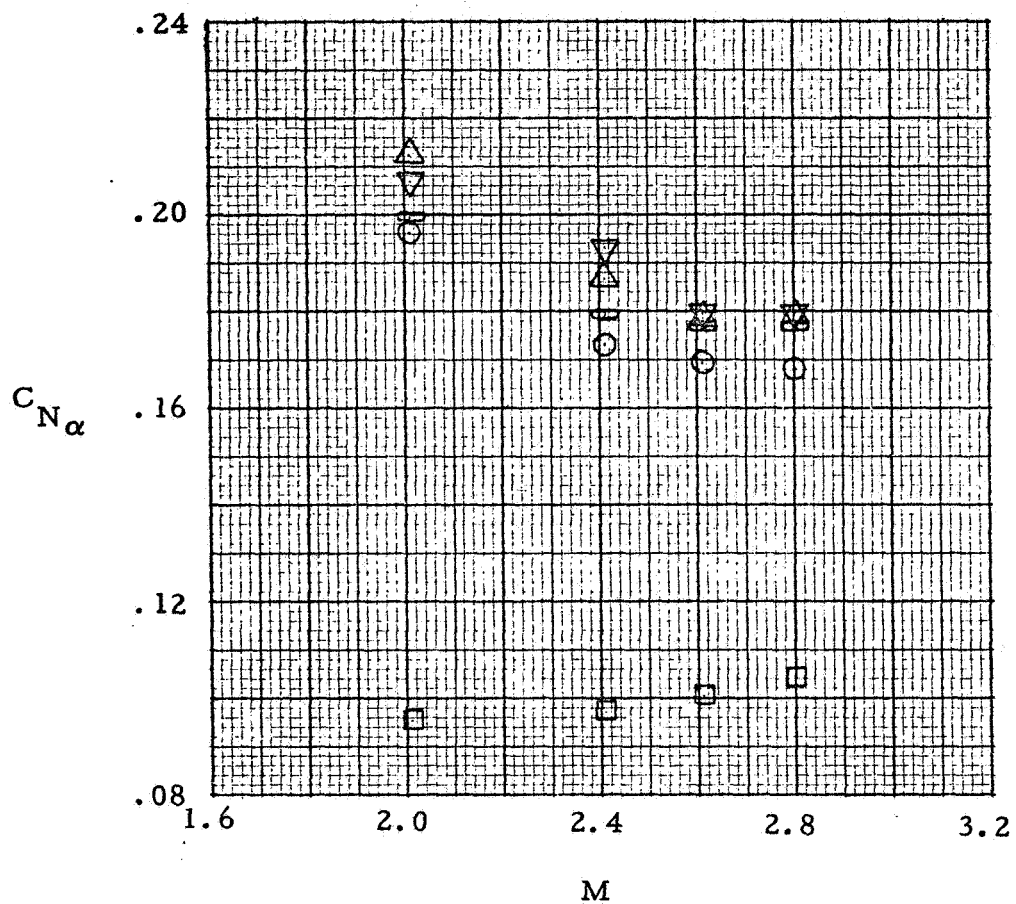
Figure 2 – Vehicle Normal Force Coefficient Derivative. (Force Test Data)

	Boom	Protub.	Fins
○	off	off	on
□	on, 0	on	off
▽	on, 0	on	on
△	on, 3°	on	on
⊖	on, 0	off	on

C_{m_α}
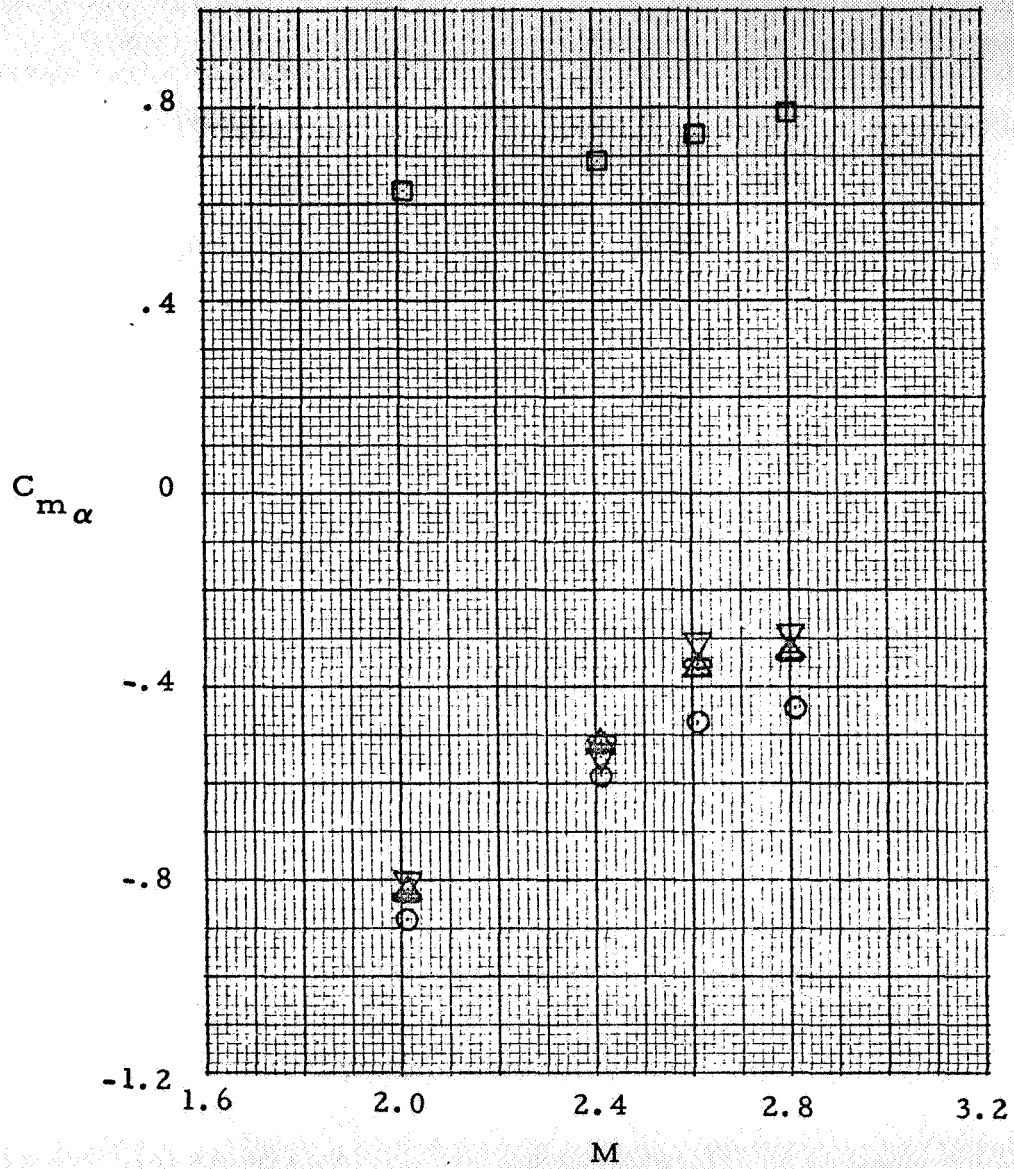
Figure 3 - Vehicle Pitching Moment Coefficient Derivative. (Force Test Data)

27
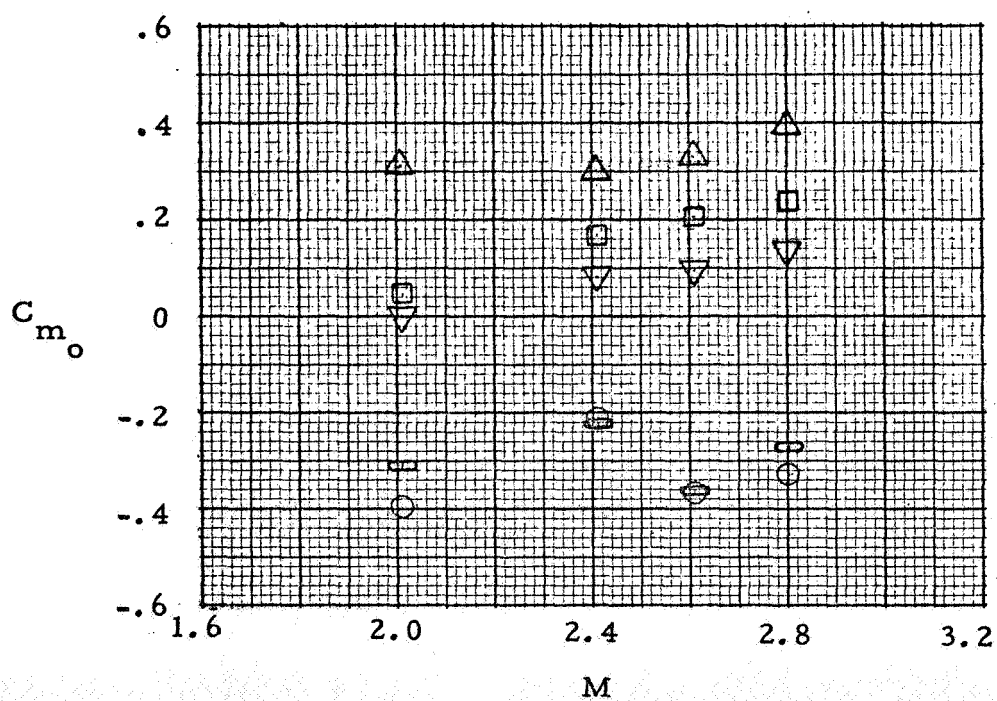
Figure 4 – Vehicle Normal Force and Pitching Moment Coefficients at $\alpha = 0$. (Force Test Data)

O fin balance (doubled)
□ vehicle balance

Note: Values do not vary
with configurations tested.

C_{N_α} FINS

.14

.10

.06

1.6   2.0   2.4   2.8   3.2

M

	Boom	Protub.	Fins
O	off	off	on
▽	on, 0	on	on
△	on, 3°	on	on
⊃	on, 0	off	on

$C_{N_{o_{FIN}}}$

.05

0

-.05

1.6   2.0   2.4   2.8   3.2

M
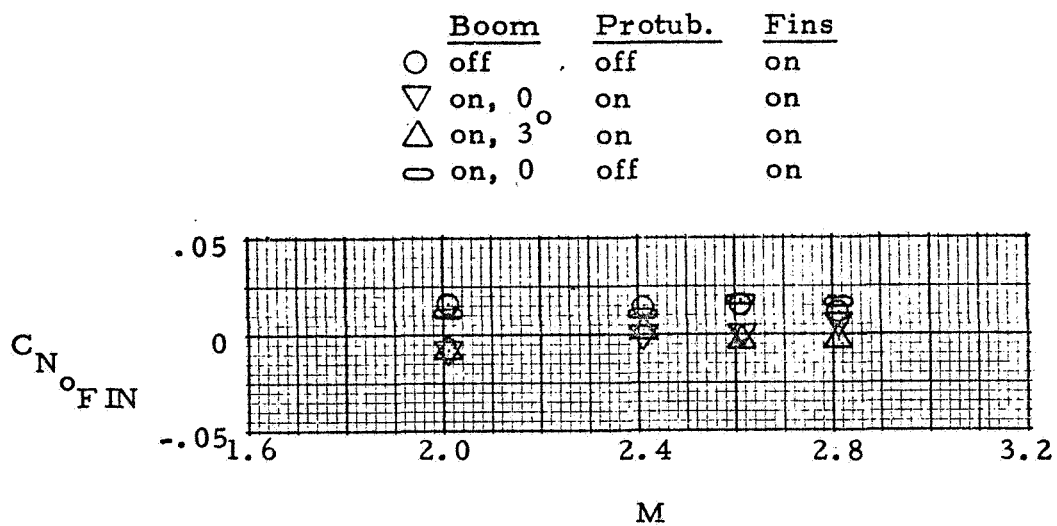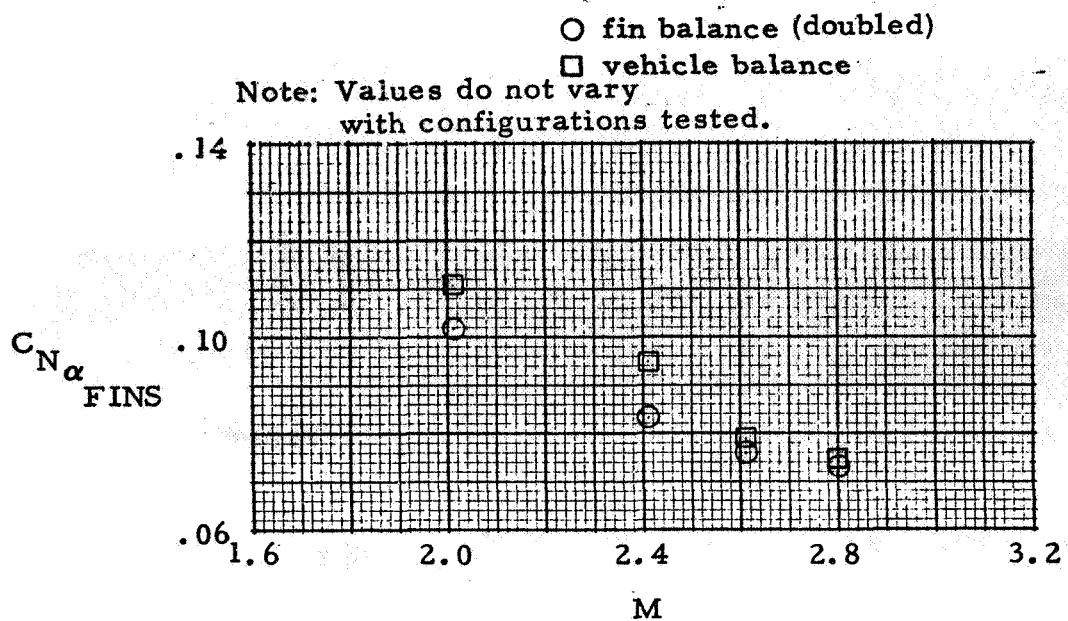
Notes: 1. Data obtained
from fin balance

2. $\delta_{FIN} = 0°$

Figure 5   — Fin Normal Force Coefficient Derivative and
Normal Force Coefficient at $\alpha = 0$.
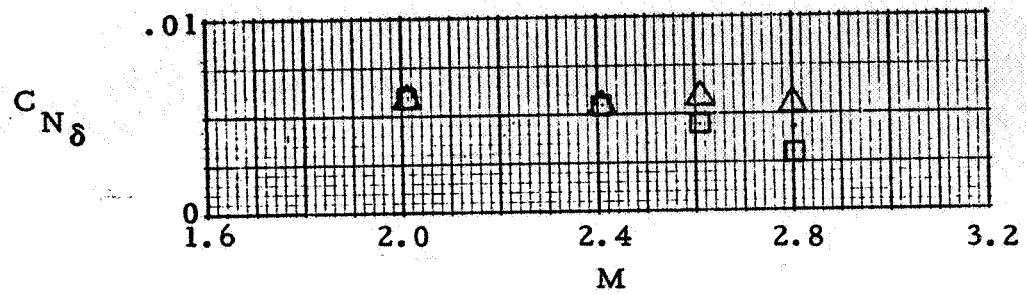
□ fin balance (doubled)
△ vehicle balance (2 surfaces deflected)
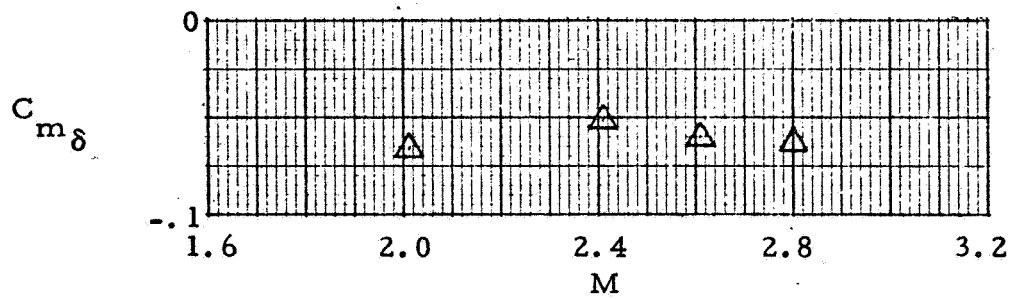
Figure 6 - Longitudinal Control Effectiveness.
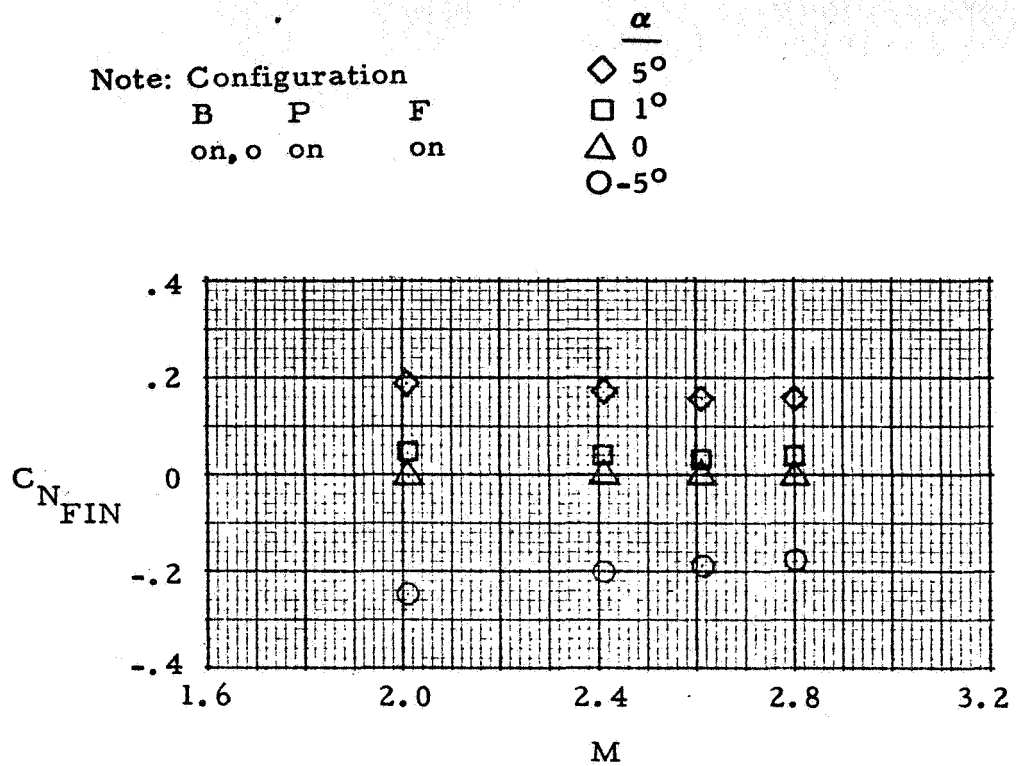
Figure 7 – Fin Normal Force Coefficient, $\delta = 0$.

31
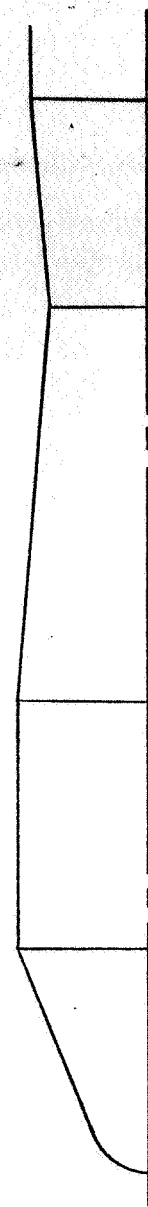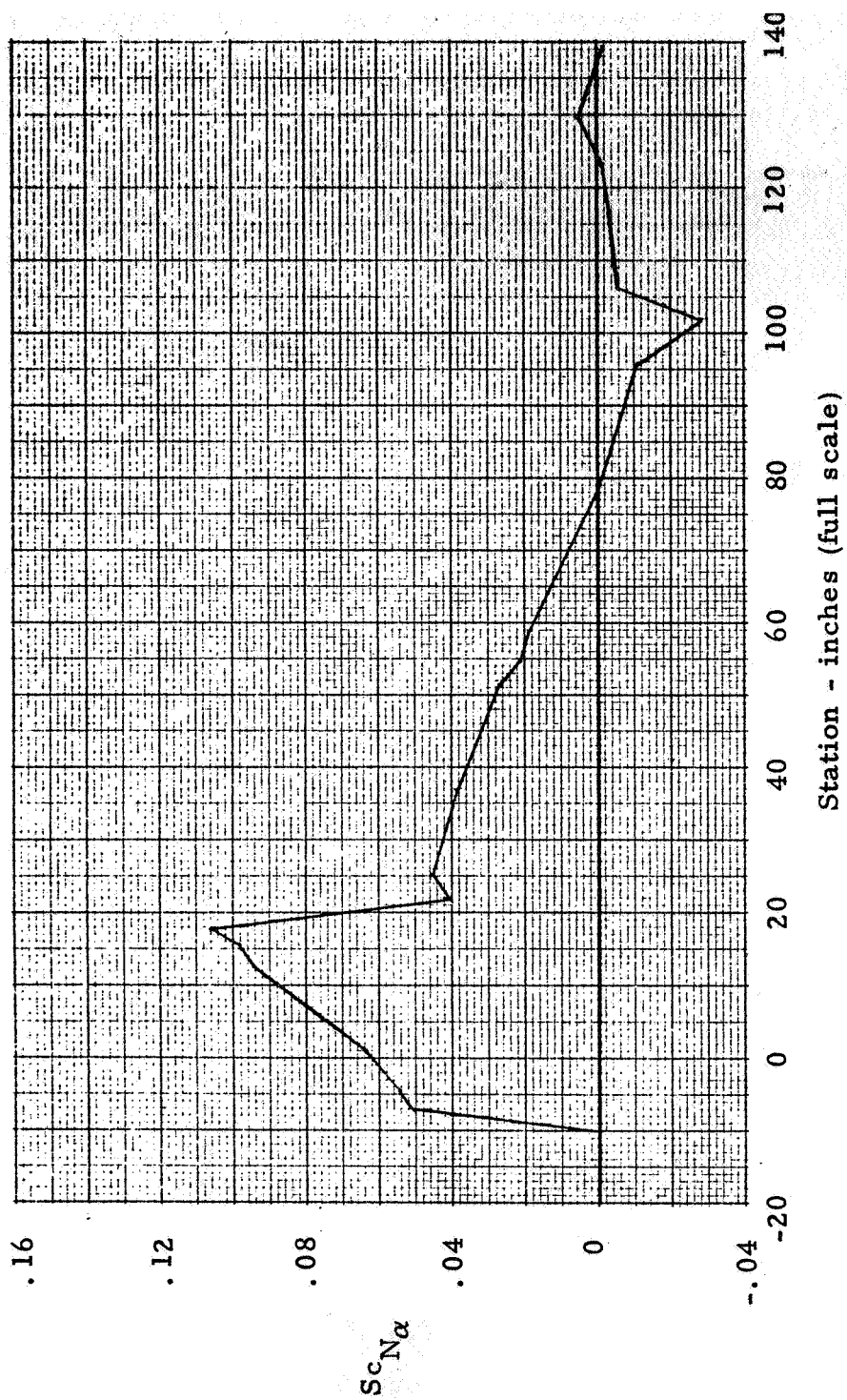
(a) Station -20 to 139.47.

Figure 8. - Normal Load Distribution, $B_{off} P_{off} F_{on}$, M = 2.01.

Station - inches (full scale)

$Sc_{N_{\alpha}}$
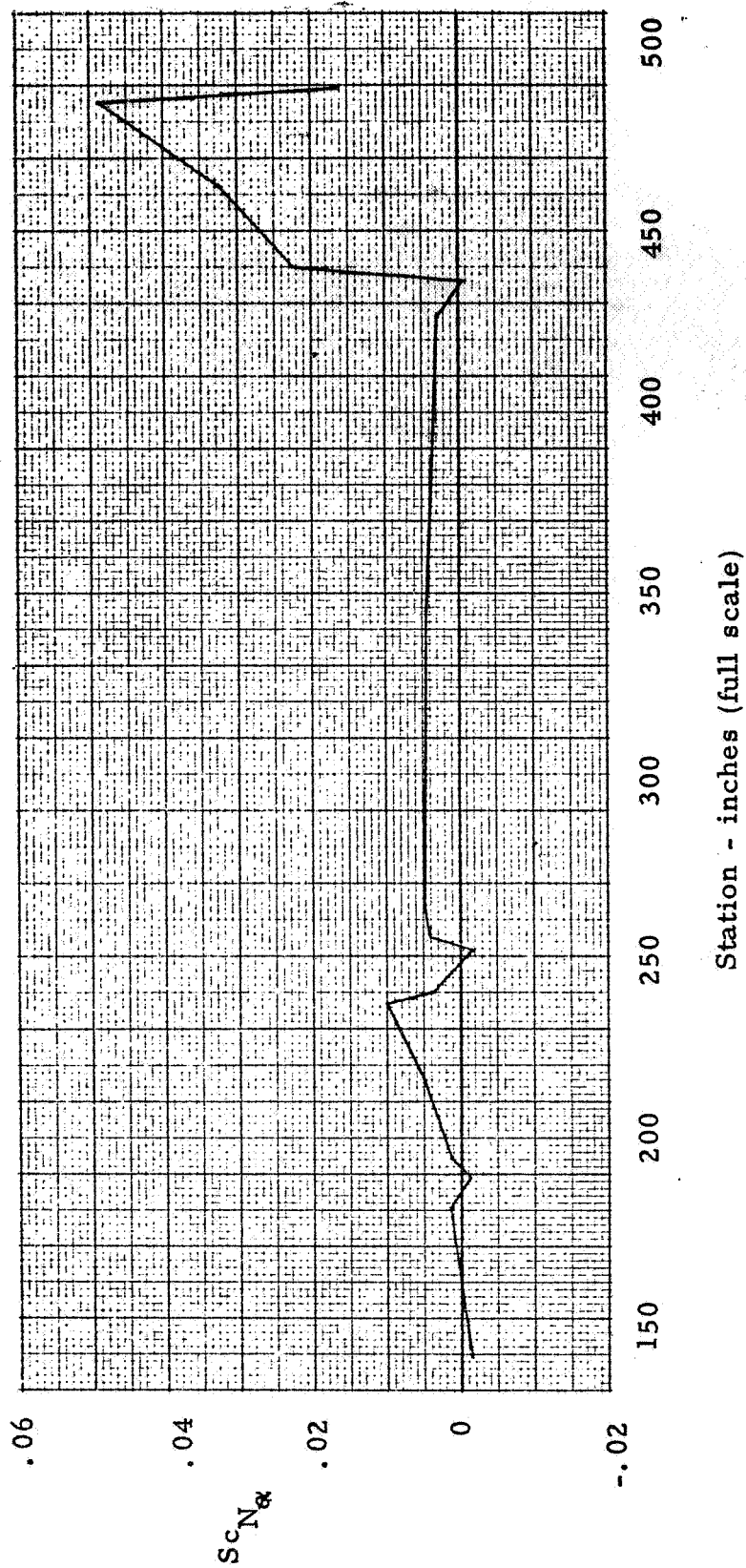
(b) Stations 139.47 to 489.39.

Figure 8 . - Continued.
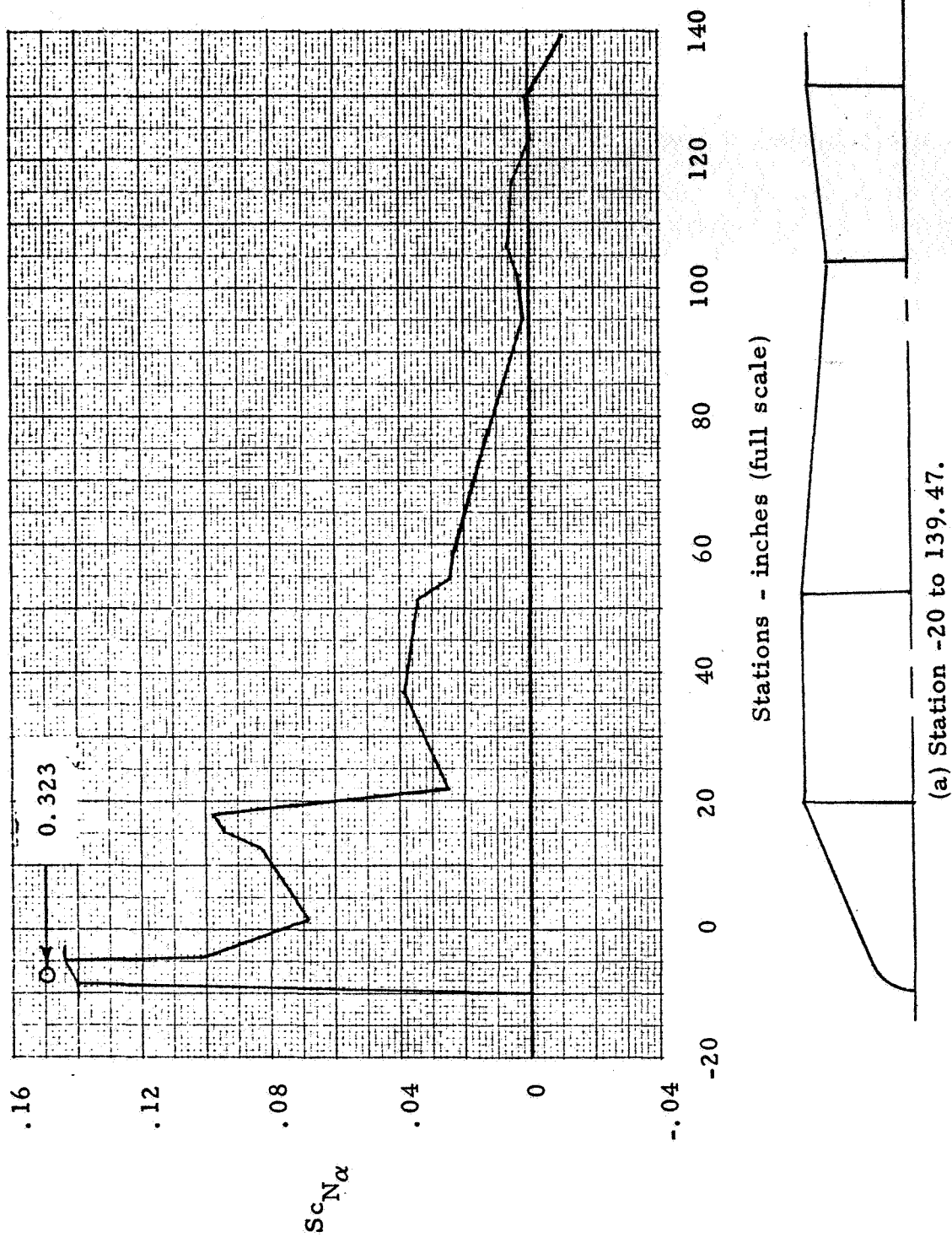
33
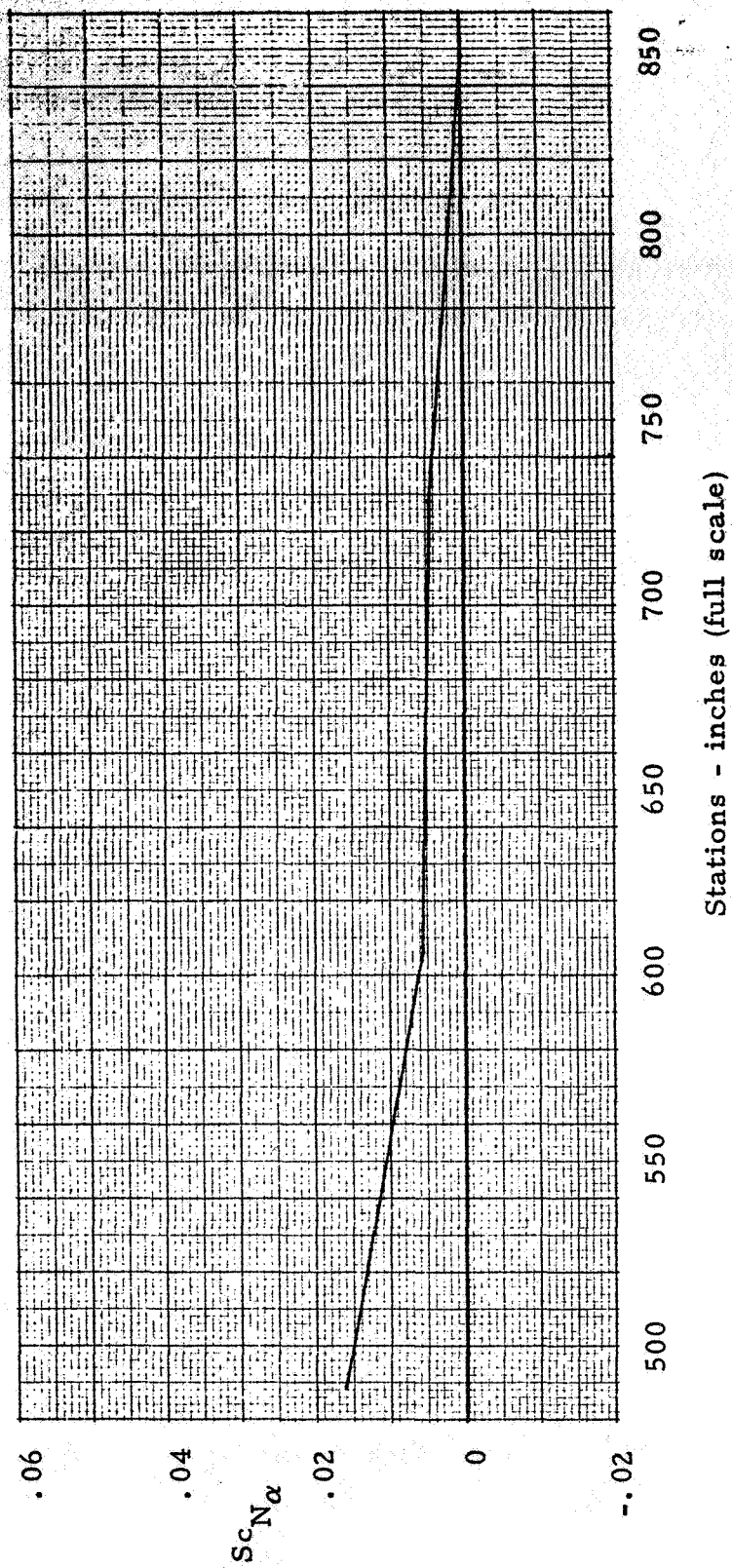
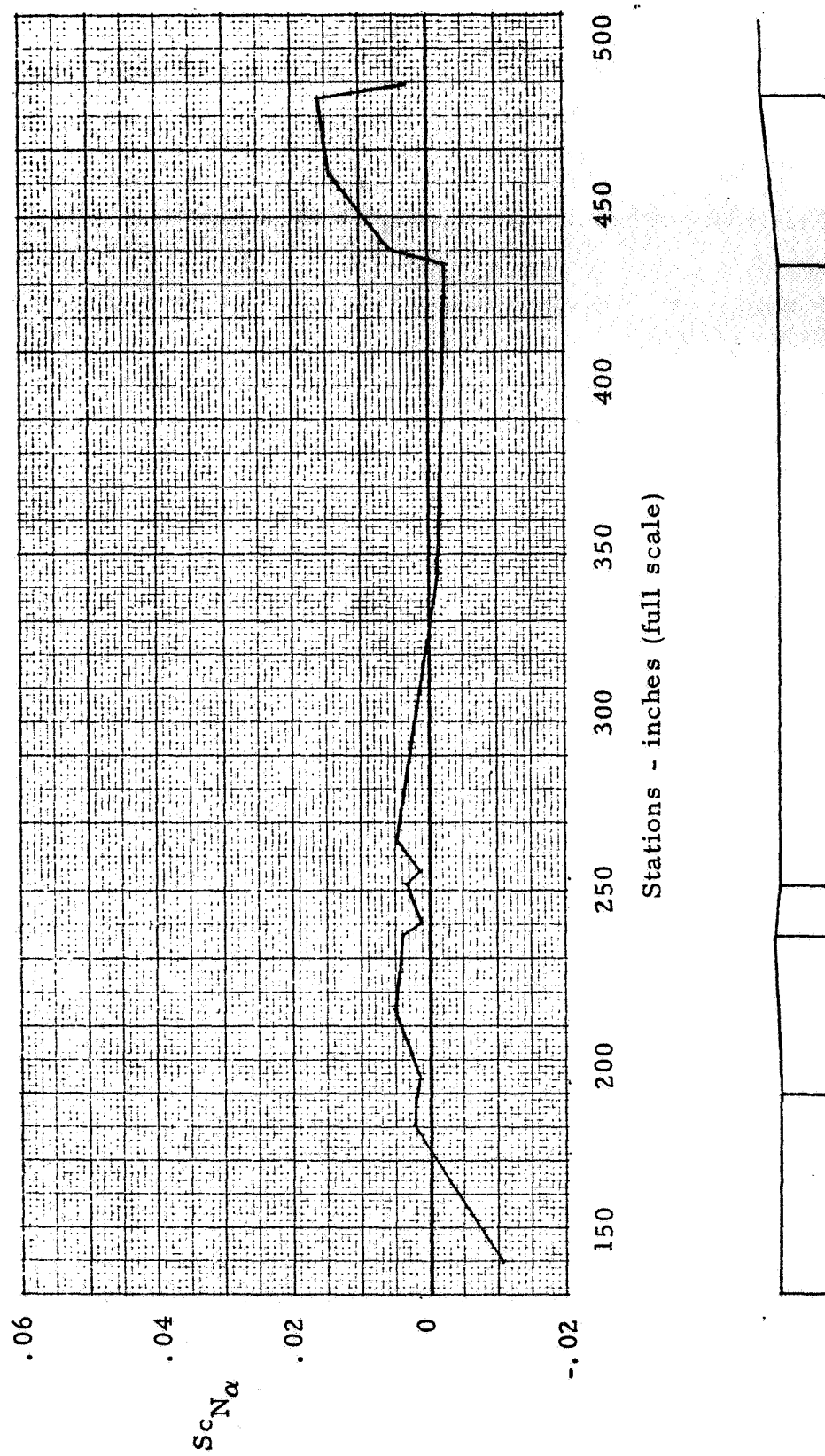(c) Stations 489.39 to 848.
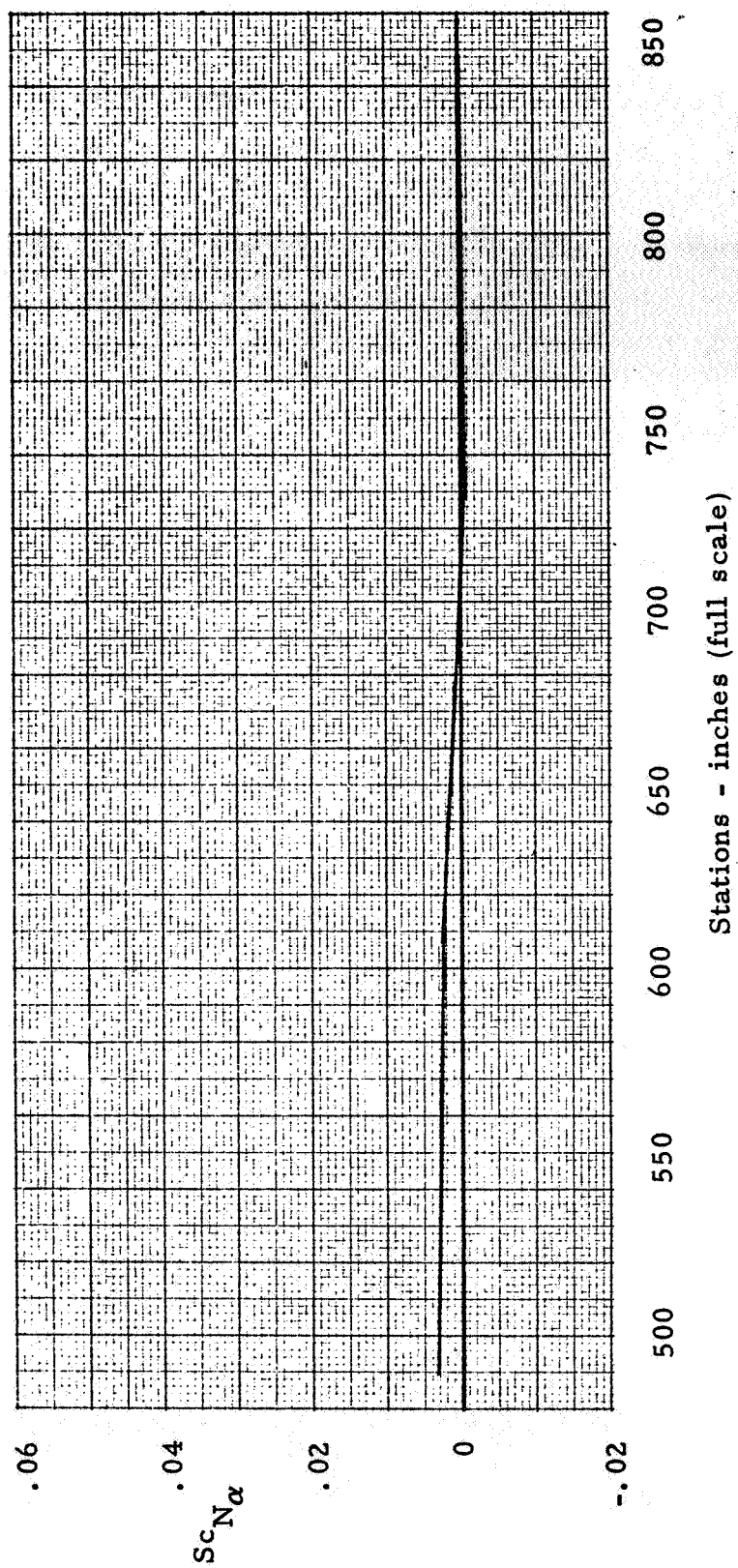
Figure 8. - Concluded.
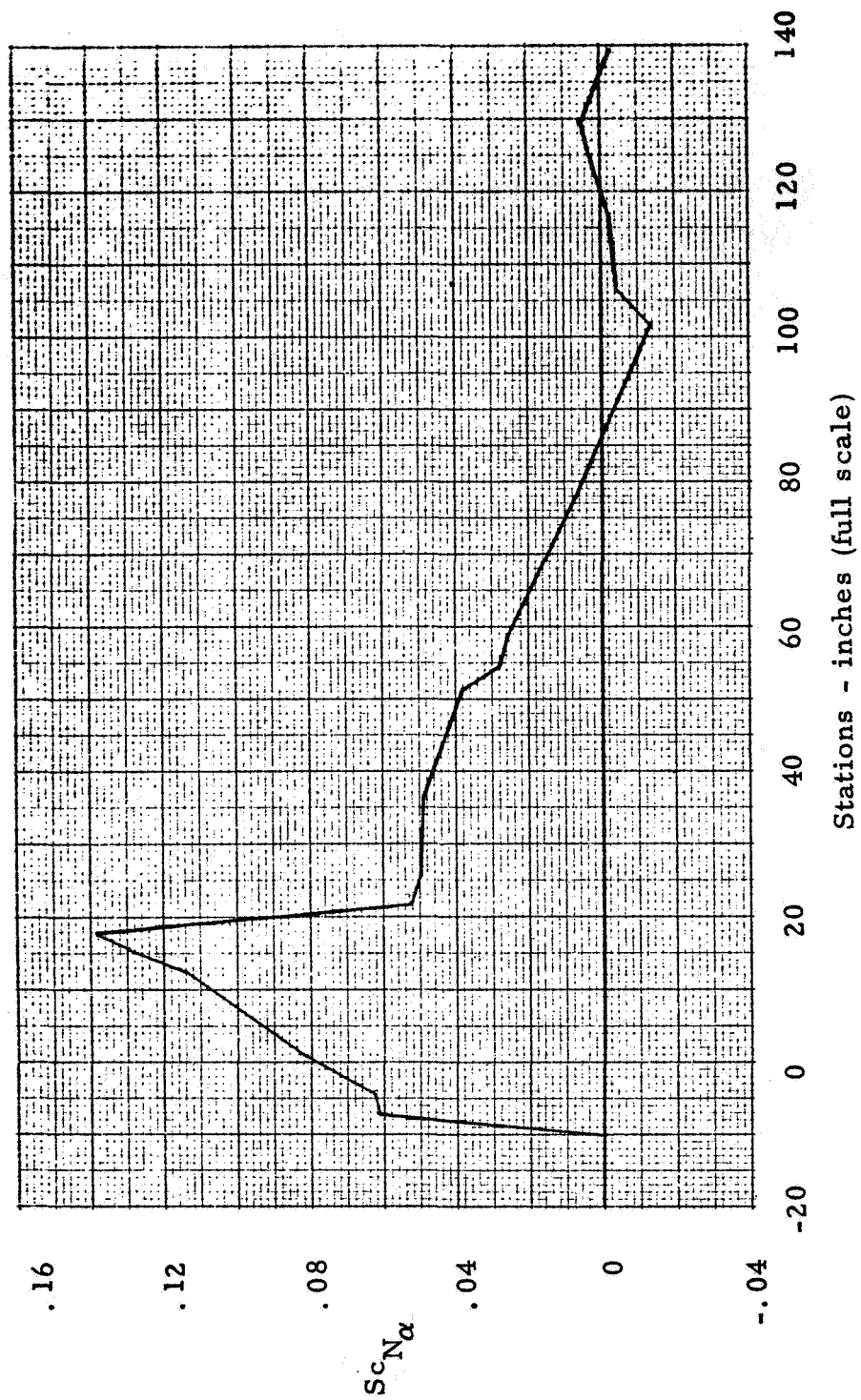
(a) Station -20 to 139.47.

Figure 9. - Normal Load Distribution, $B_{off}P_{off}F_{on}$, M = 2.41.

(b) Stations 139.47 to 489.39.
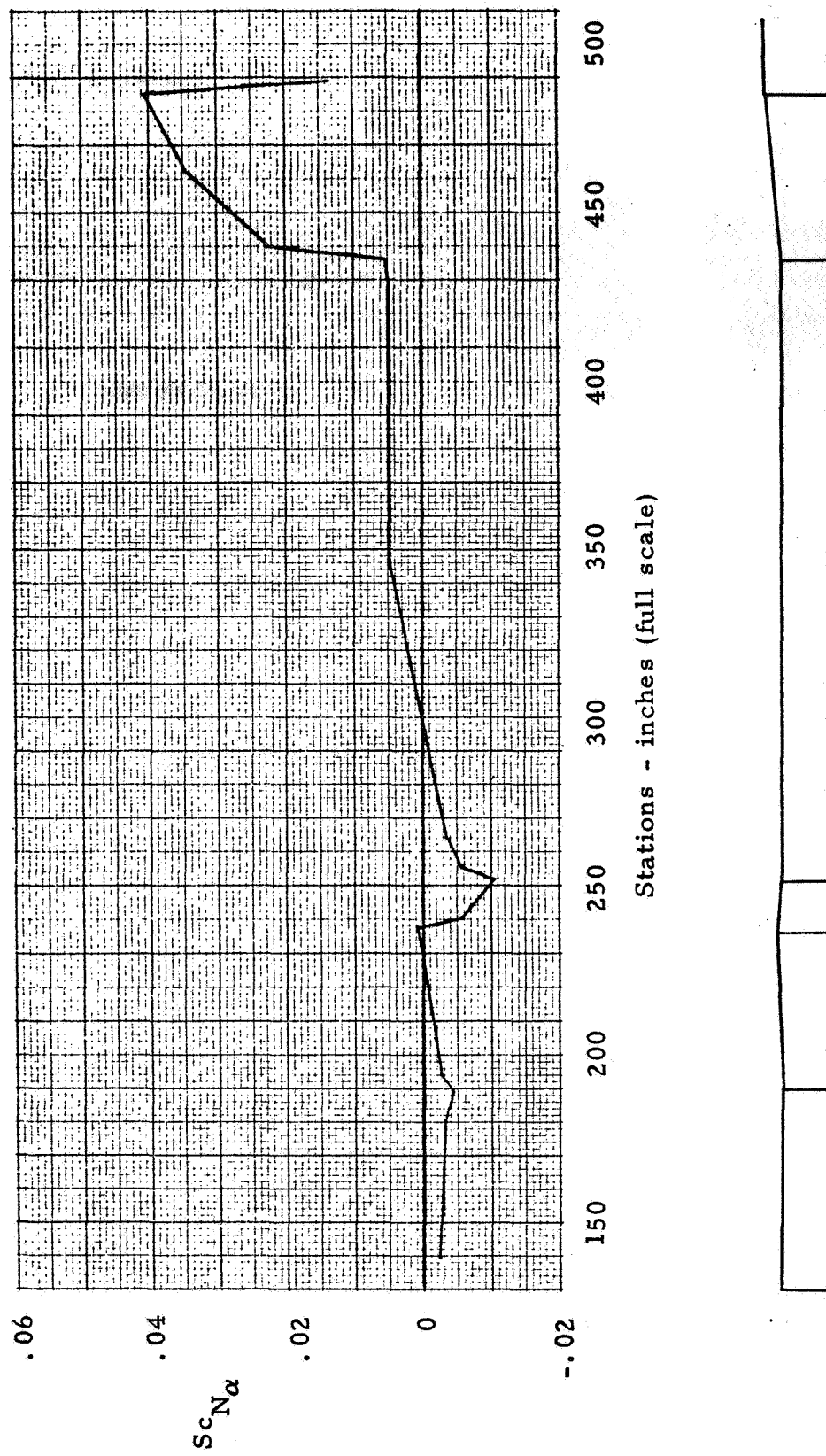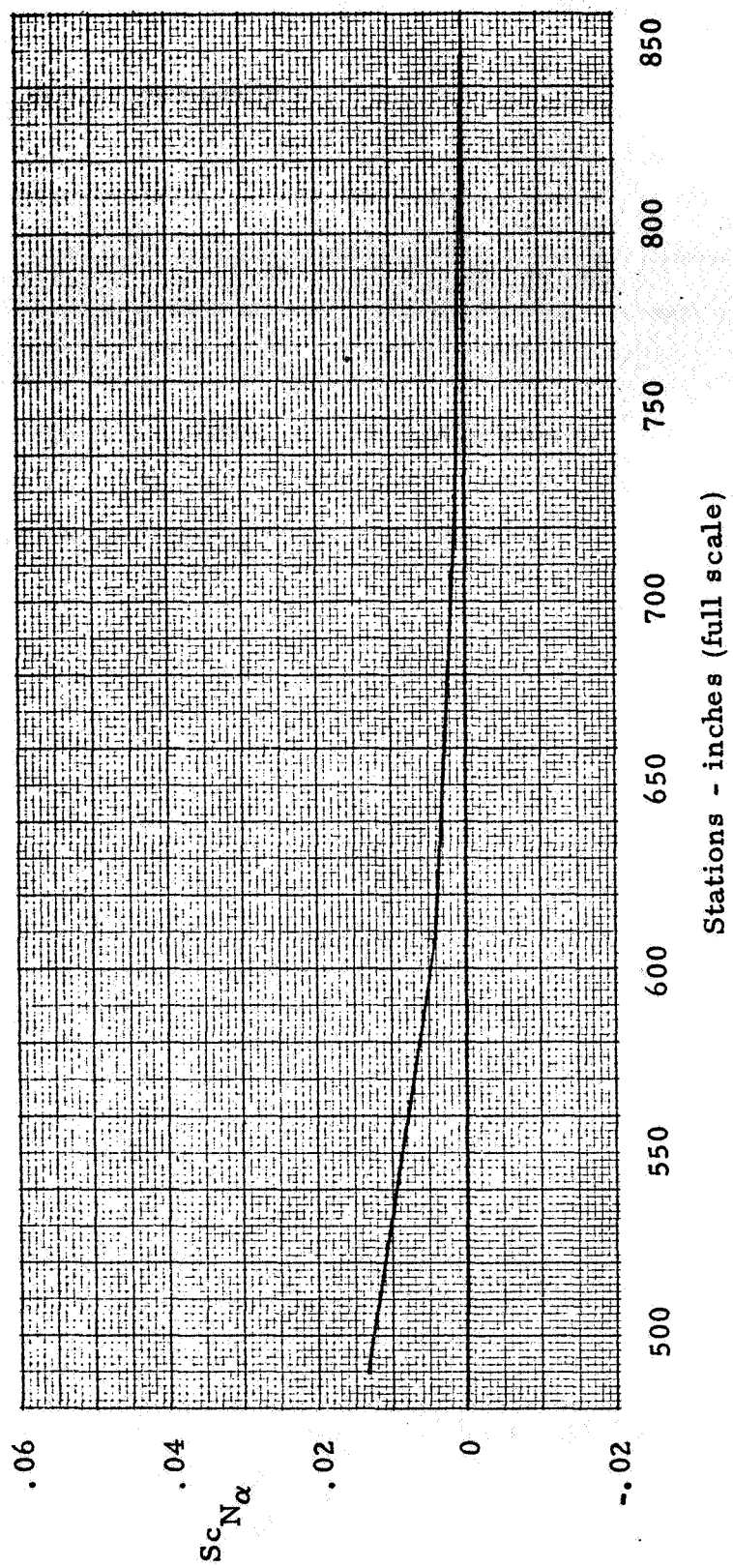
Figure 9. - Continued.

(c) Stations 489.39 to 848.

Figure 9. - Concluded.

37

Stations - inches (full scale)
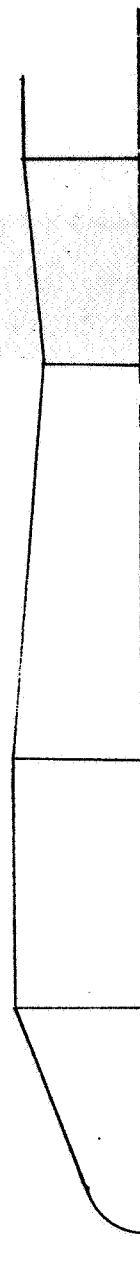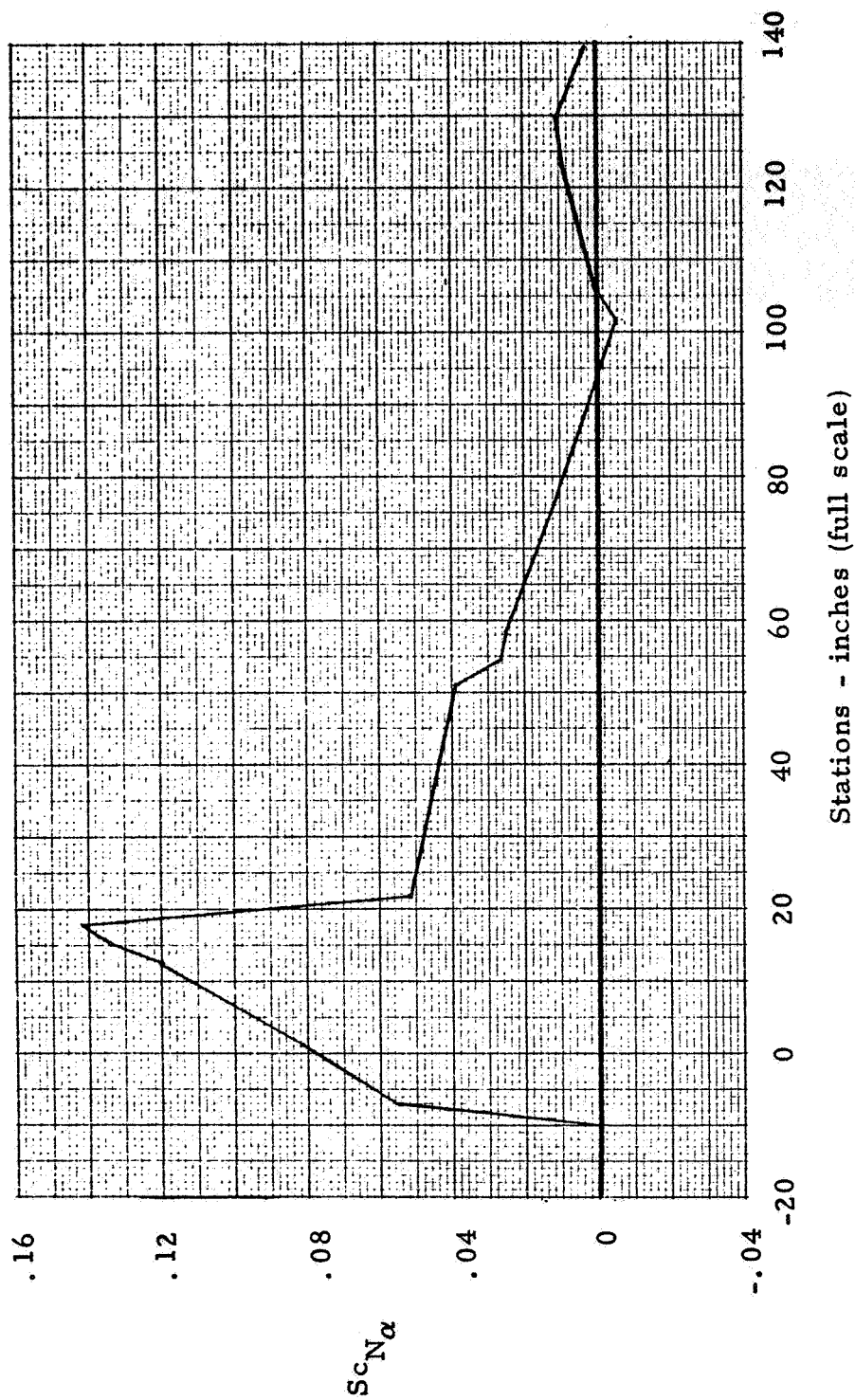
(a) Station -20 to 139.47.

Figure 10. - Normal Load Distribution, $B_{off}P_{off}F_{on}$, $M = 2.61$.
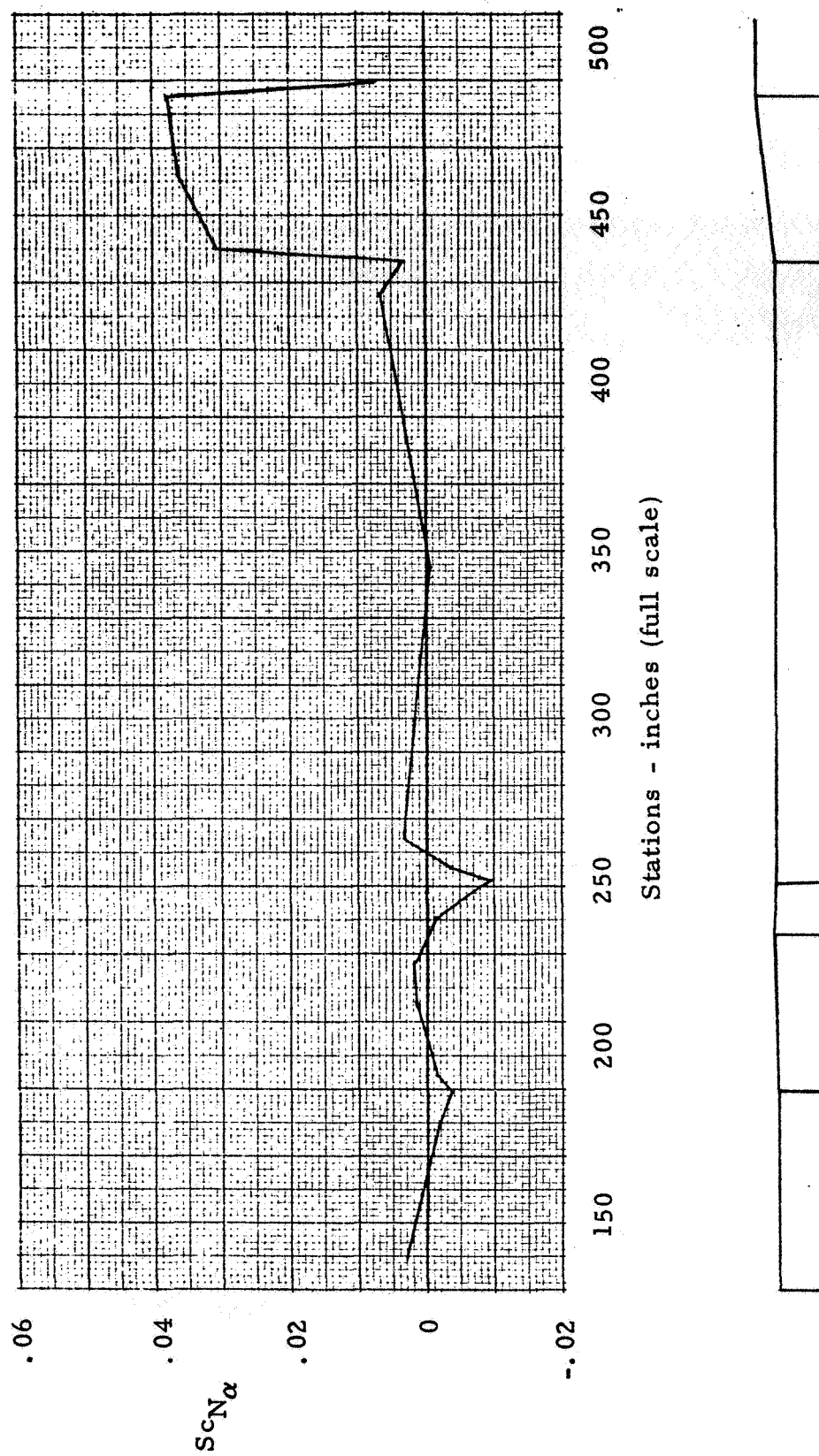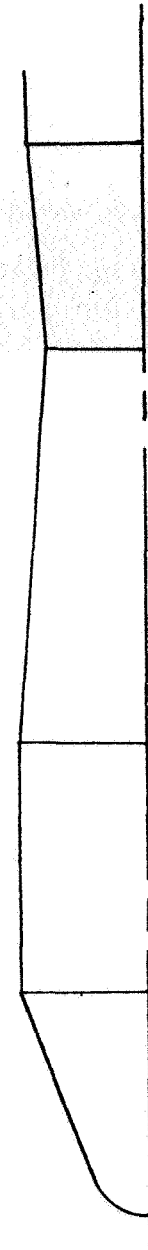
(b) Stations 139.47 to 489.39.

Figure 10. - Continued.

39
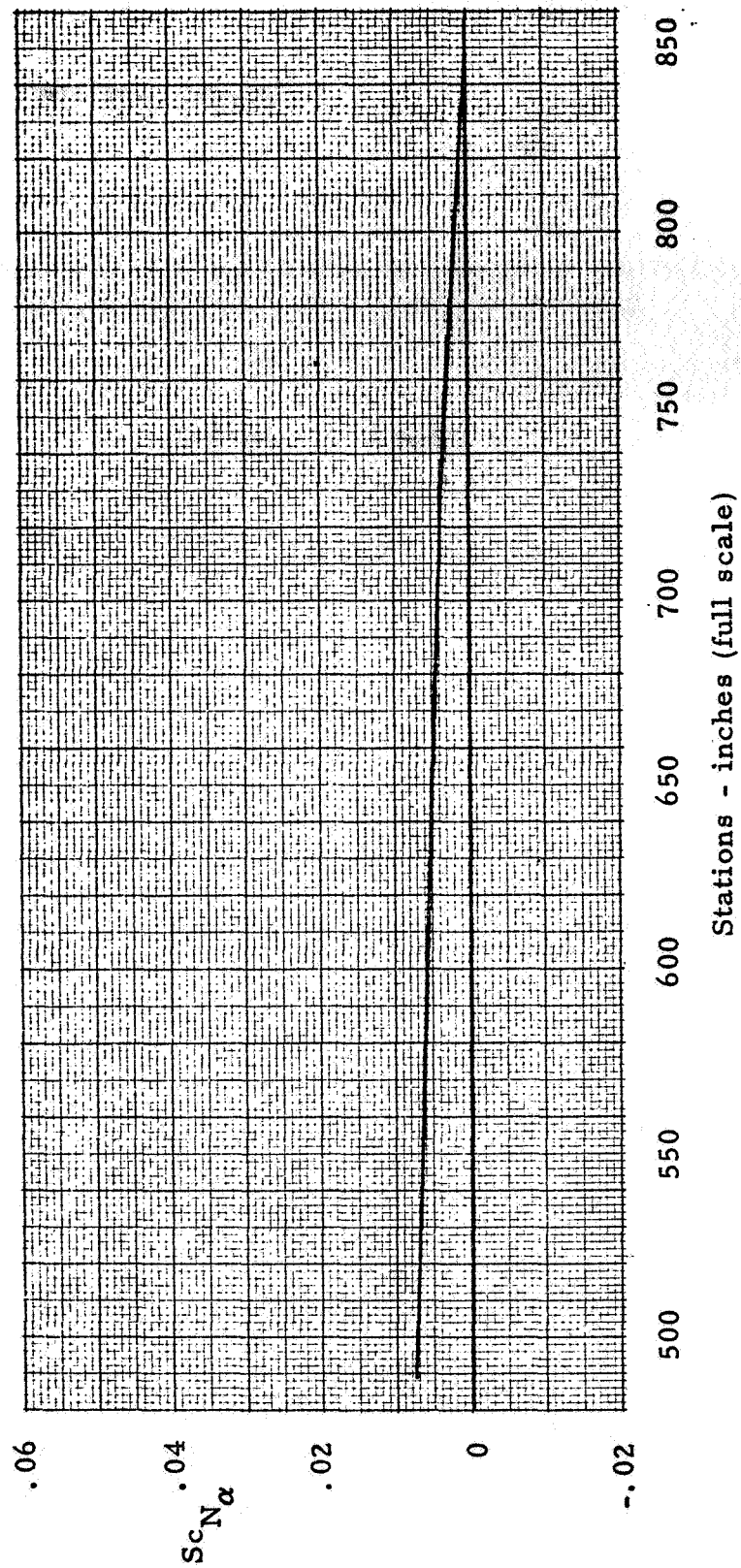
(c) Stations 489.39 to 848.

Figure 10. - Concluded.
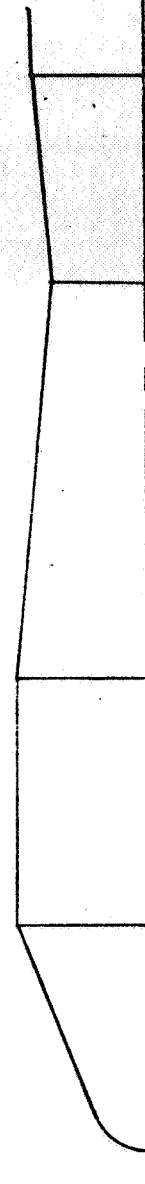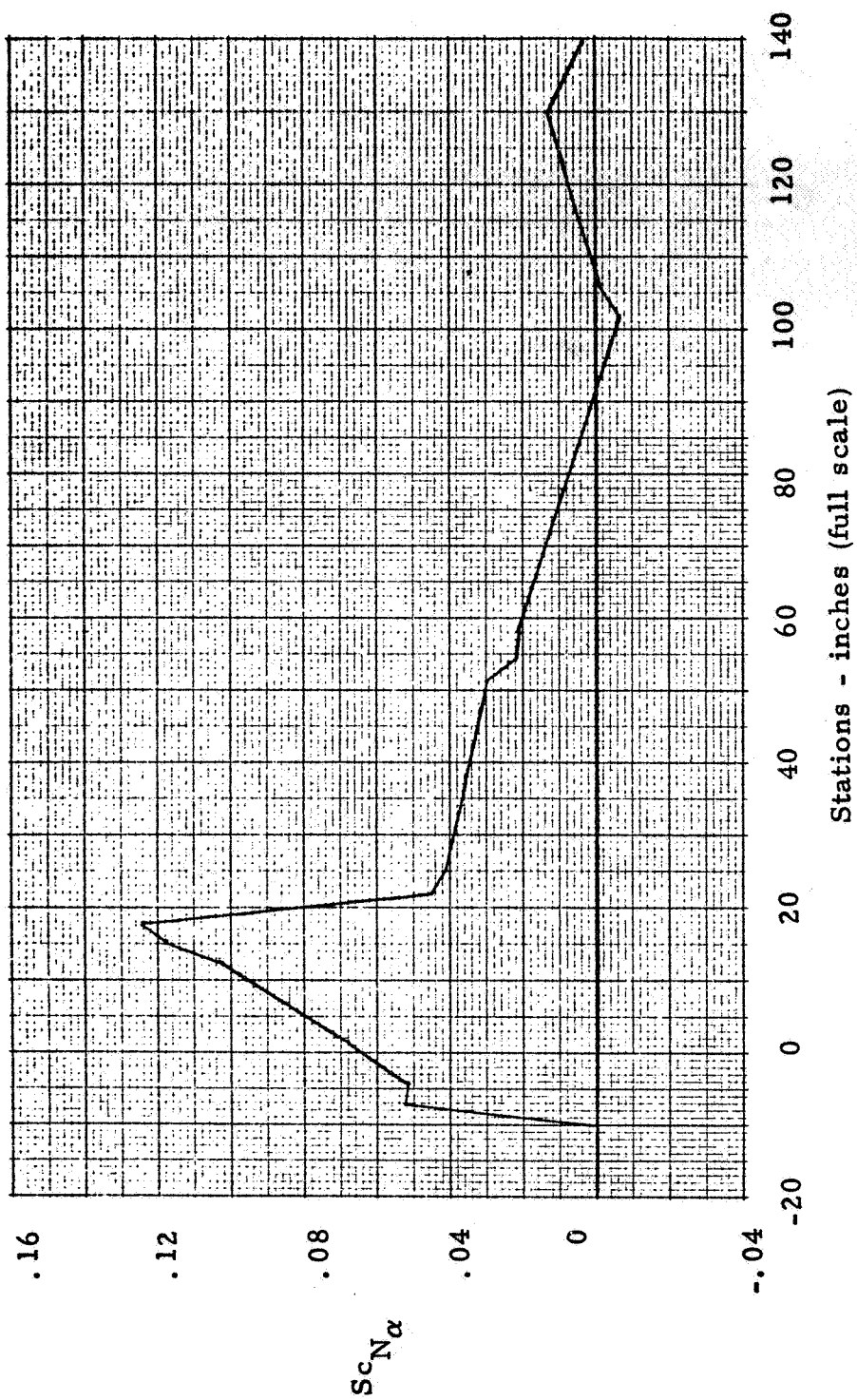
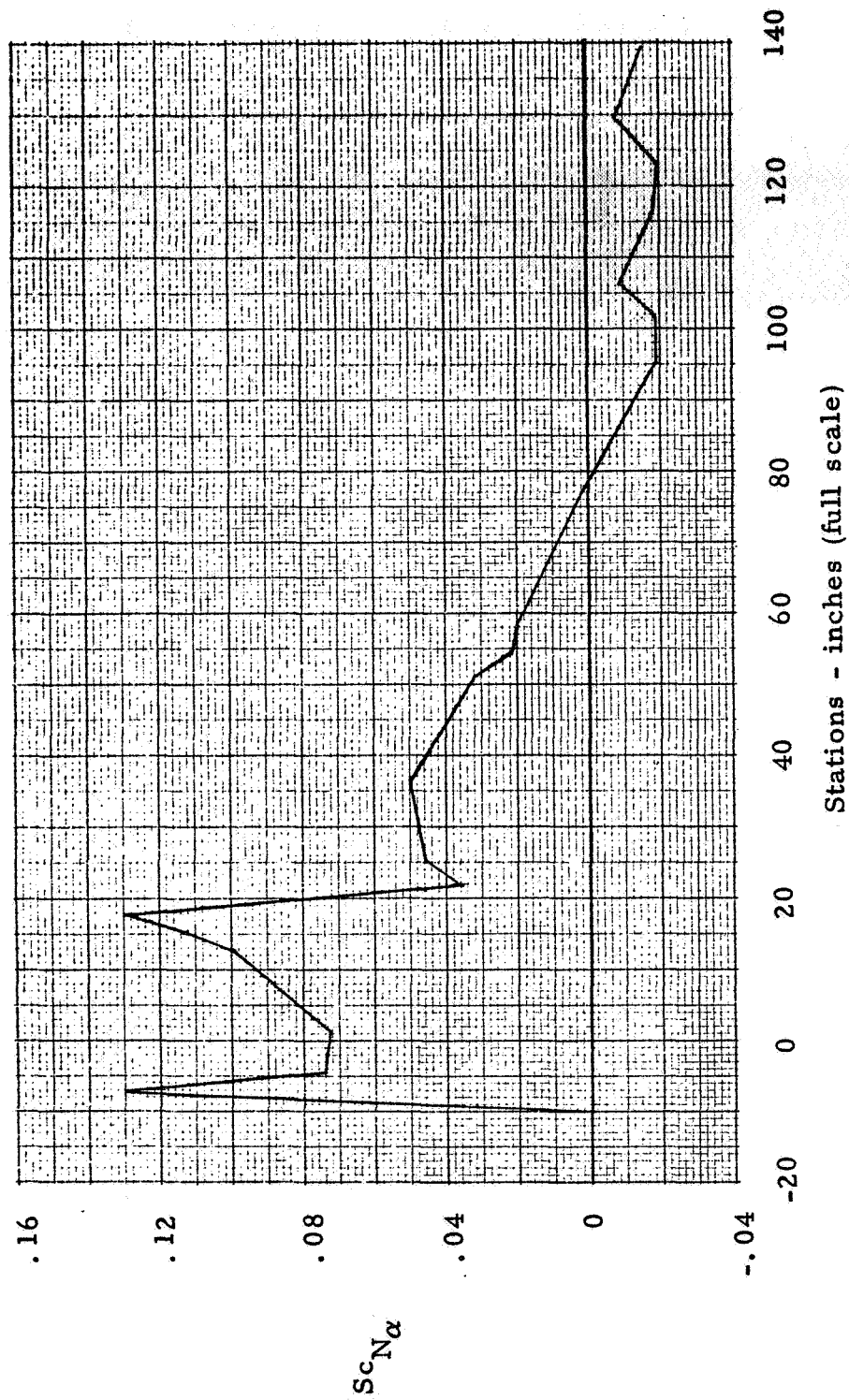Figure 11. - Normal Load Distribution, $B_{off}P_{off}F_{on}$, $M = 2.80$.

(a) Station -20 to 139.47.

(b) Stations 139.47 to 489.39.
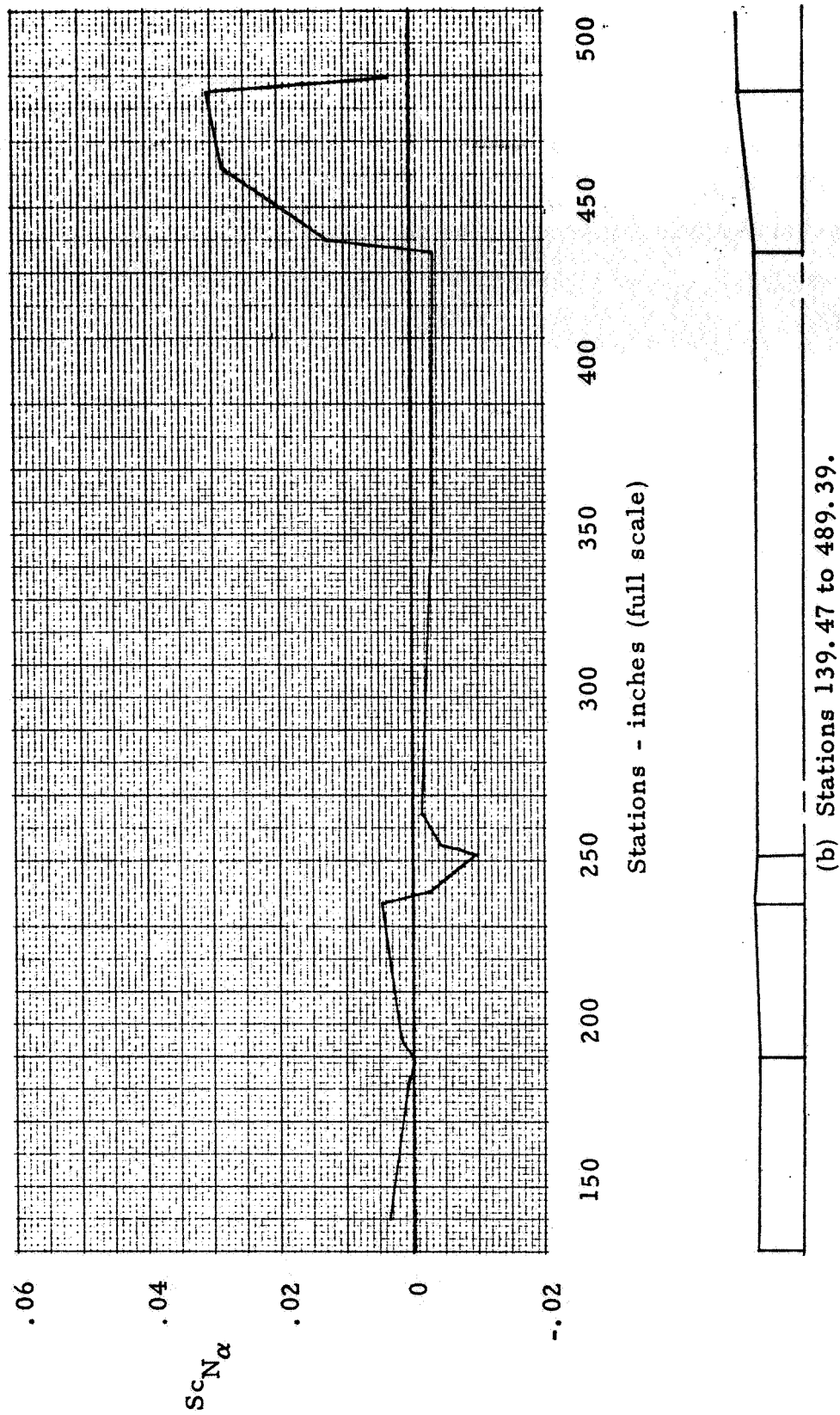
Figure 11. - Continued.
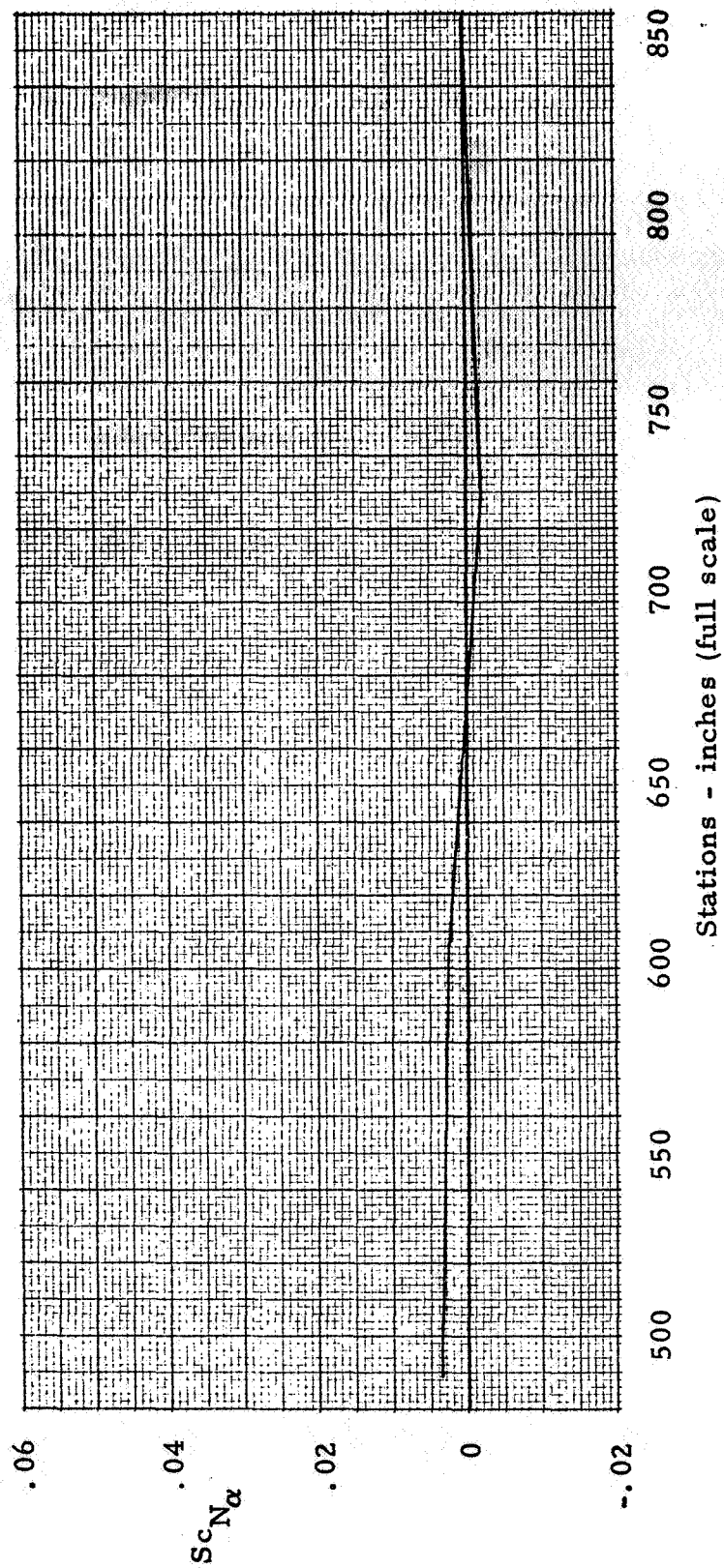
(c) Stations 489.39 to 848.

Figure 11. - Concluded.

43

Stations - inches (full scale)

Sc_{N_α}
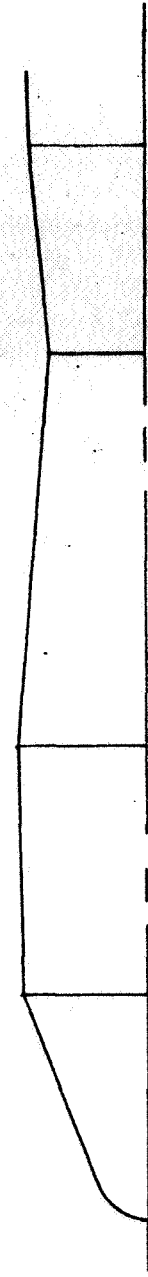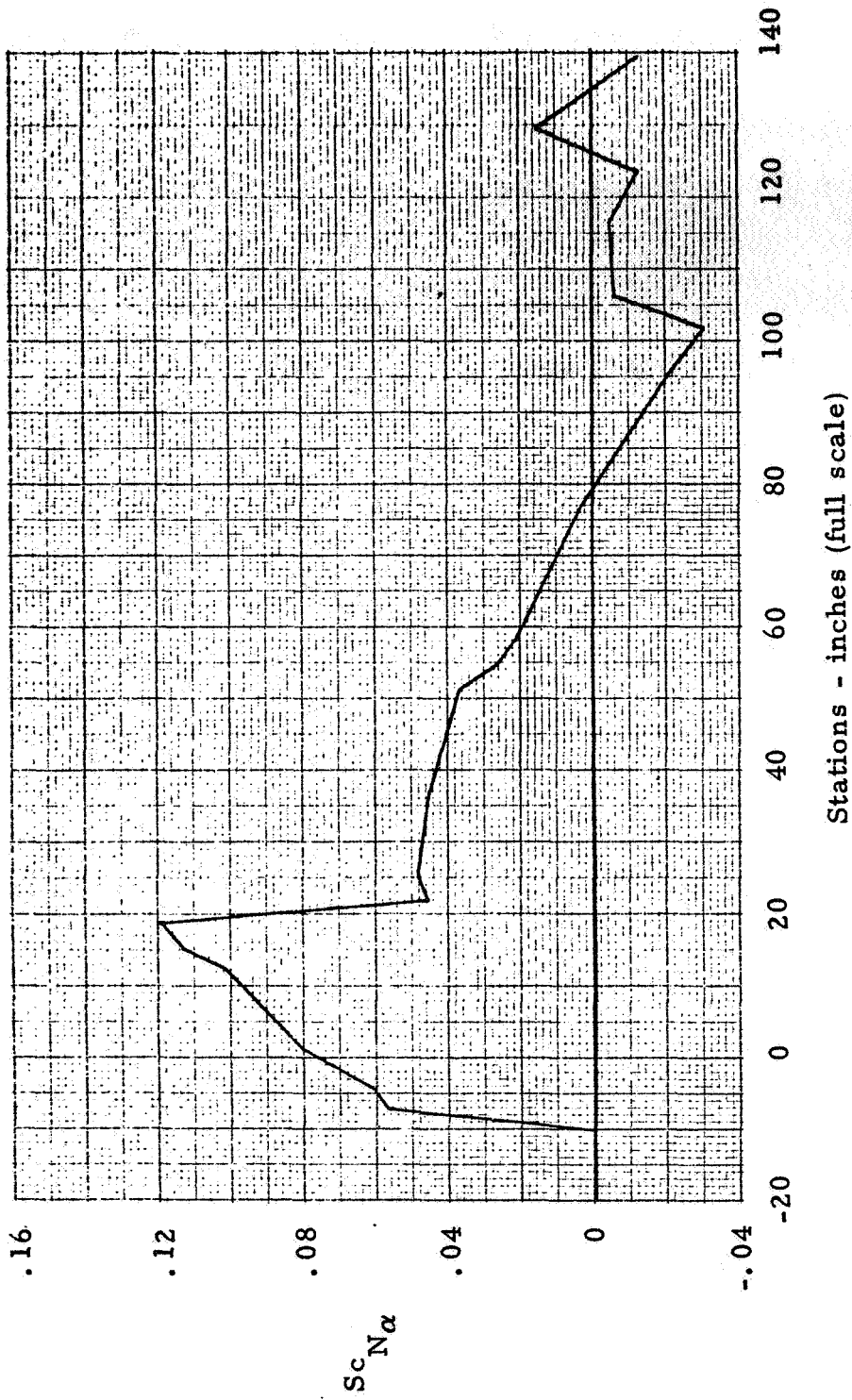
(a) Station -20 to 139.47.

Figure 12. - Normal Load Distribution, $B_{off} P_{on} F_{on}$, M = 2.01.
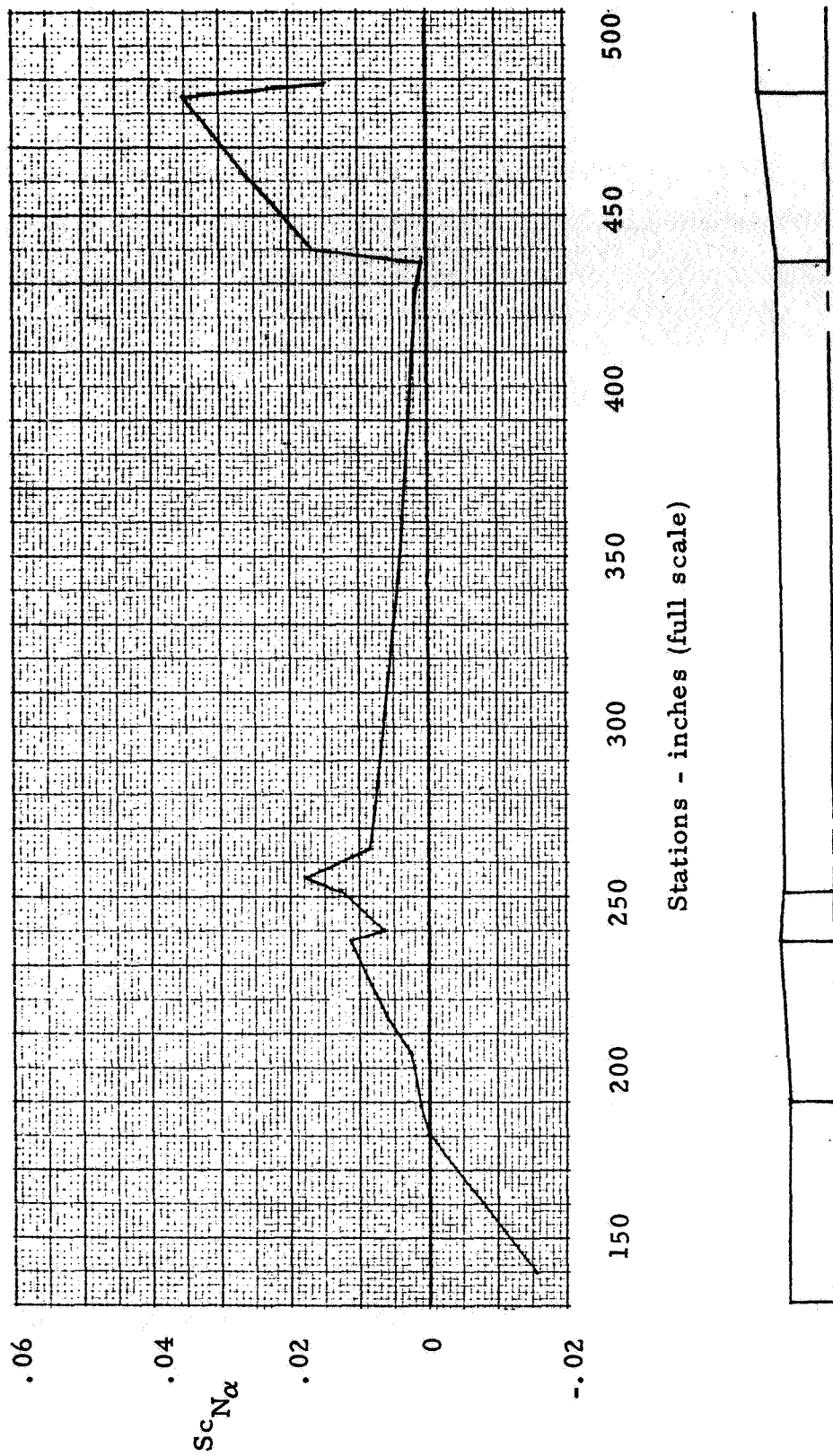
44
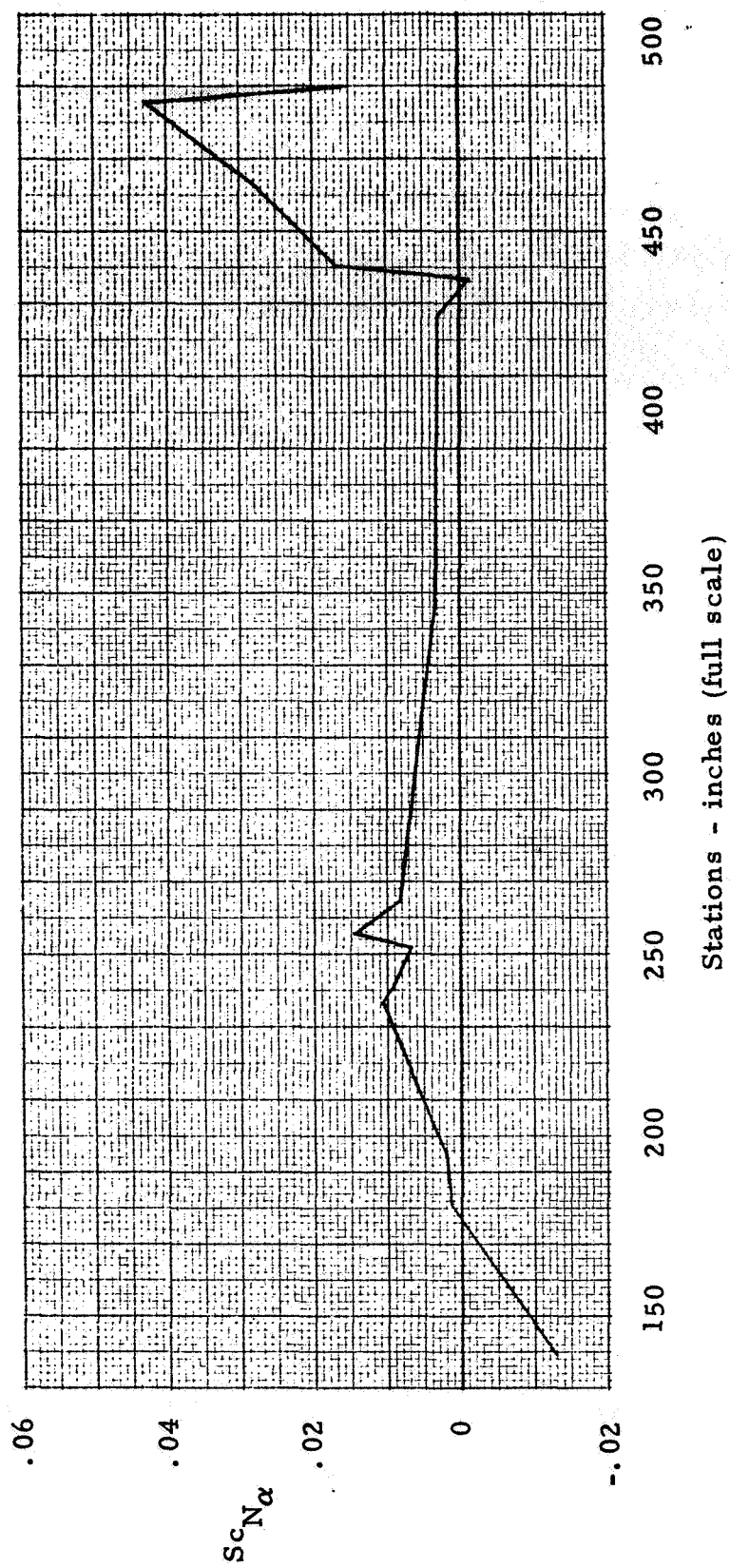
(b) Stations 139.47 to 489.39.

Figure 12. - Continued.
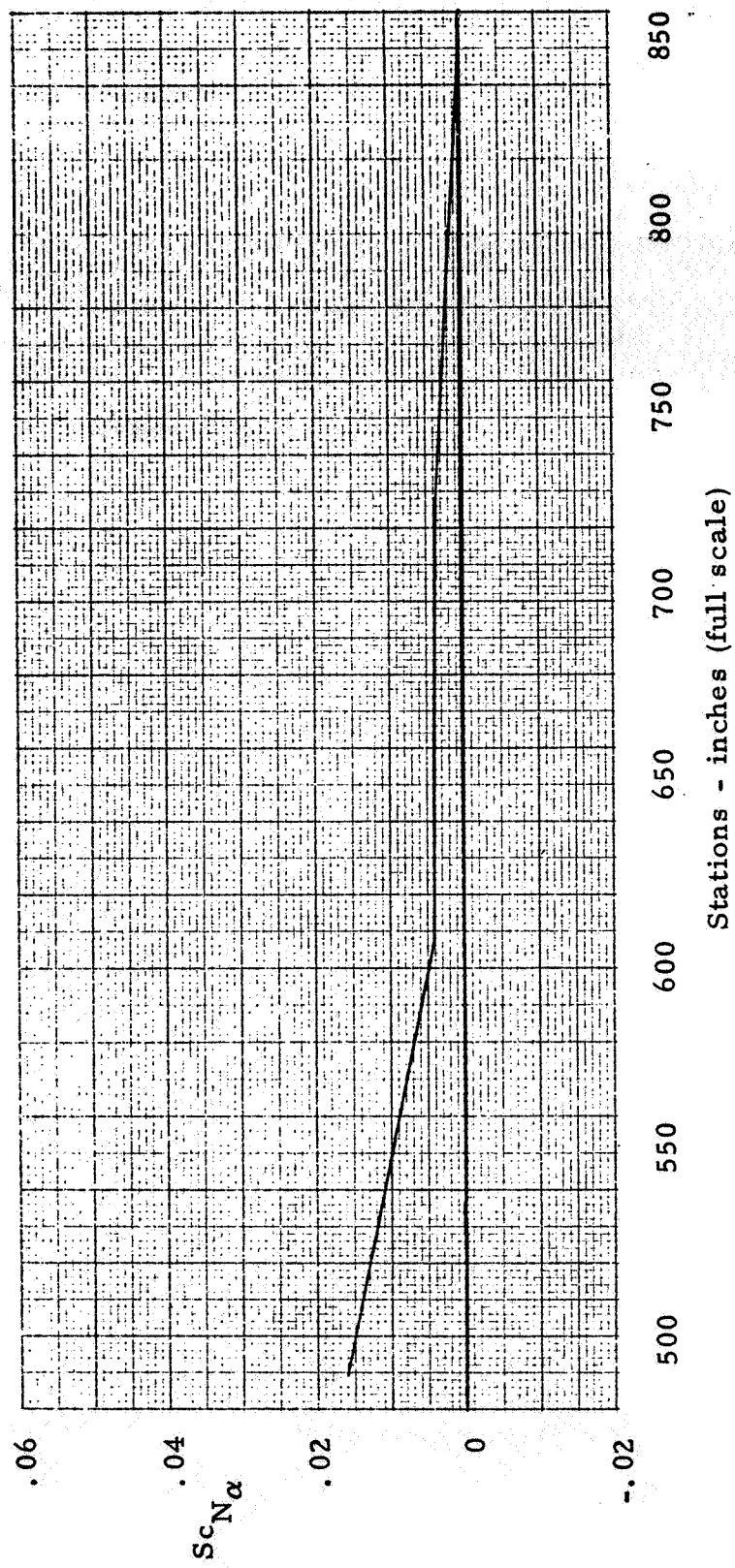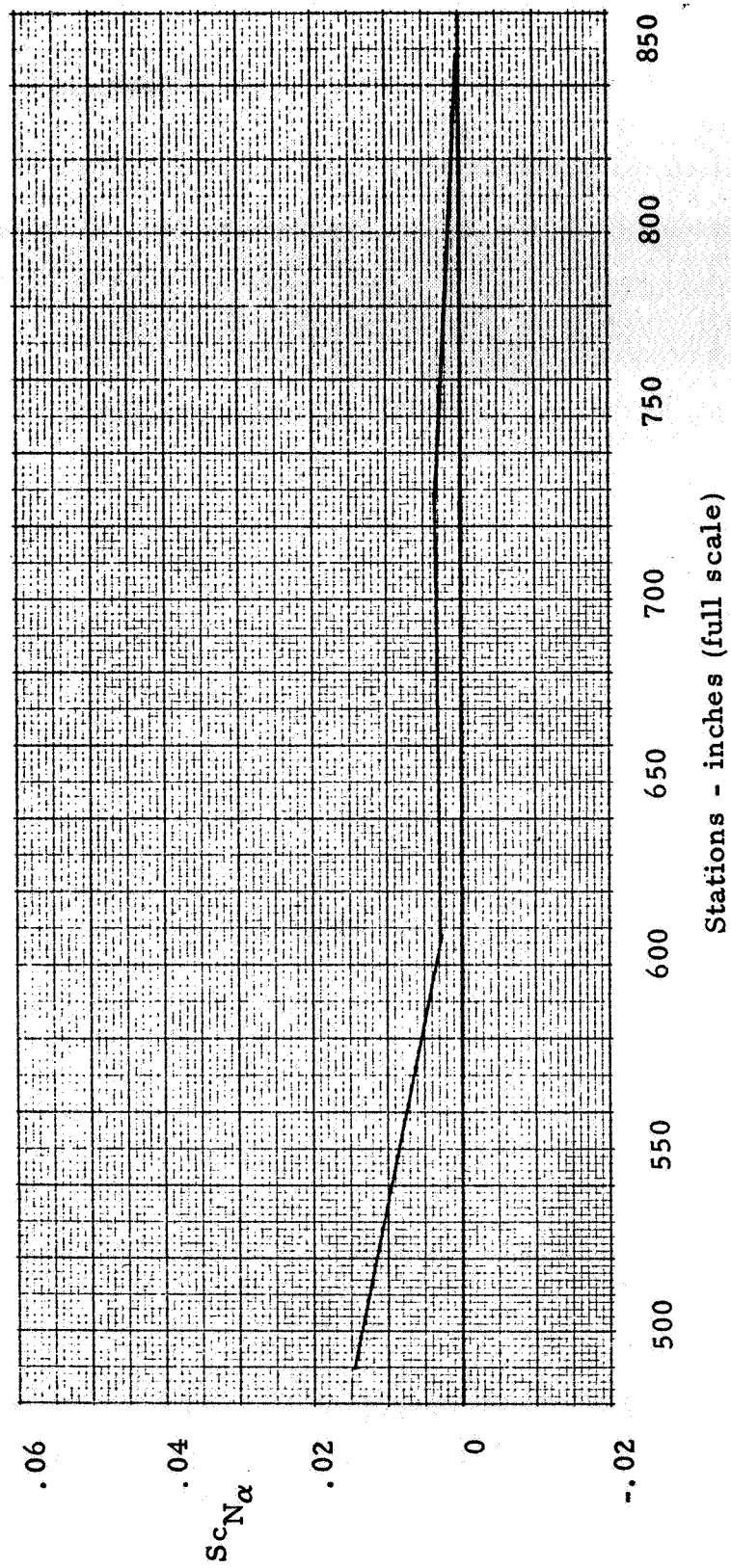
(c) Stations 489.39 to 848.

Figure 12. - Concluded.
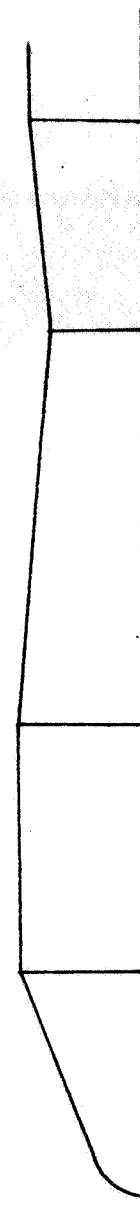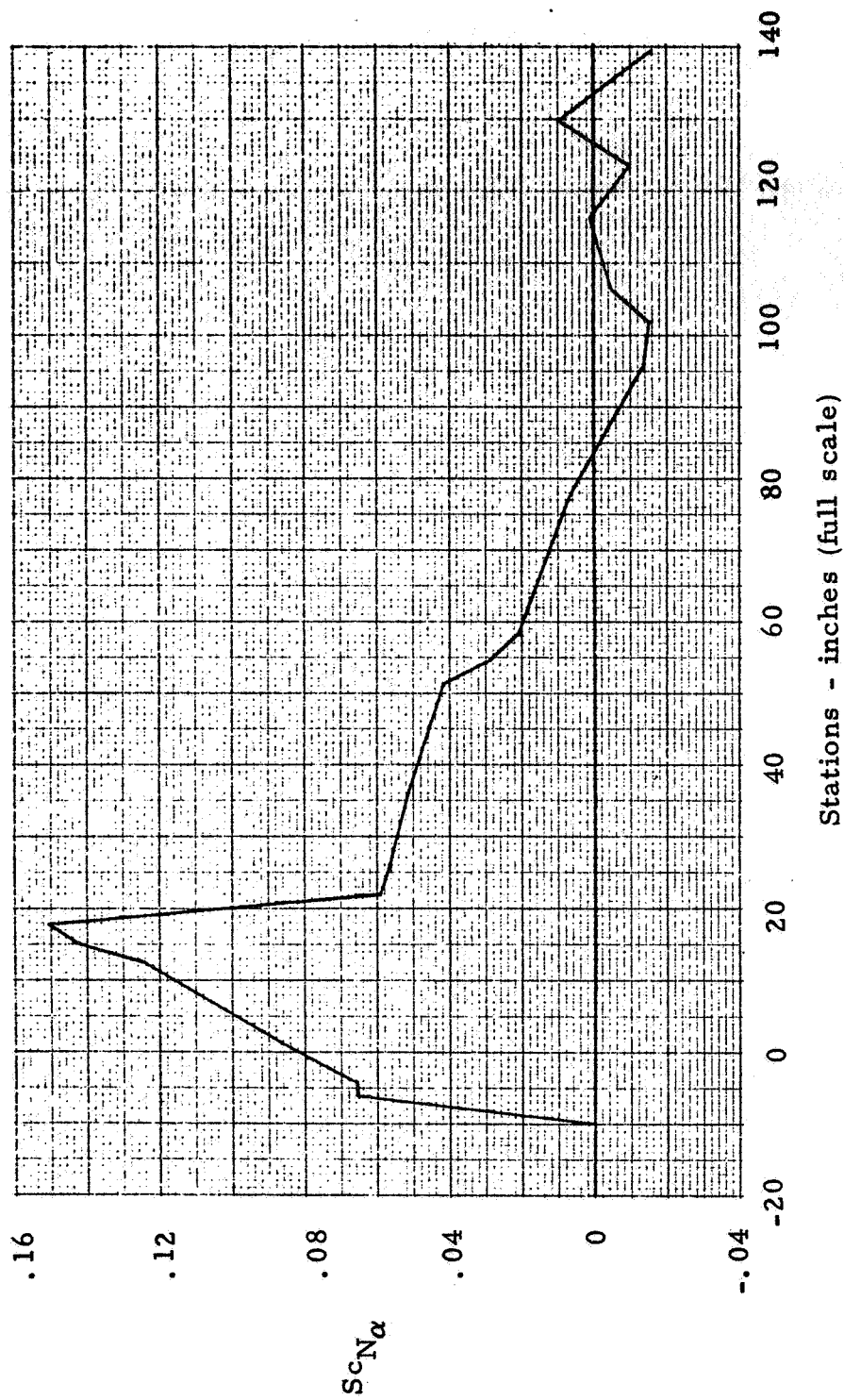
Figure 13. - Normal Load Distribution, $B_{off}P_{on}F_{on}$, M = 2.41.
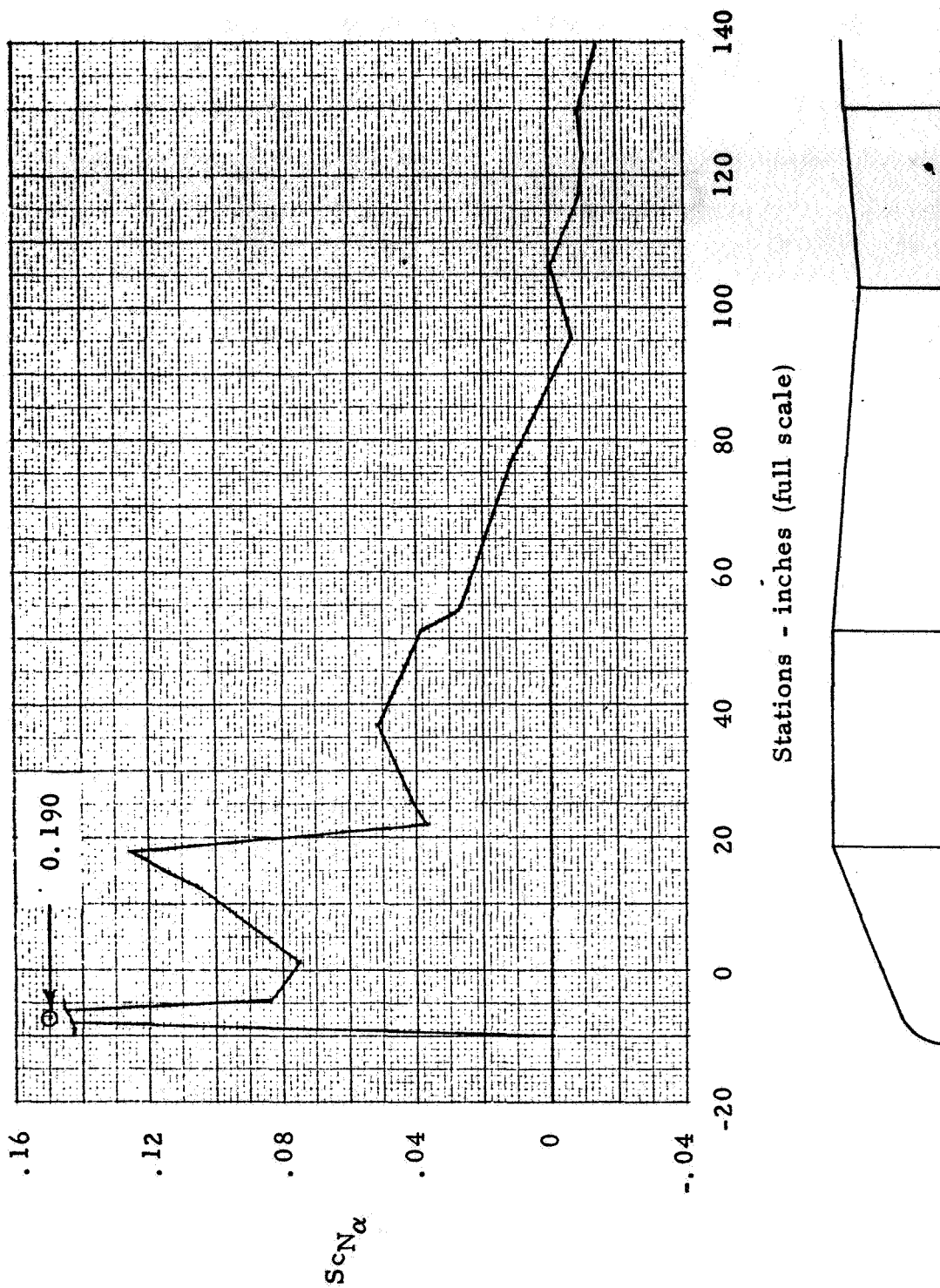
(a) Station -20 to 139.47.

Stations - inches (full scale)
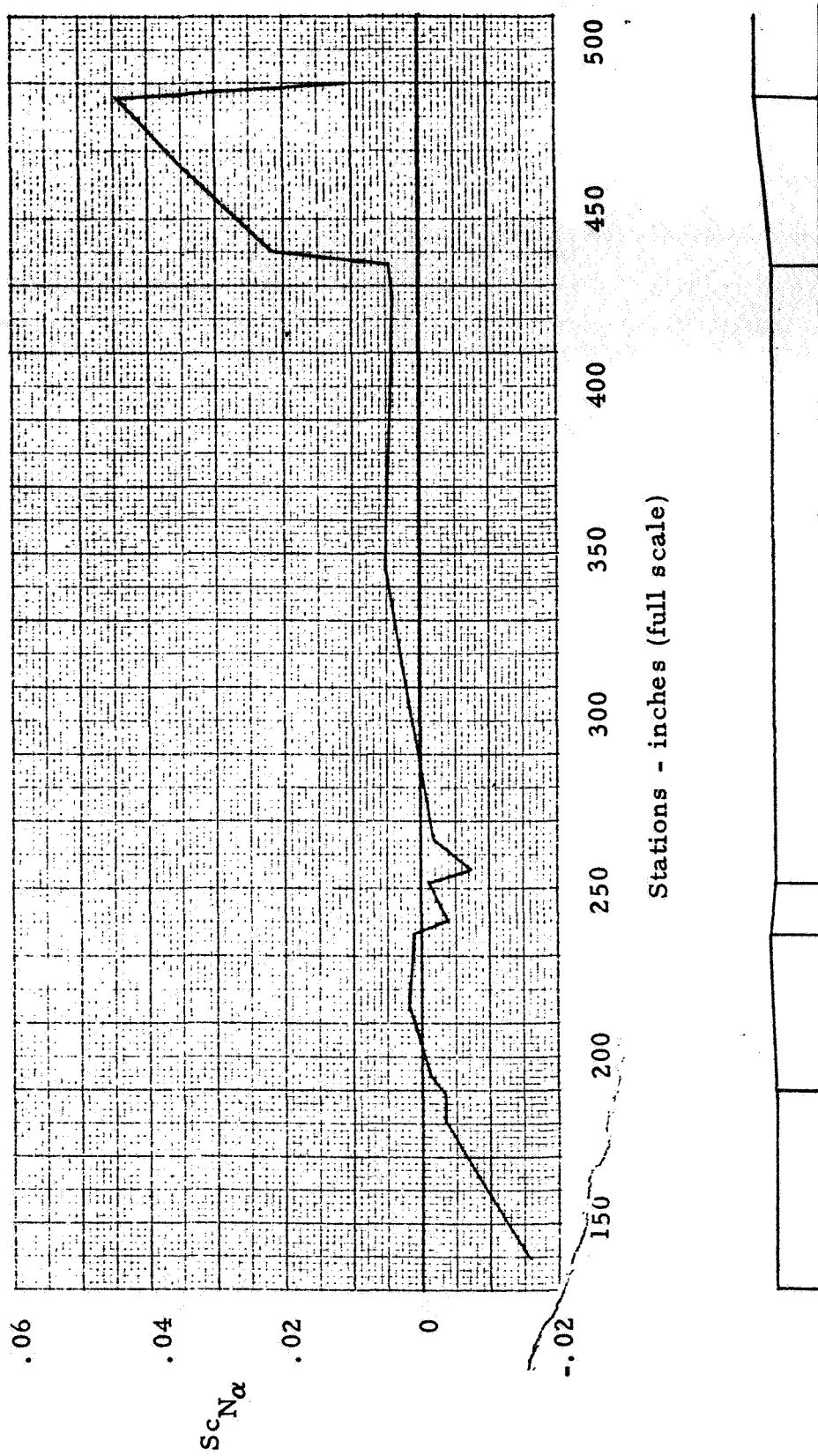
(b) Stations 139.47 to 489.39.

Figure 13. - Continued.
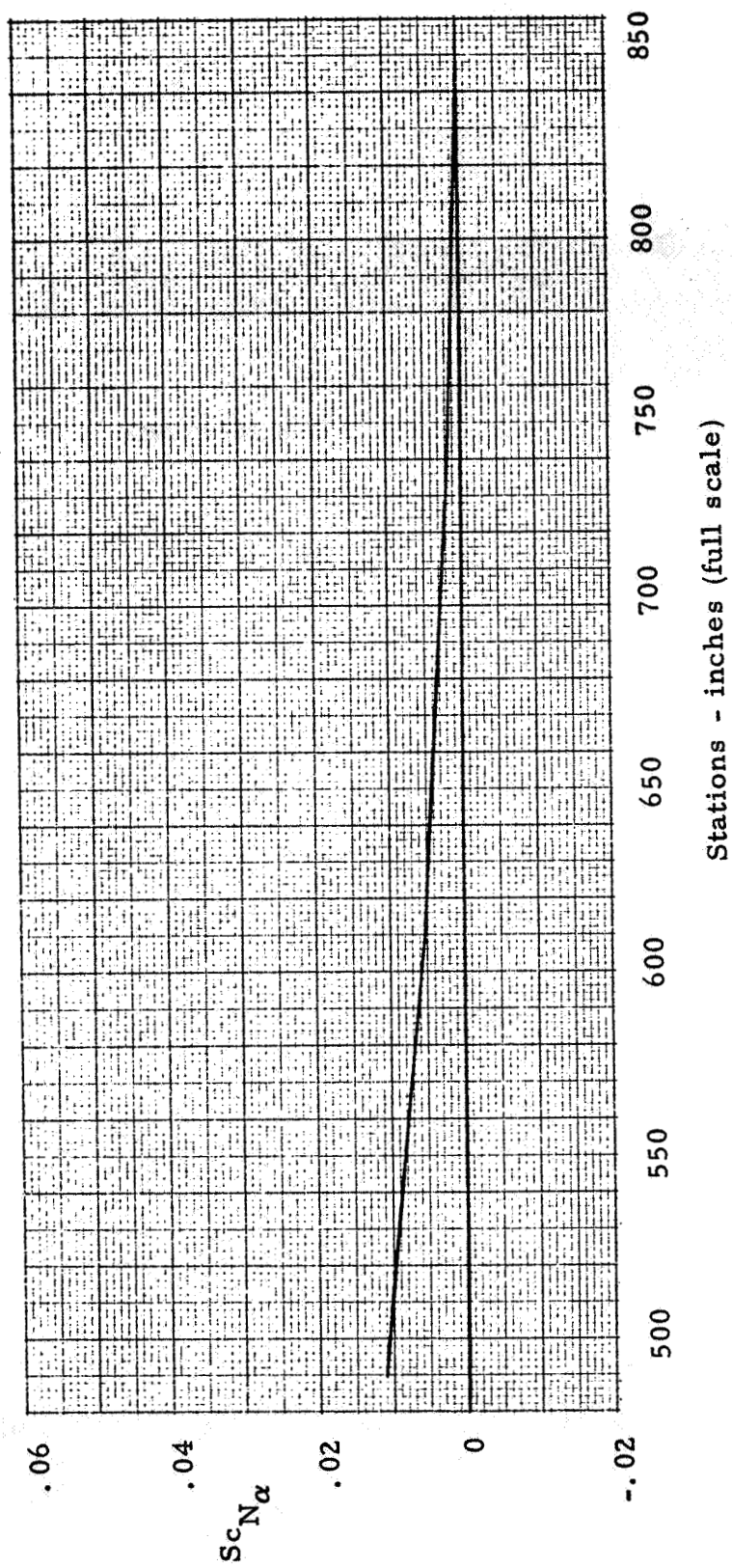
(c) Stations 489.39 to 848.

Figure 13. - Concluded.

Stations - inches (full scale)
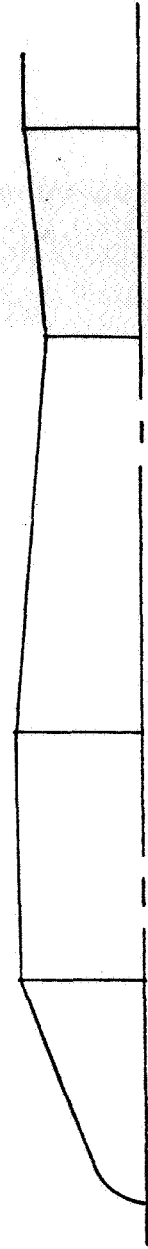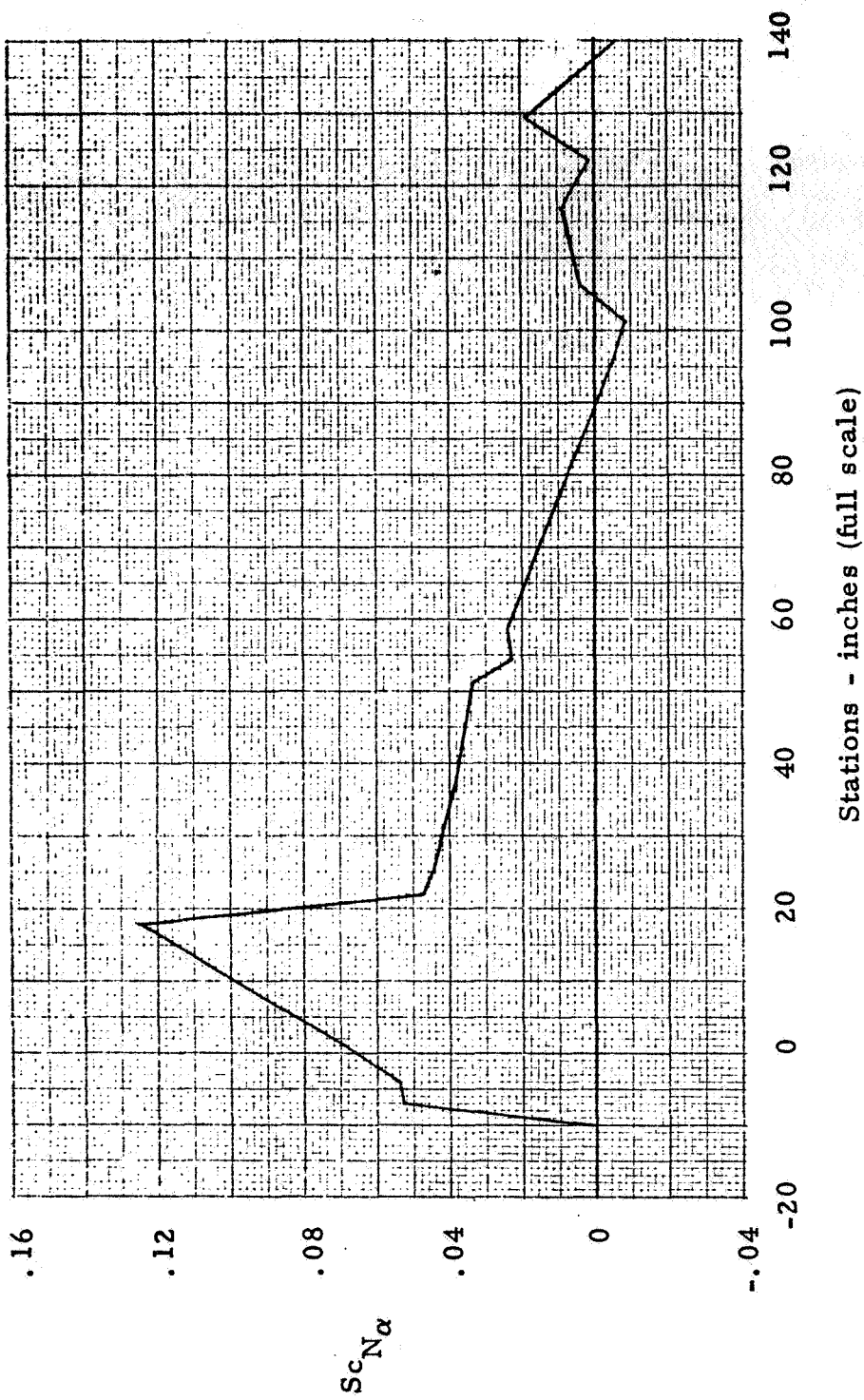
(a) Station -20 to 139.47.

Figure 14. - Normal Load Distribution, $B_{off} P_{on} F_{on}$, M = 2.61.
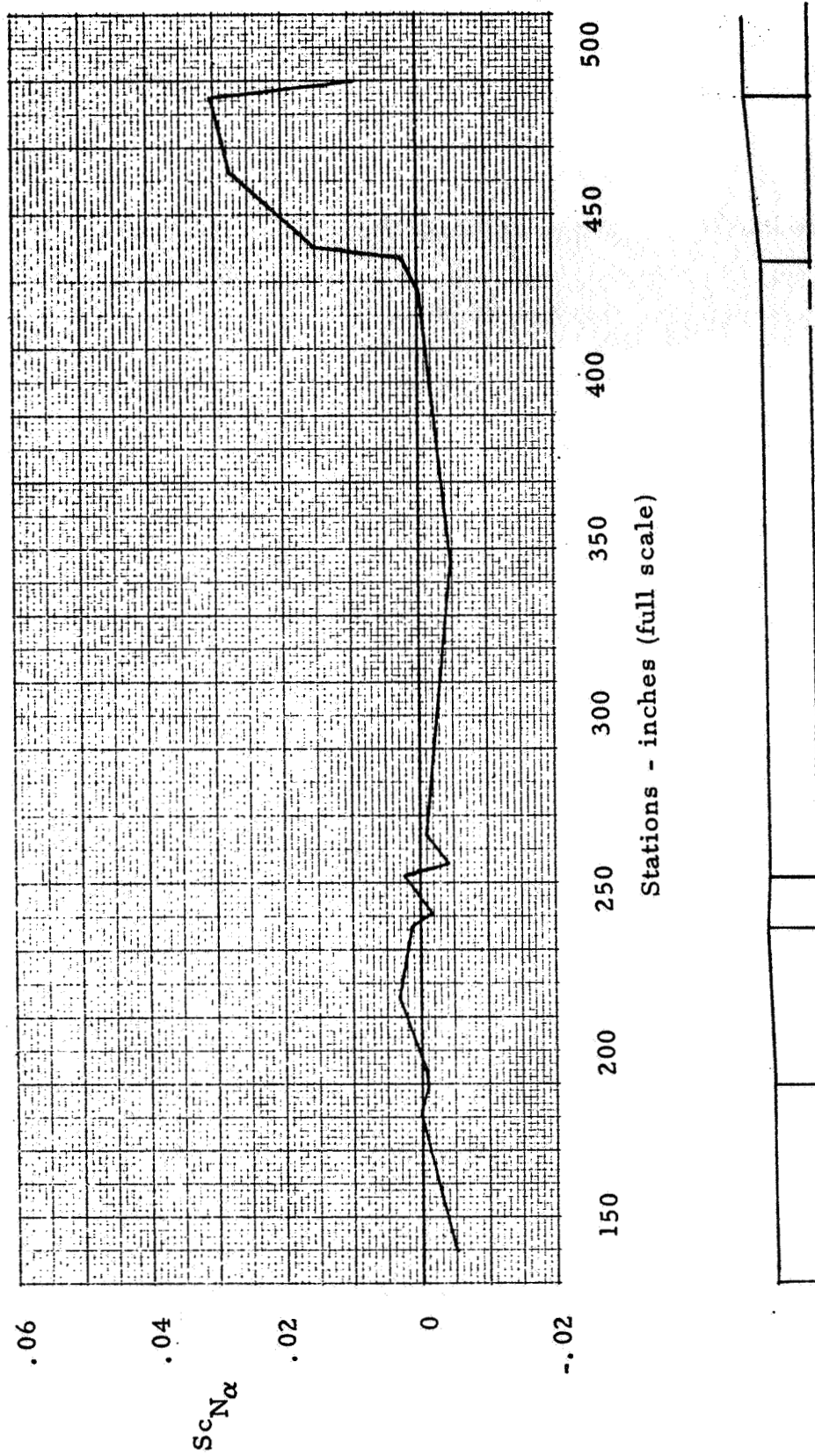
(b) Stations 139.47 to 489.39.

Figure 14. - Continued.
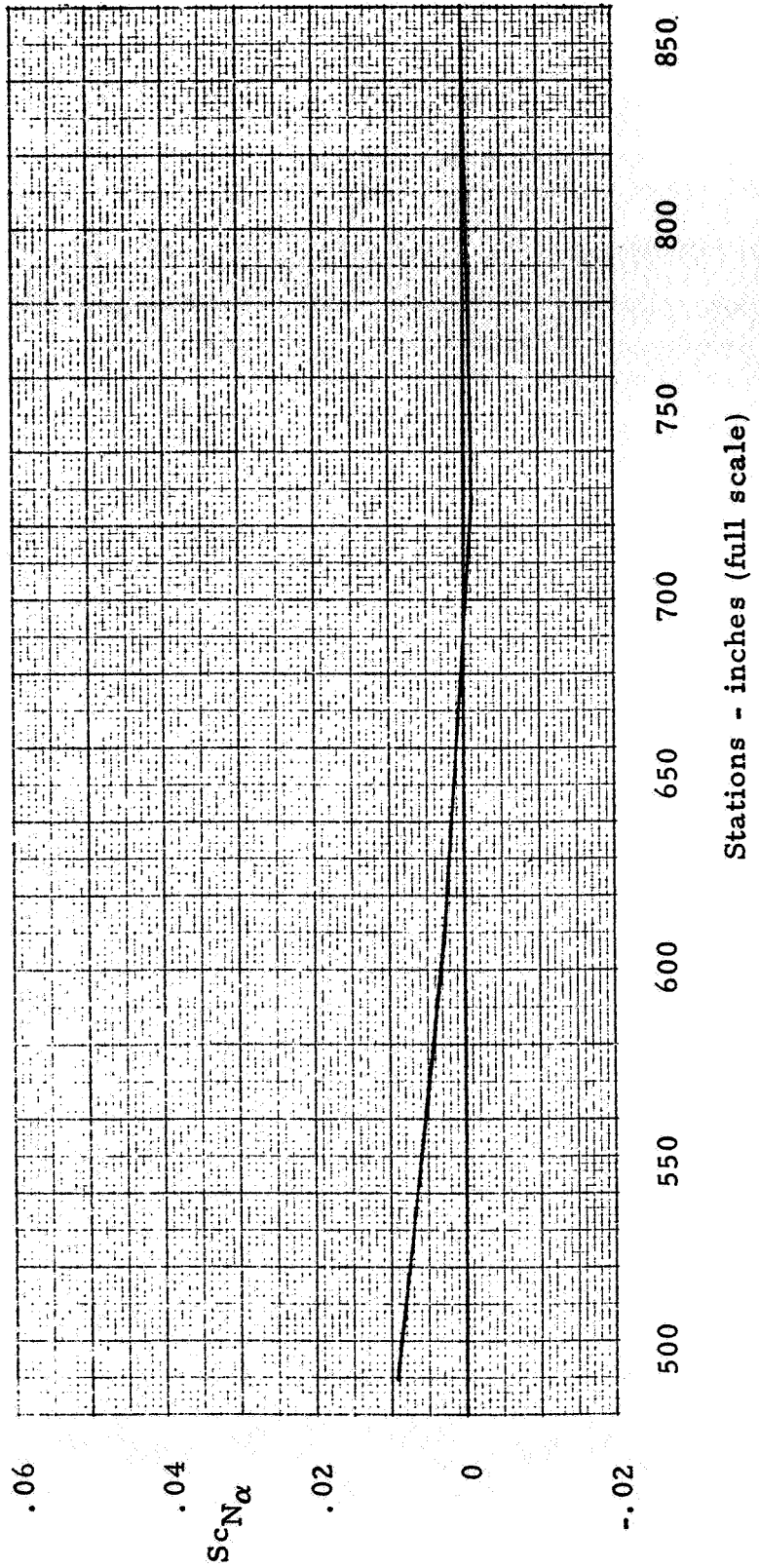
(c) Stations 489.39 to 848.

Figure 14. - Concluded.
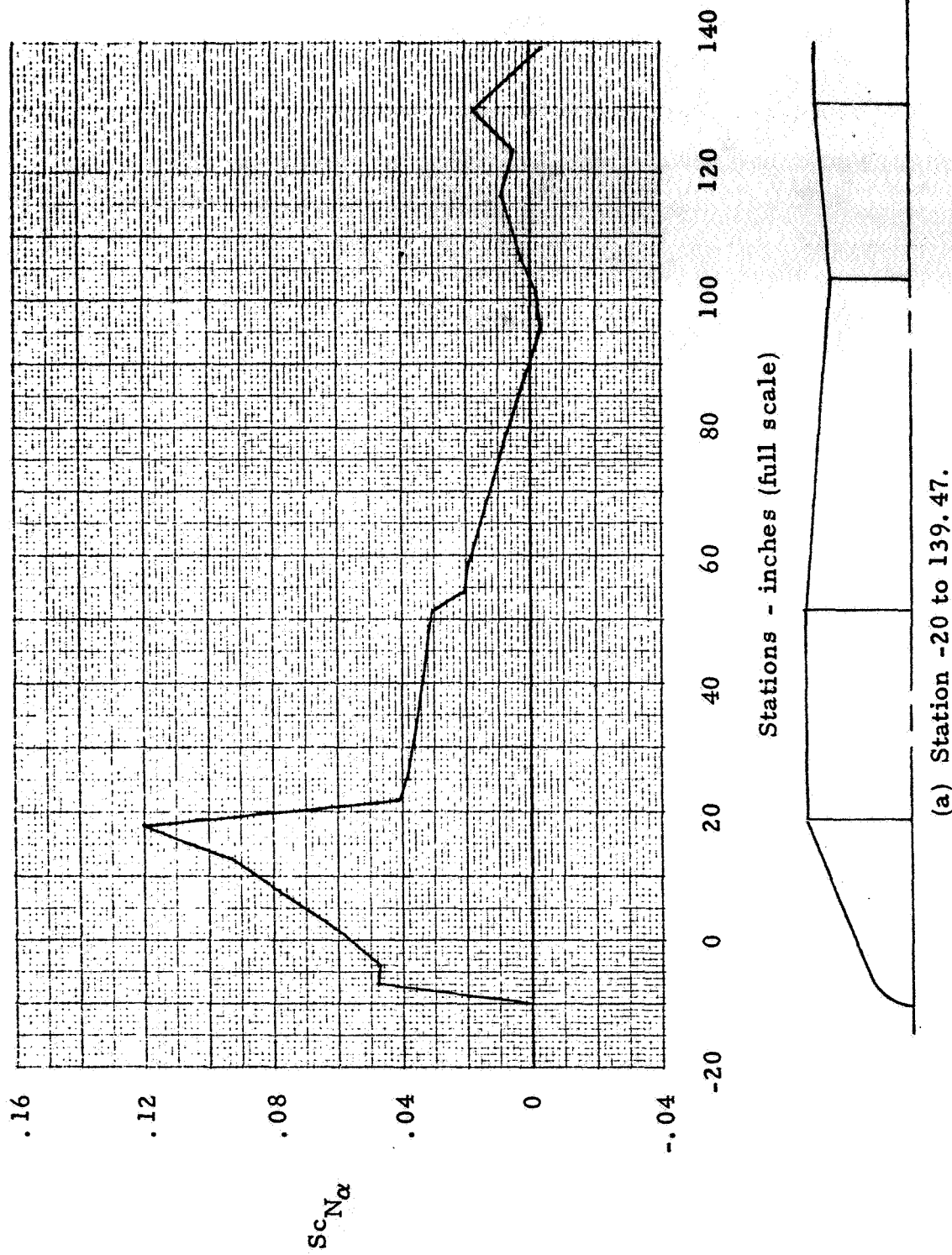
Figure 15. - Normal Load Distribution, $B_{off}P_{on}F_{on}$, $M = 2.80$.

(a) Station -20 to 139.47.
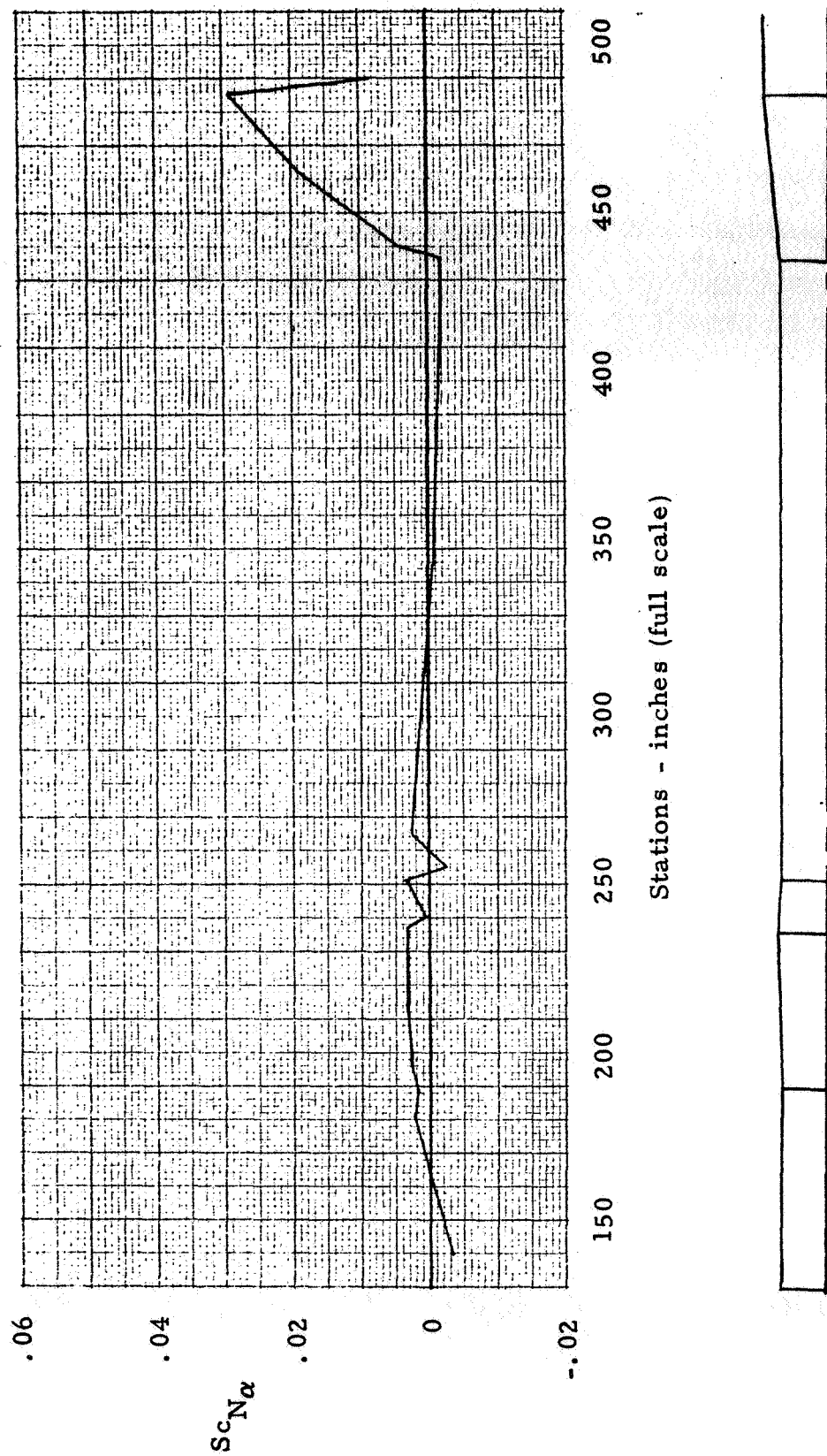
(b) Stations 139.47 to 489.39.

Figure 15. - Continued.
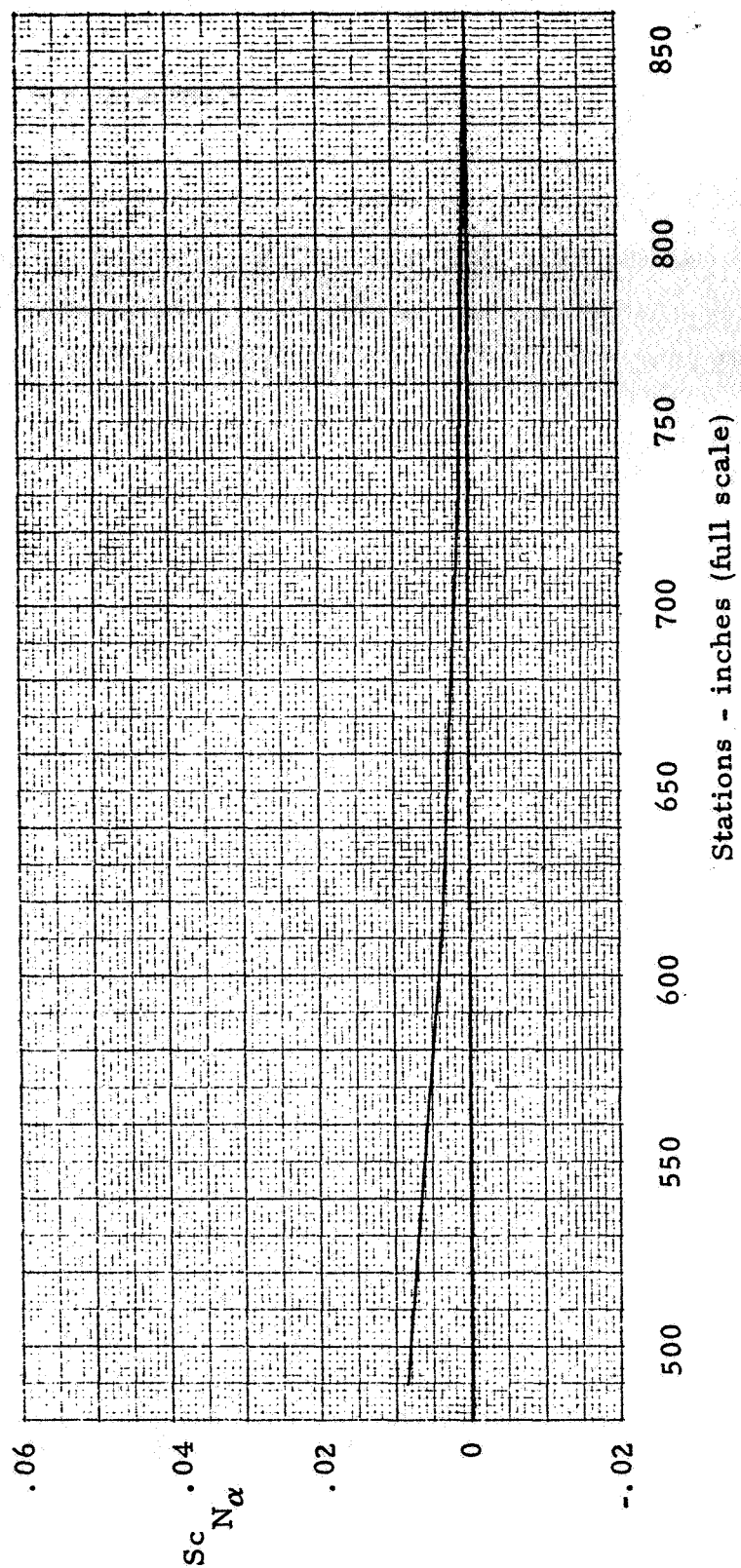
(c) Stations 489.39 to 848.

Figure 15. - Concluded.

55
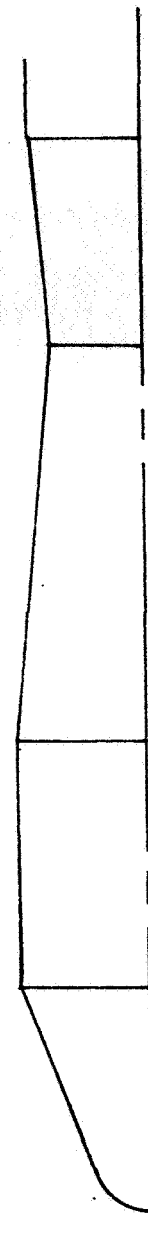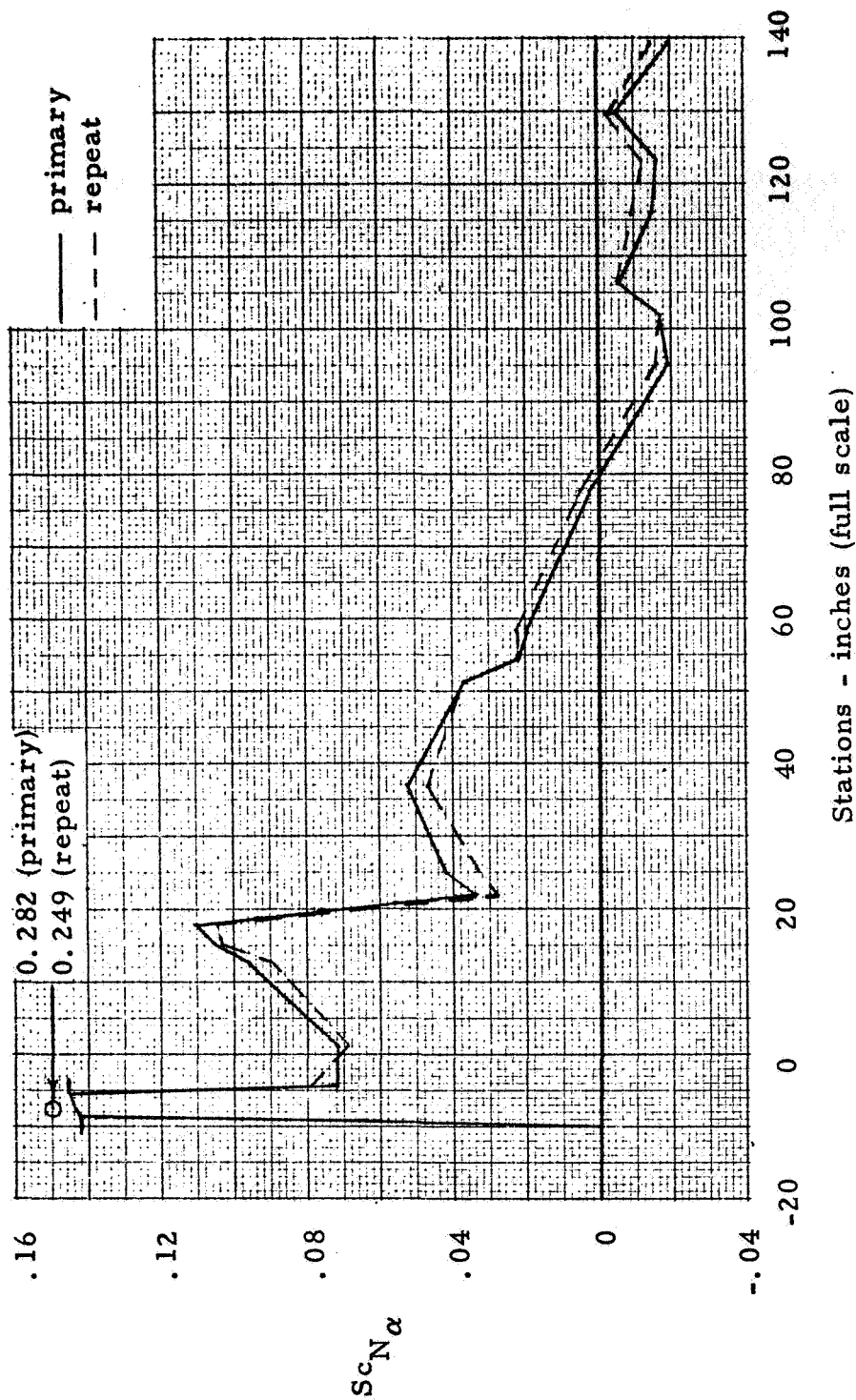
(a) Station -20 to 139.47.

Figure 16. - Normal Load Distribution, $B^0_{on} P_{on} F_{on}$, $M = 2.01$.

56
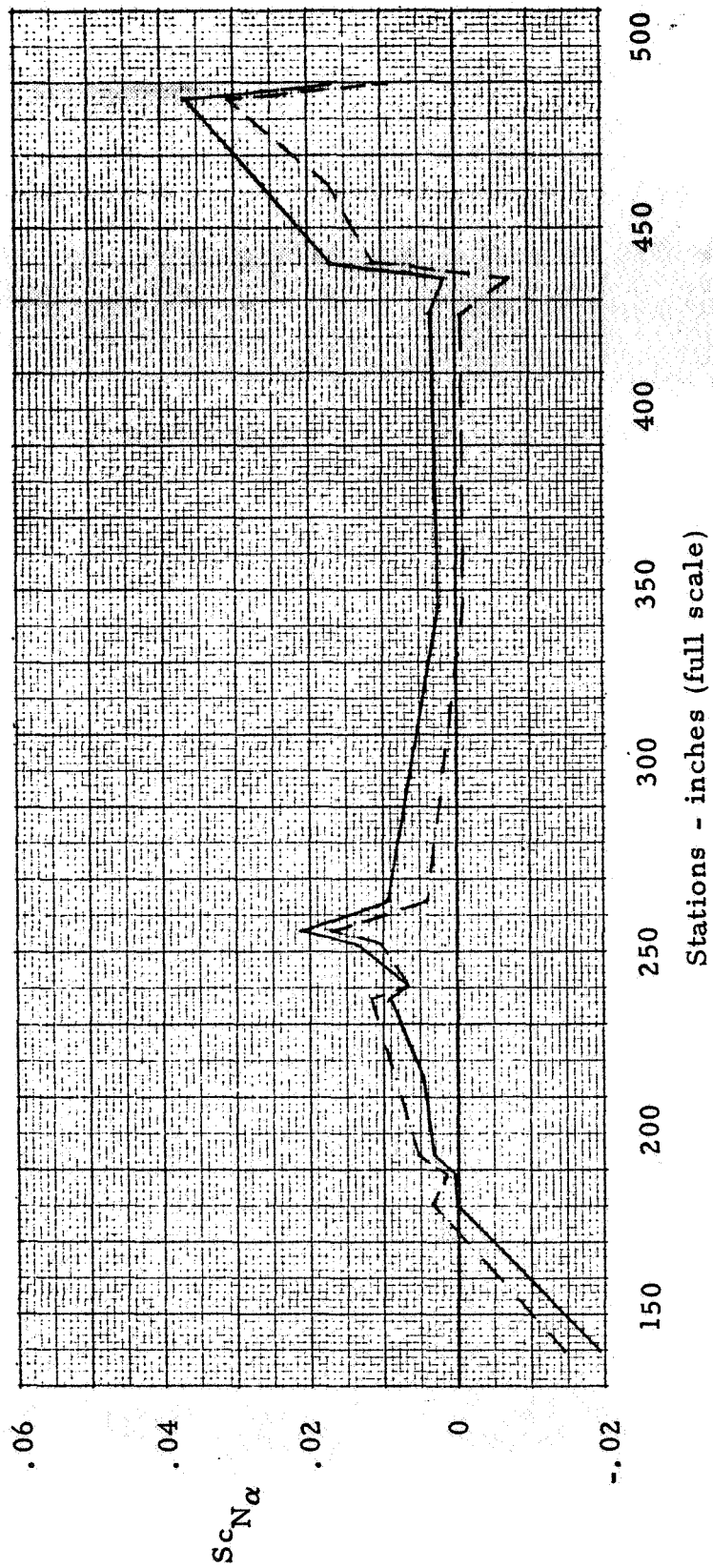
(b) Stations 139.47 to 489.39.

Figure 16. - Continued.

primary
repeat

Sc_{N_α}

Stations - inches (full scale)
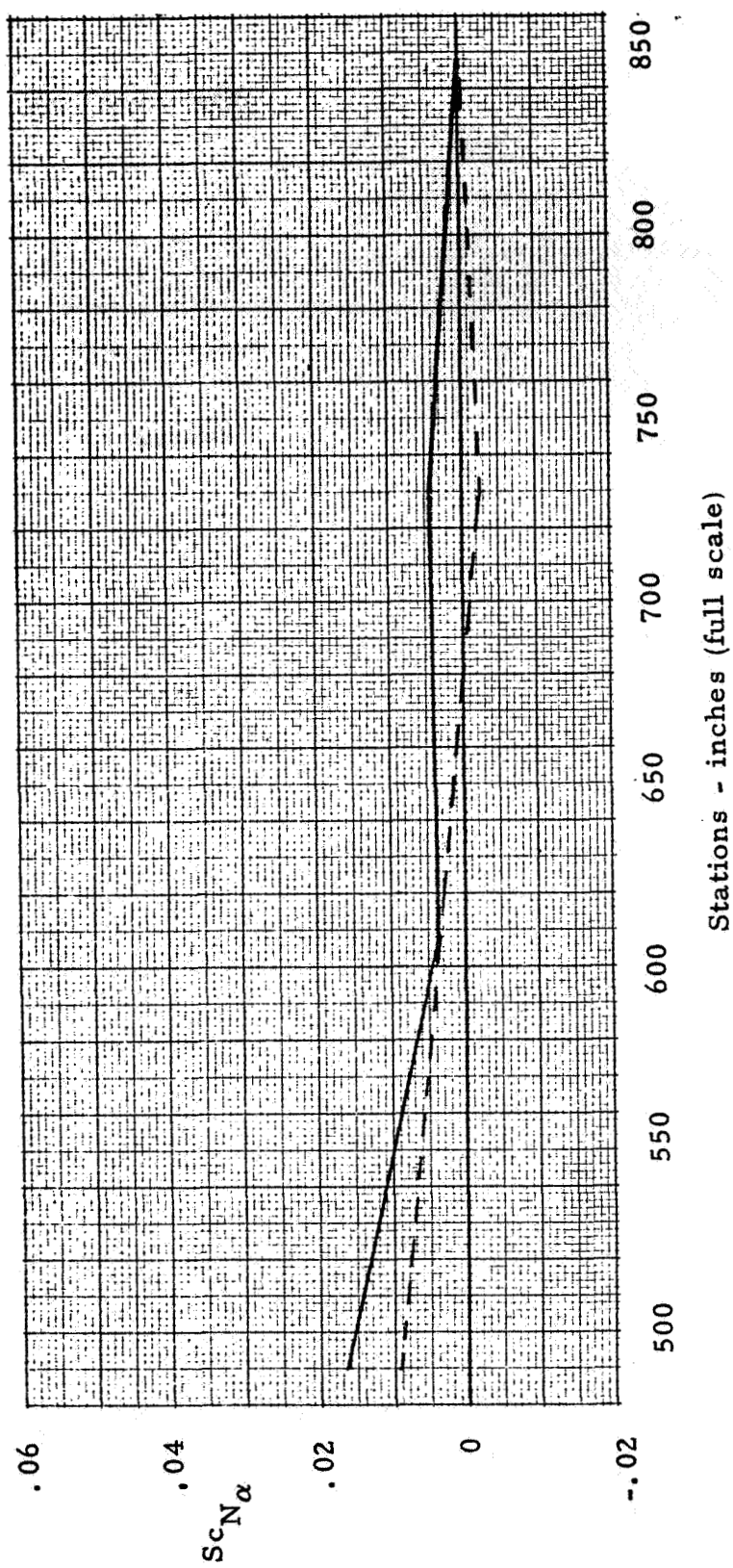
(c) Stations 489.39 to 848.

Figure 16. - Concluded.
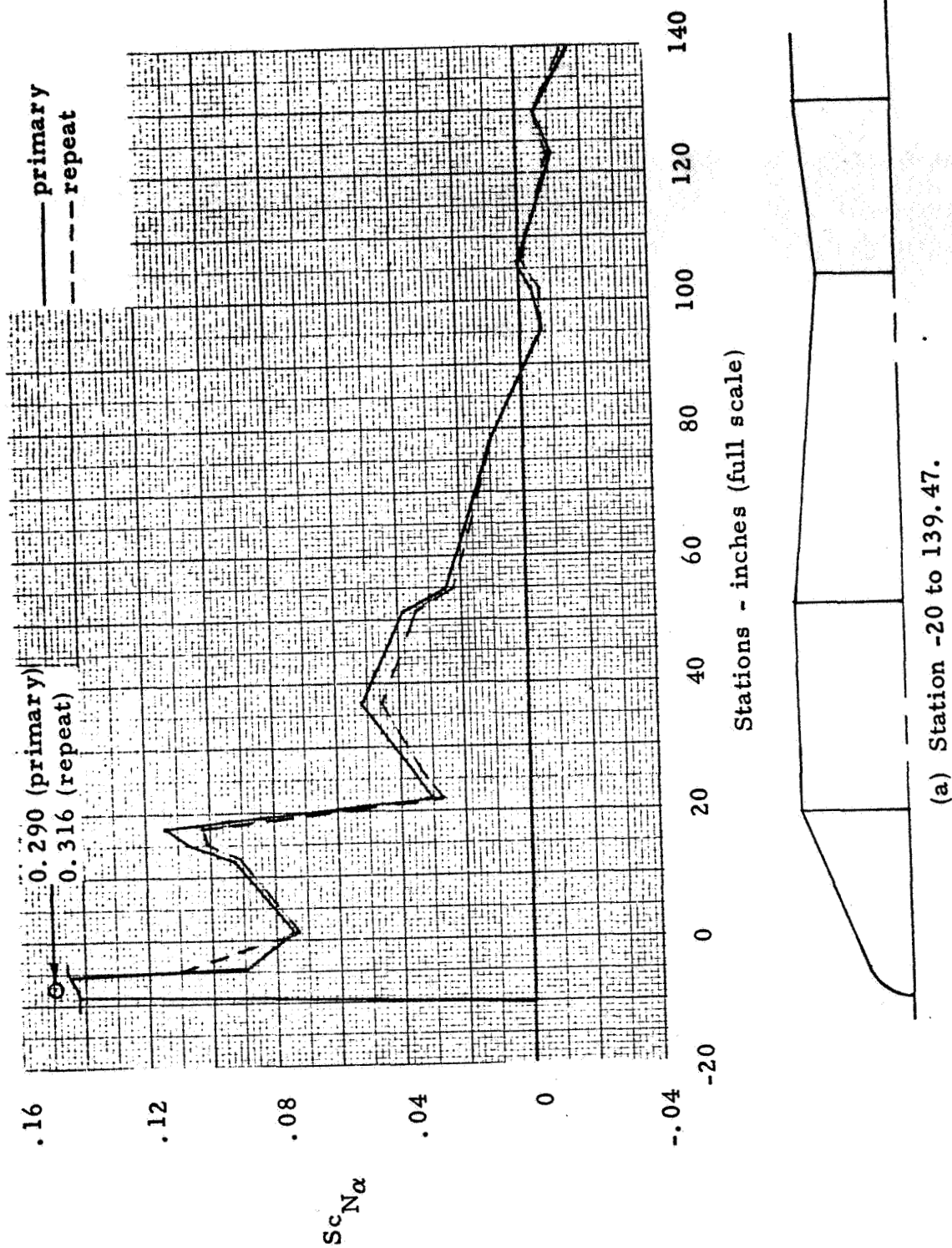
Figure 17. - Normal Load Distribution, $B_{on}^0 P_{on} F_{on}$, $M = 2.41$.

(a) Station -20 to 139.47.
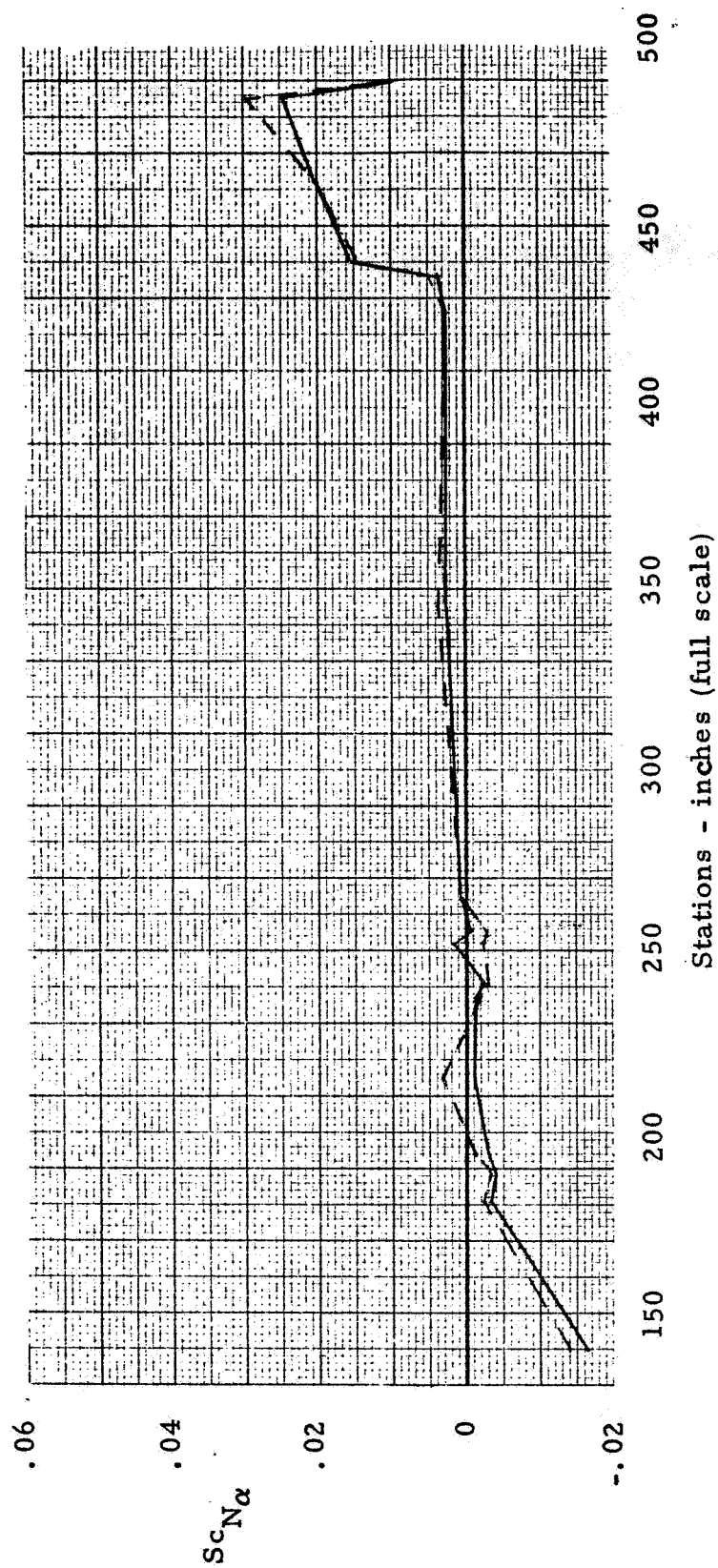
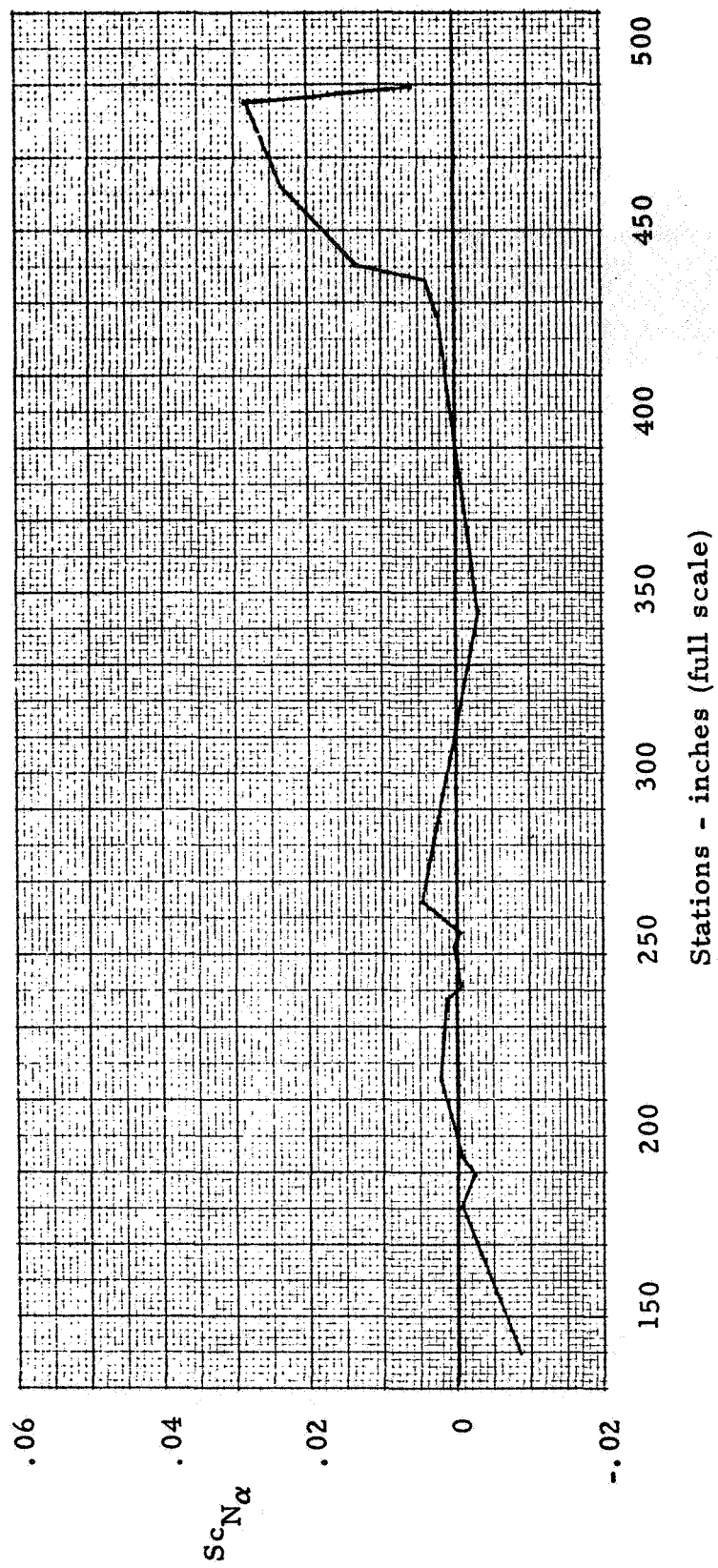(b) Stations 139.47 to 489.39.

Figure 17. - Continued.
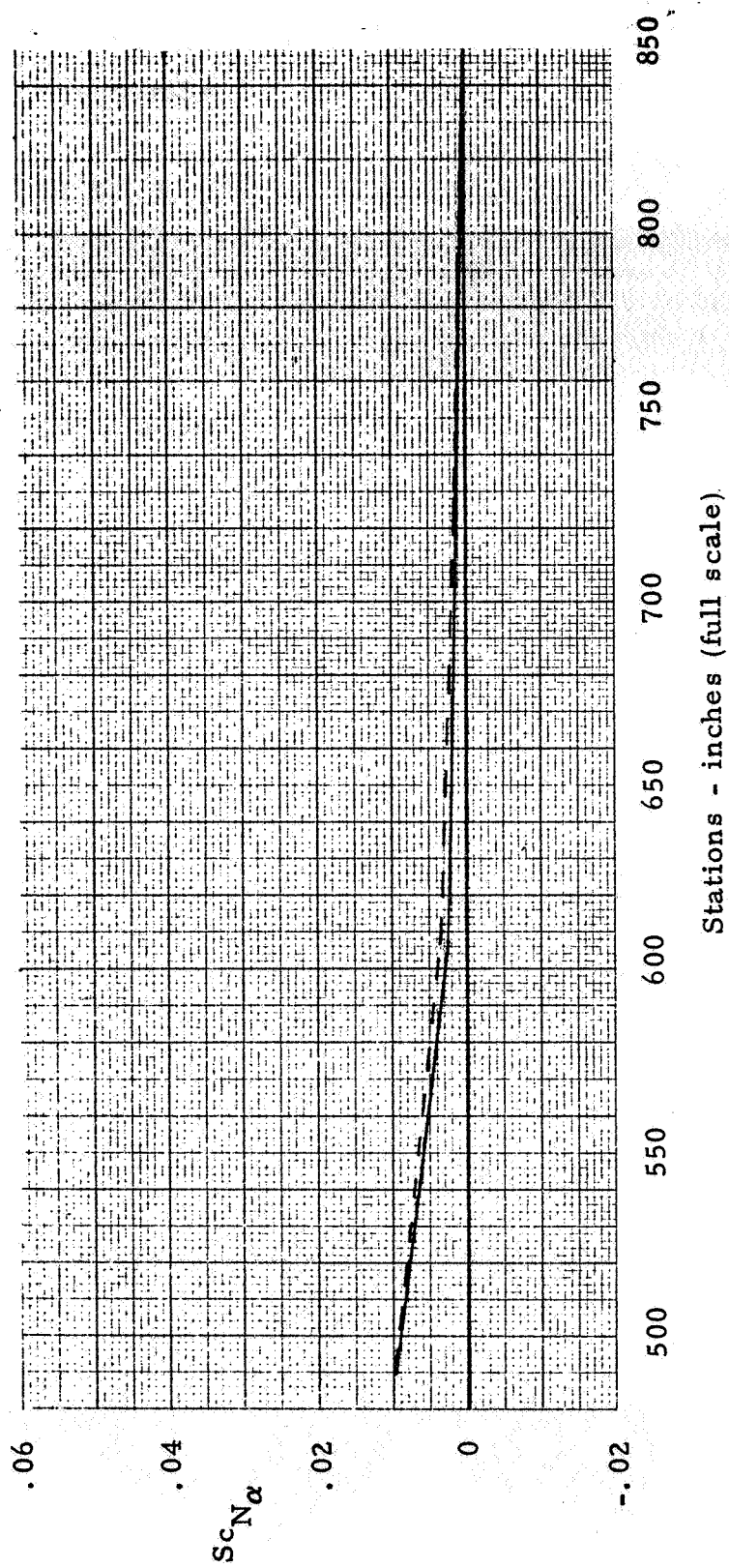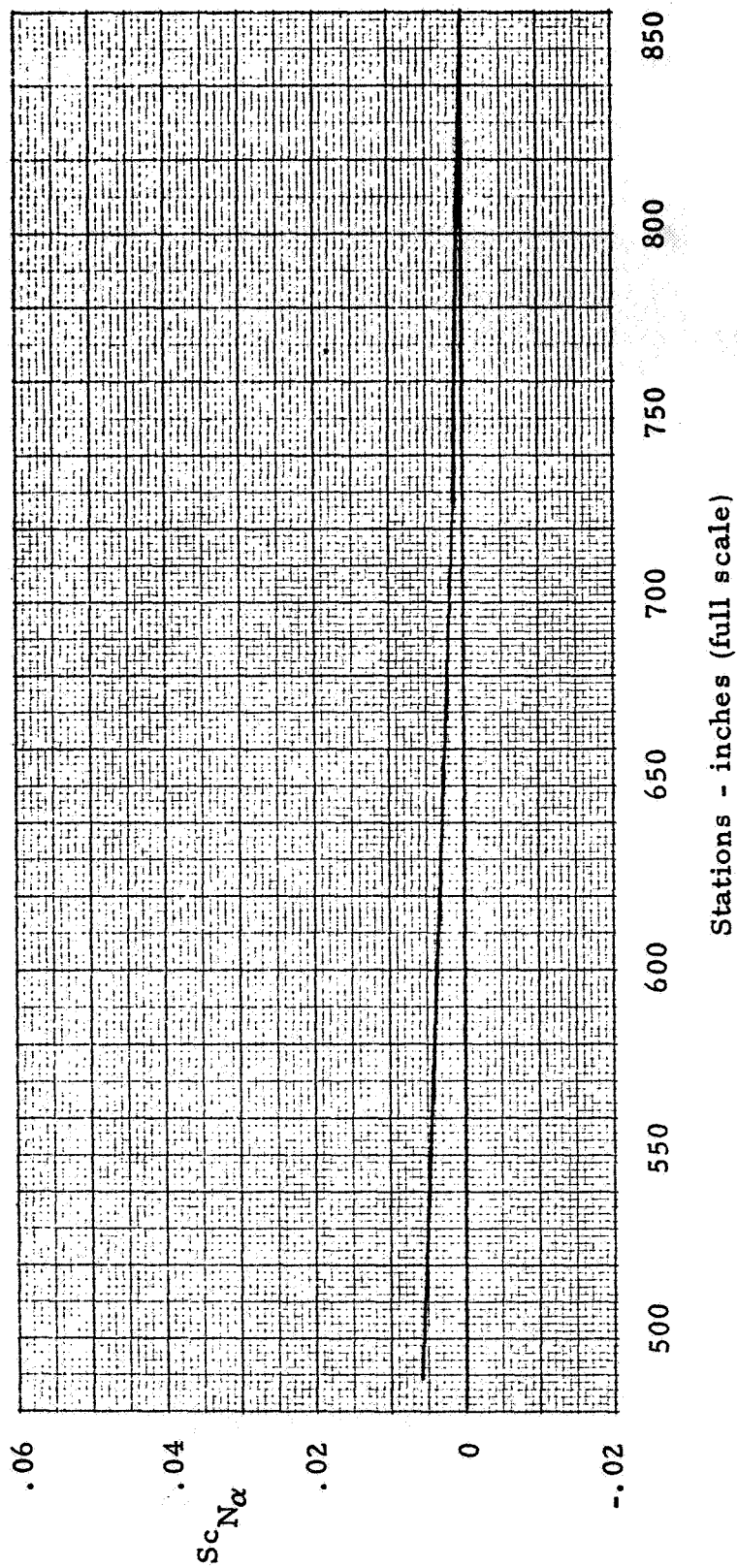
(c) Stations 489.39 to 848.

Figure 17. - Concluded.

61

(a) Station -20 to 139.47.
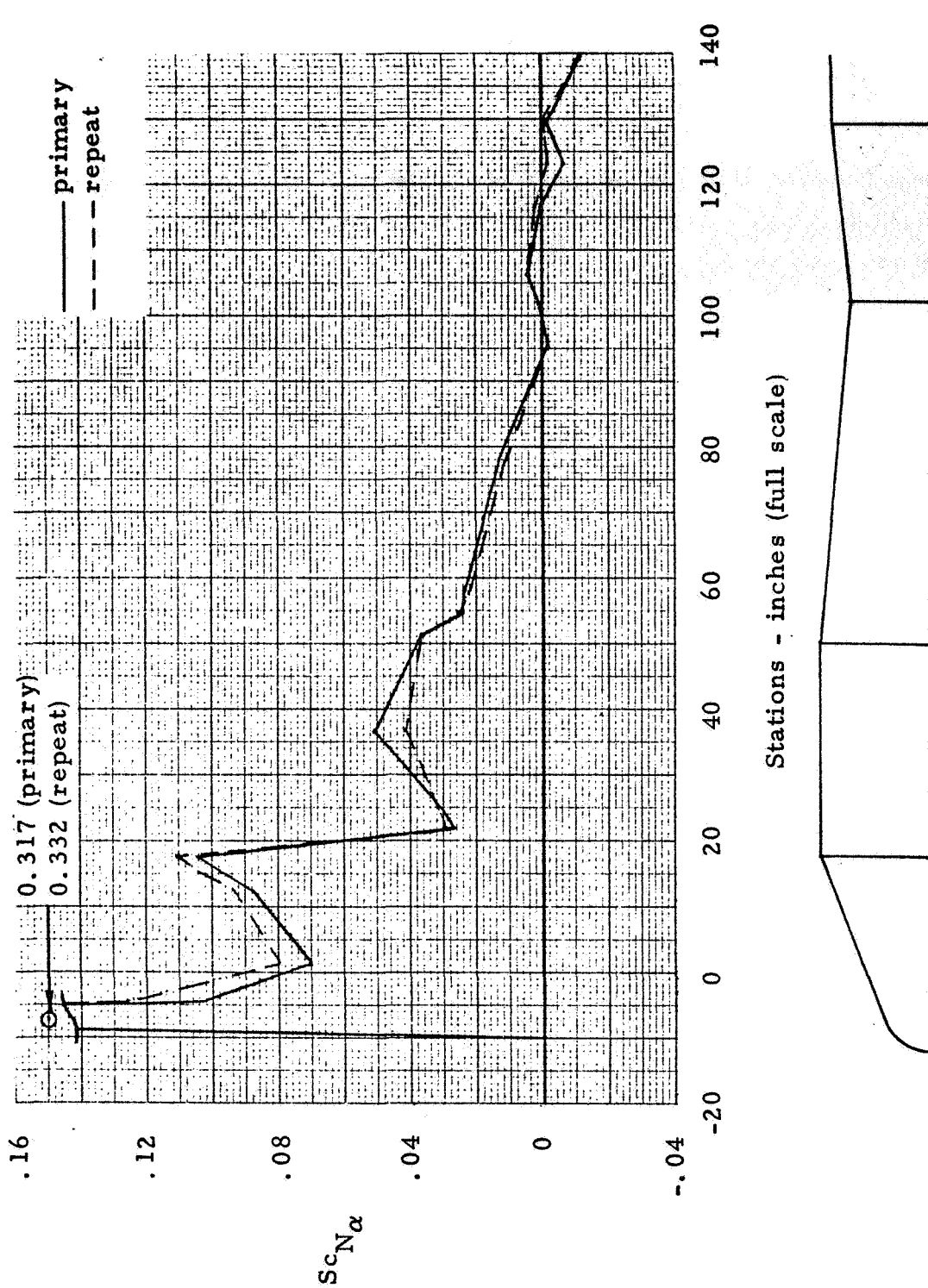
Figure 18. – Normal Load Distribution, $B^0_{on} P_{on} F_{on}$, M = 2.61.
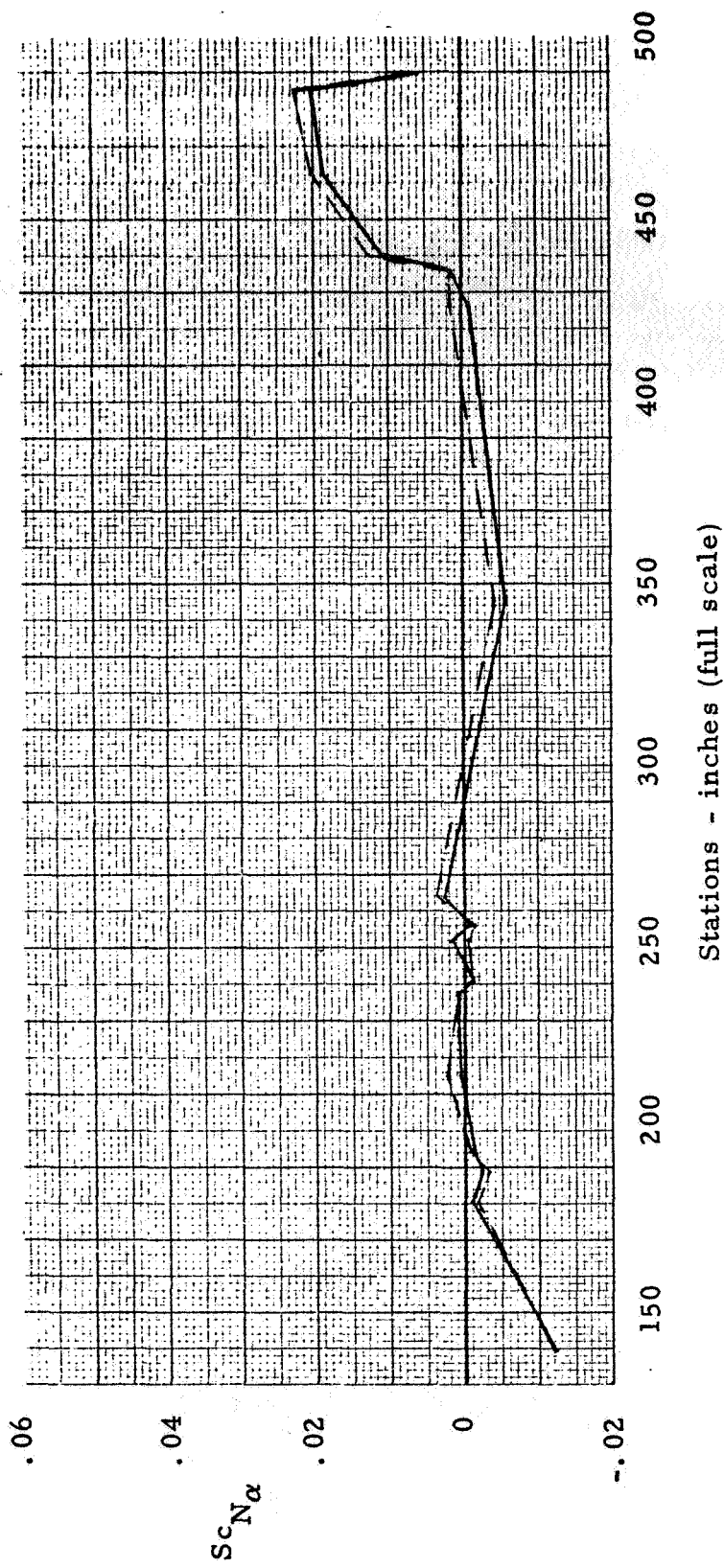
(b) Stations 139.47 to 489.39.

Figure 18. - Continued.
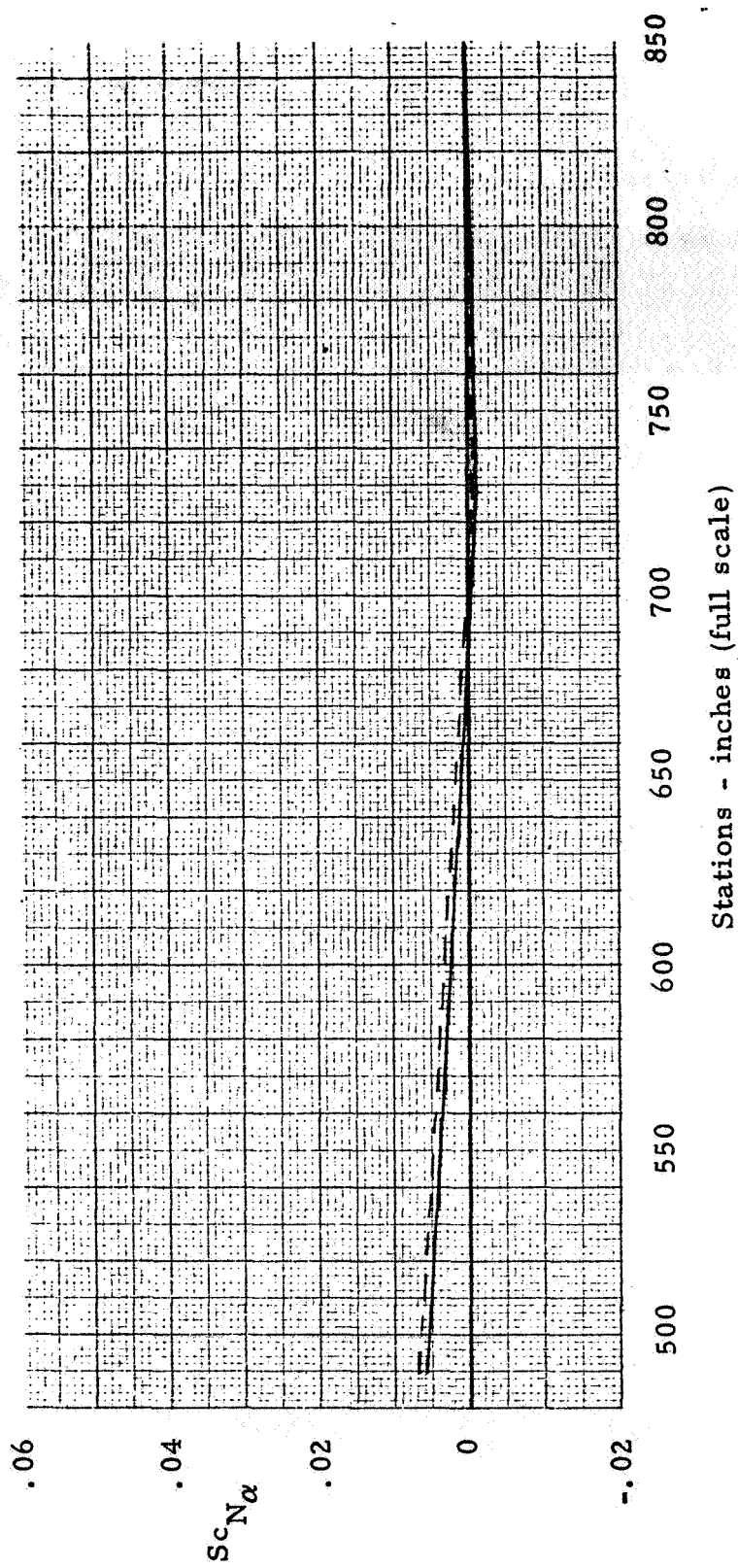
(c) Stations 489.39 to 848.
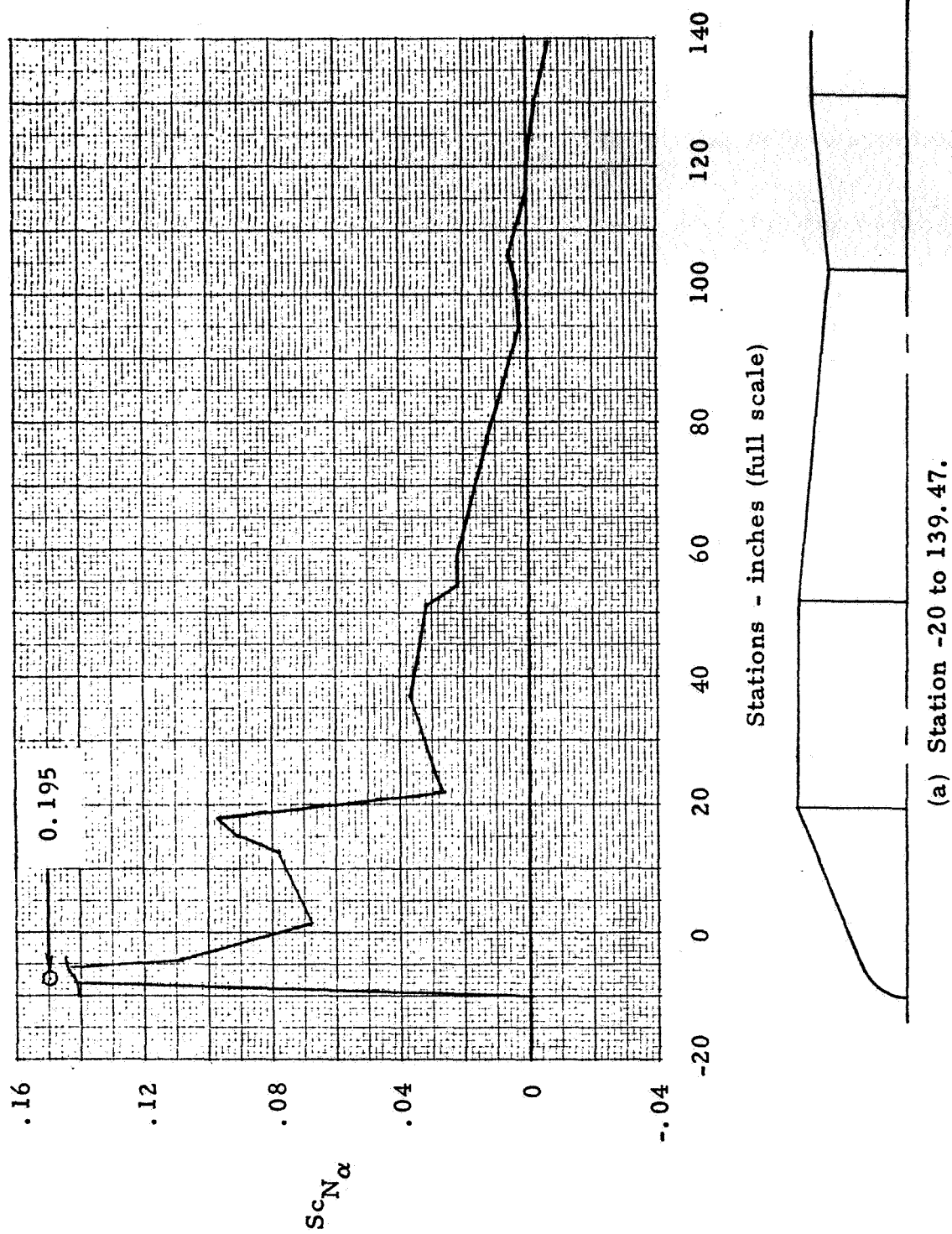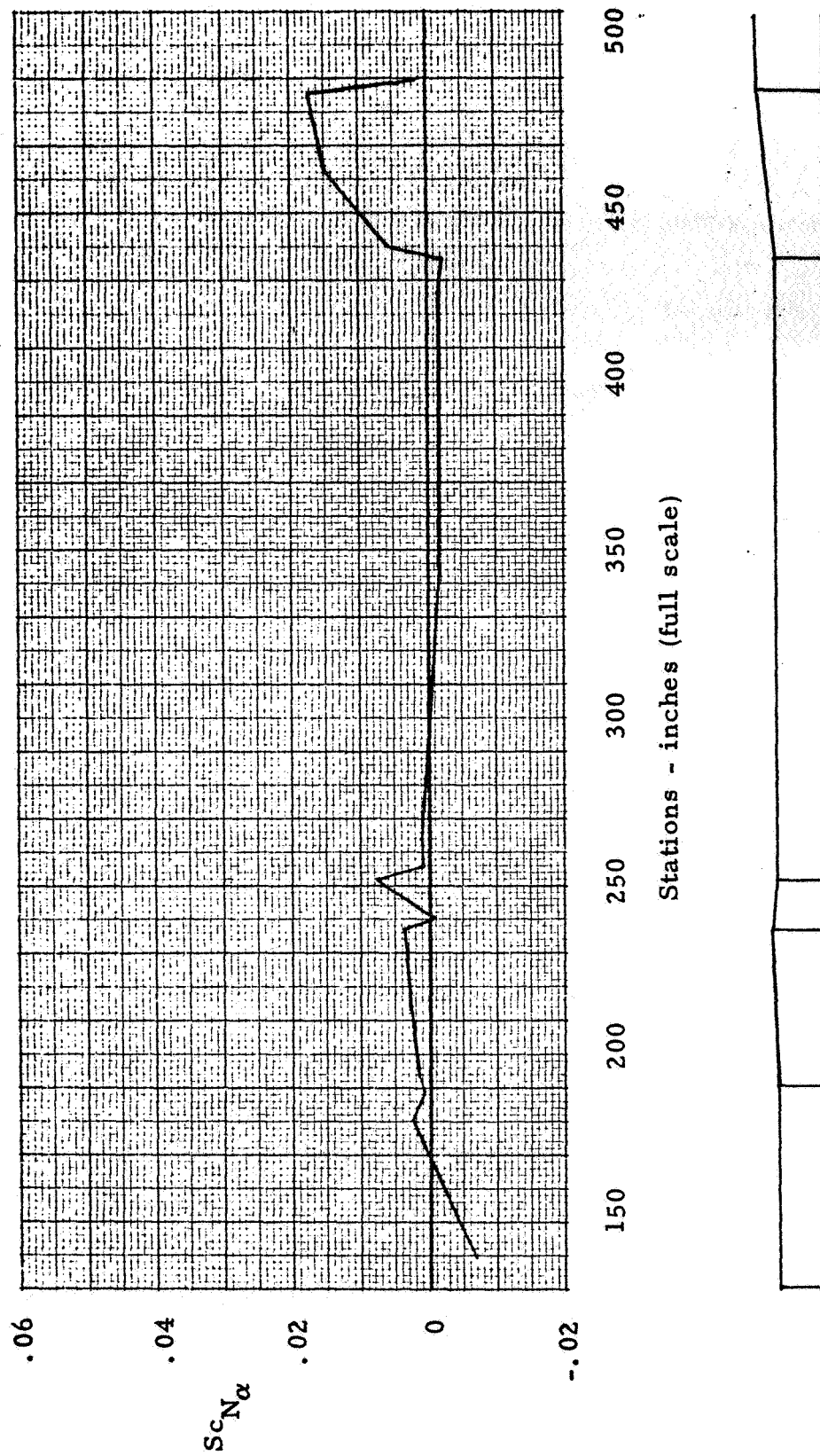
Figure 18. - Concluded.

Figure 19. - Normal Load Distribution, $B_{on}^0 P_{on} F_{on}$, M = 2.80.

(a) Station -20 to 139.47.

(b) Stations 139.47 to 489.39.

Figure 19. - Continued.

(c) Stations 489.39 to 848.

Figure 19. - Concluded.

Figure 20. - Normal Load Distribution, $B^3_{on} \, P_{on} F_{on}$, M = 2.01.

(a) Station -20 to 139.47.

(b) Stations 139.47 to 489.39.

Figure 20. - Continued.

(c) Stations 489.39 to 848.

Figure 20. - Concluded.

(a) Station -20 to 139.47.

Figure 21. - Normal Load Distribution, $B^3_{on} P_{on} F_{on}$, M = 2.41.

71

(b) Stations 139.47 to 489.39.
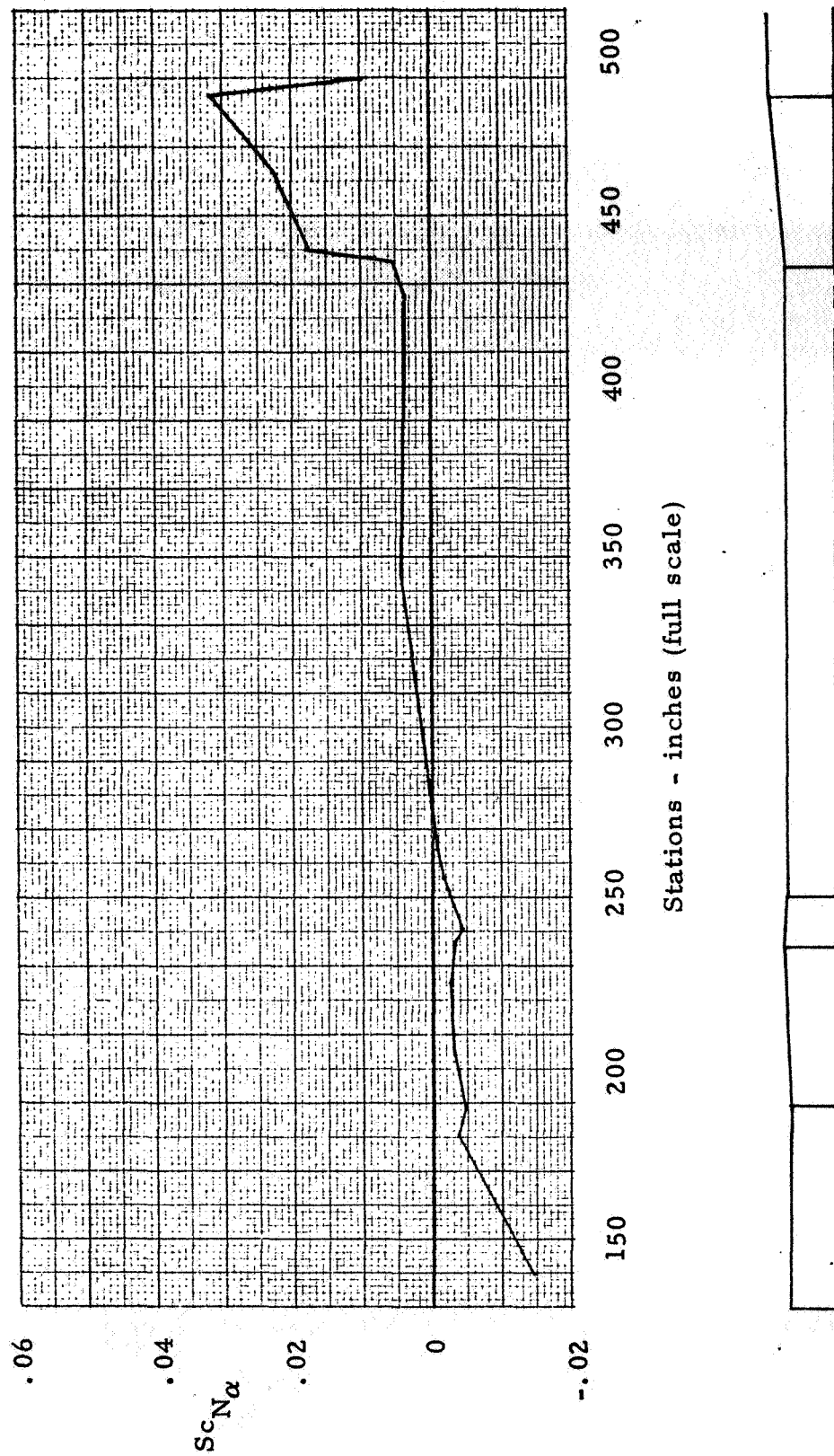
Figure 21. - Continued.
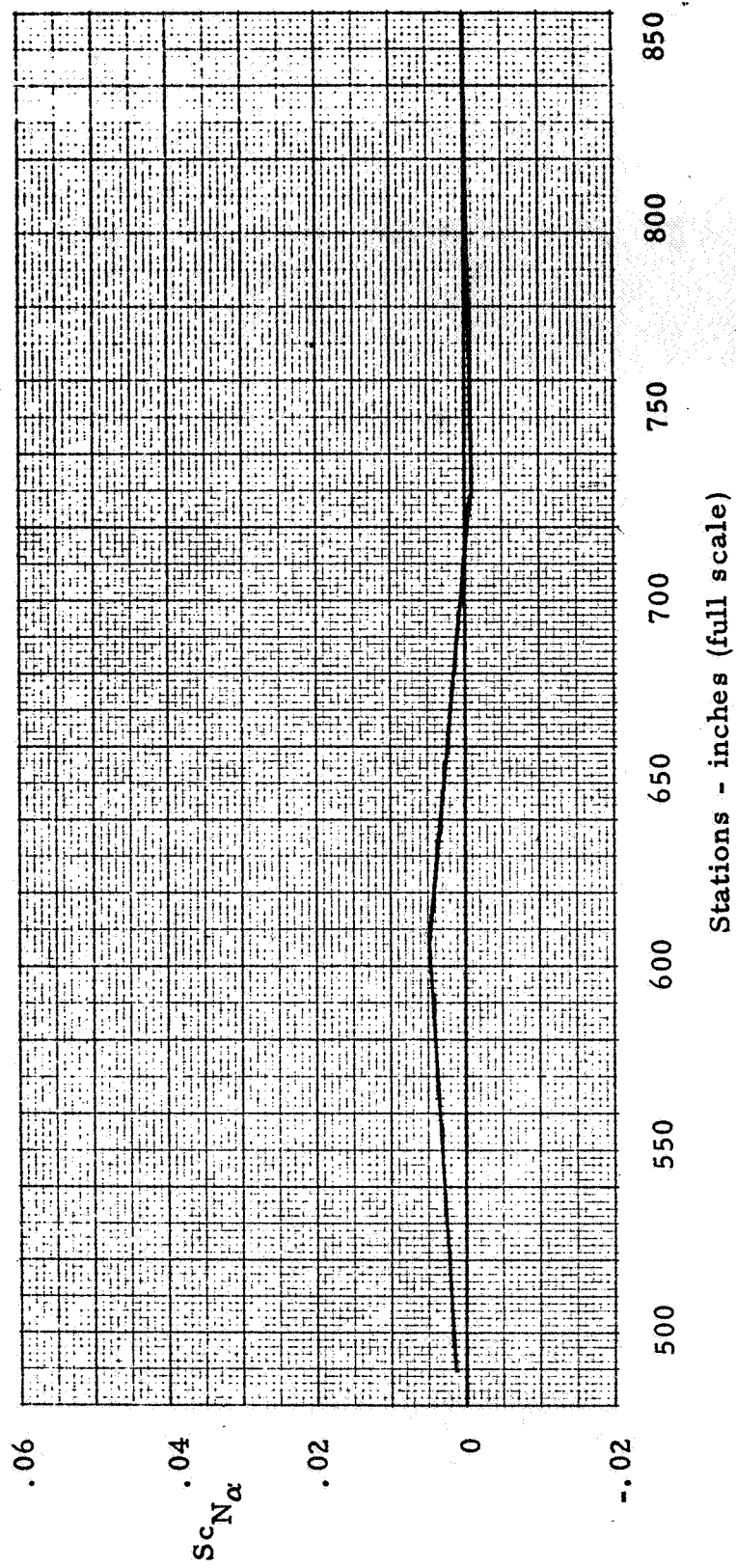
72
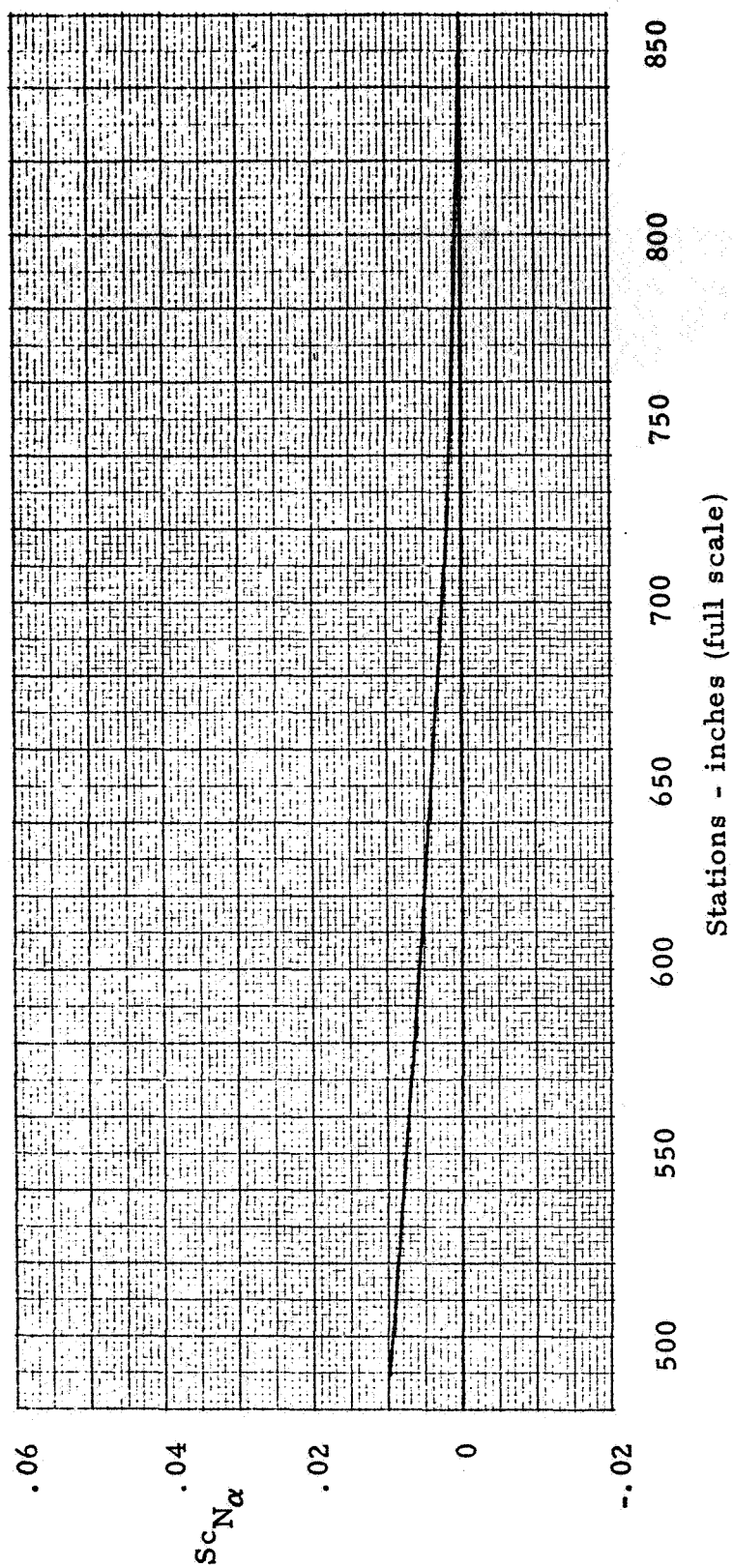
(c) Stations 489.39 to 848.

Figure 21. - Concluded.

73
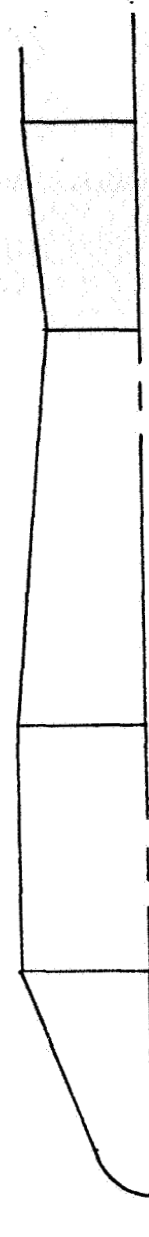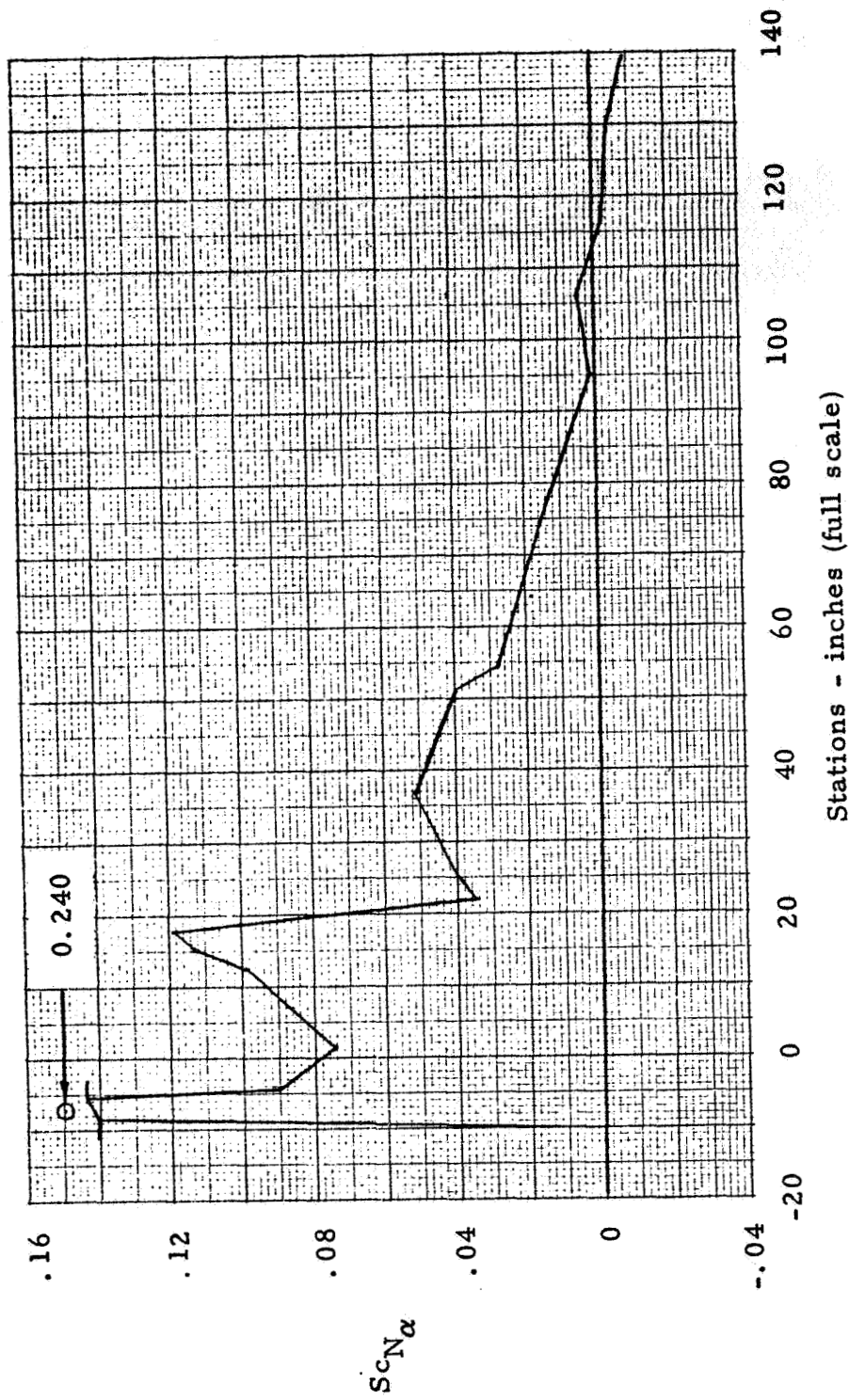
(a) Station -20 to 139.47.

Figure 22. - Normal Load Distribution, $B^3_{on} F_{on} F_{on}$, M = 2.61.

(b) Stations 139.47 to 489.39.

Figure 22. - Continued.

(c) Stations 489.39 to 848.

Figure 22. - Concluded.

76

Figure 23. – Normal Load Distribution, $B^3_{on}P_{on}F_{on}$, $M = 2.80$.

(a) Station -20 to 139.47.

(b) Stations 139.47 to 489.39.

Figure 23. - Continued.

(c) Stations 489.39 to 848.

Figure 23. – Concluded.

	Boom	Protub.	Fins
O	off	off	on
[]	on, 0	on	on
◻	on, 0	on	on (Repeat)
△	on, 3	on	on
◊	off	on	on

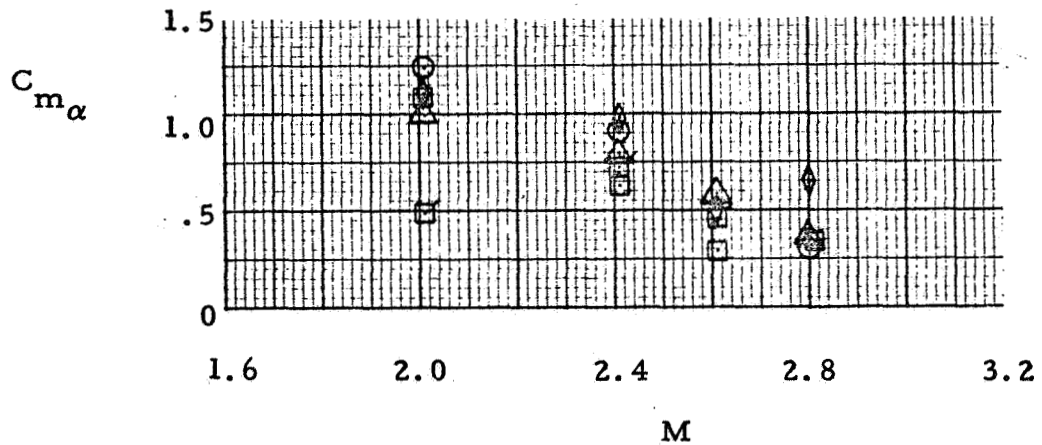Note: Pressure data were integrated over the body only, therefore, fin contributions are not included.

C_{N_α}
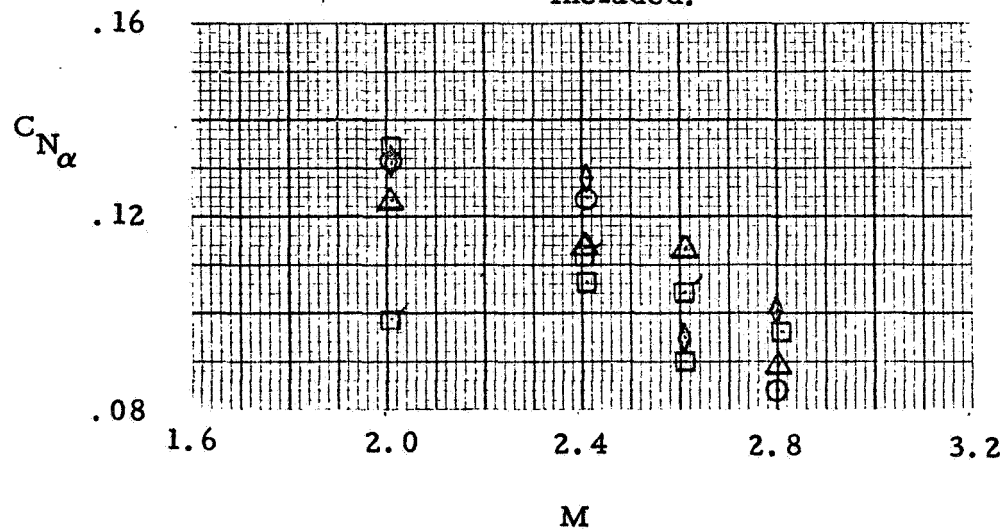
Figure 24. - Vehicle Normal Force Coefficient Derivatives (Pressure Test Data).

Figure 25. - Vehicle Pitching Moment Coefficient
Derivatives (Pressure Test Data)

	Boom	Protub.	Fins
○	off	off	on
□	on, 0	on	on
◁	on, 0	on	on (Repeat)
△	on, 3	on	on
◊	off	on	on

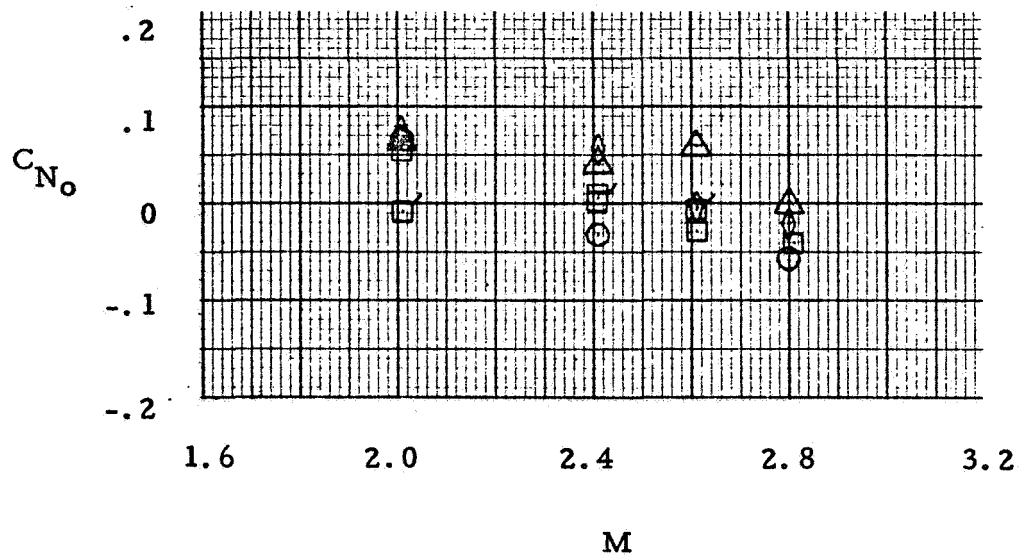Note: Pressure data were integrated over the body only, therefore, fin contributions are not included.

Figure 26. - Vehicle Normal Force Coefficient at $\alpha = 0°$ (Pressure Test Data)

		Boom	Protub.	Fins
Pressure Test Data	□	on, 0	on	on
	◻′	on, 0	on	on (Repeat)
Force Test Data	⊂	on, 0	on	off

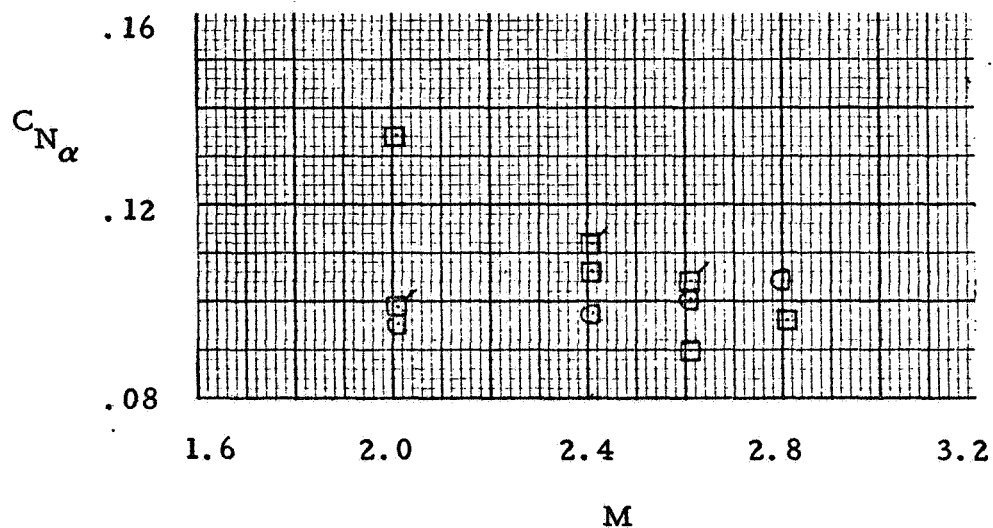Note: Pressure data were integrated over the body only, therefore, fin contributions are not included.

Figure 27. - Correlation of Vehicle Normal Force Coefficient Derivative

		Boom	Protub.	Fins
Pressure Test Data	□	on, 0	on	on
	◪	on, 0	on	on (Repeat)
Force Test Data	◖	on, 0	on	off

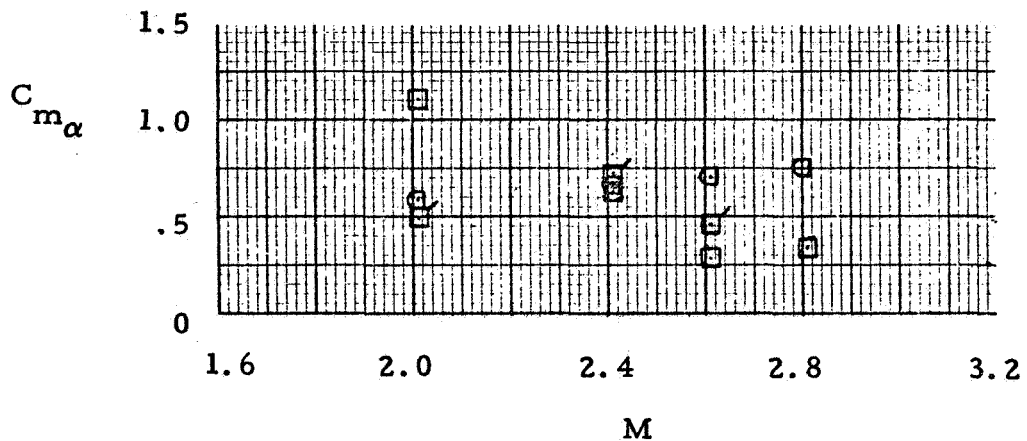Note: Pressure data were integrated over the body only; therefore, fin contributions are not included.

Figure 28. - Correlation of Vehicle Pitching Moment Coefficient Derivative

		Boom	Protub.	Fins
Pressure Test Data	⊡	on, 0	on	on
	⊡	on, 0	on	on (Repeat)
Force Test Data	⊡	on, 0	on	off

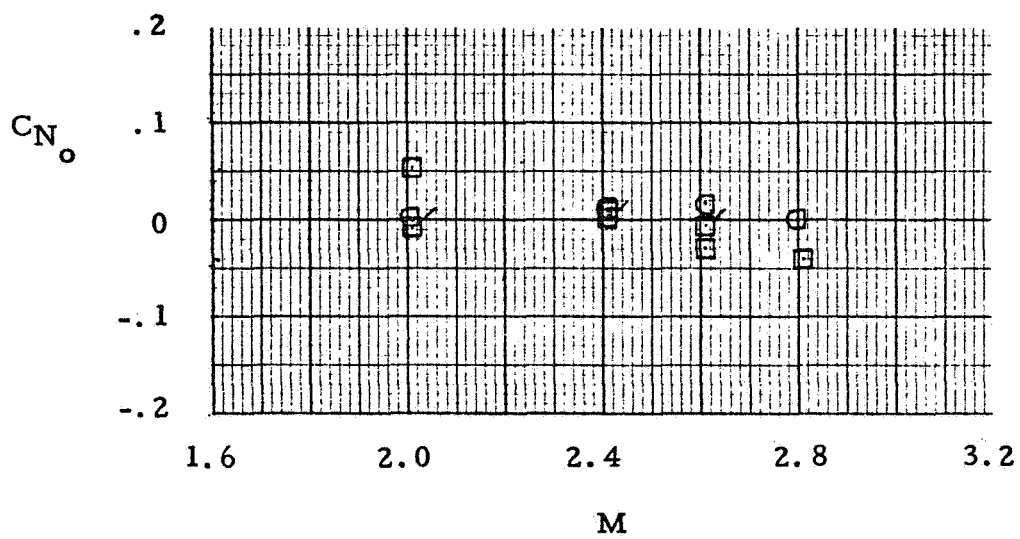Note: Pressure data were integrated over the body only, therefore, the fin contributions are not included.

Figure 29. – Correlation of Normal Force
Coefficient at $\alpha = 0^{\circ}$